NASA Contractor Report 182031

CALCULATION OF FLIGHT VIBRATION LEVELS OF THE AH-1G HELICOPTER AND CORRELATION WITH EXISTING FLIGHT VIBRATION MEASUREMENTS

R. Sopher and W.J. Twomey

SIKORSKY AIRCRAFT DIVISION
UNITED TECHNOLOGIES DIVISION
STARTFORD, CT 06601-1381

Contract NAS1-17499

April 1990

National Aeronautics and
Space Administration

Langley Research Center
Hampton, Virginia 23665-5225

FOREWORD

Sikorsky Aircraft has been conducting a study of finite element modeling of helicopter airframes to predict vibration. This work is being performed under U. S. Government Contract NAS1-17499. The contract is monitored by the NASA Langley Research Center, Structures Directorate.

This report describes the RDYNE analysis used by Sikorsky for the coupled rotor/airframe correlation study, the specifics of the application of the analysis to the AH-1G, and the correlation of theory and test. Key NASA and Sikorsky personnel are listed below.

NASA LANGLEY

Panice H. Clark, Contracting Officer

Joseph W. Owens, Contract Specialist

John H. Cline, Technical Representative

Raymond G. Kvaternik, Leader Rotorcraft Structural Dynamics Group

SIKORSKY

Dennis Prebensen, Contract Administrator

Wen-Liu Miao, Chief of Dynamics

Robert Sopher, Supervisor Dynamics Methods

W. J. Twomey, Senior Dynamics Engineer

Vincent Wu, Dynamics Engineer

TABLE OF CONTENTS

1. INTRODUCTION

INTRODUCTION

The NASA Langley Research Center is sponsoring a rotorcraft structural dynamics program with the overall objective to establish in the United States a superior capability to utilize finite element analysis models for calculations to support industrial design of helicopter airframe structures. Viewed as a whole, the program is planned to include efforts by NASA, Universities, and the U.S. Helicopter Industry. In the initial phase of the program, teams from the major U.S. manufacturers of helicopter airframes will apply extant finite element analysis methods to calculate static internal loads and vibrations of helicopter airframes of both metal and composite construction, conduct laboratory measurements of the structural behavior of these airframes, and perform correlations between analysis and measurements to build up a basis upon which to evaluate the results of the applications. To maintain the necessary scientific observation and control, emphasis throughout these activities will be on advance planning, documentation of methods and procedures, and thorough discussion of results and experiences, all with industry-wide critique to allow maximum technology transfer between companies. The finite element models formed in this phase will then serve as the basis for the development, application and evaluation of both improved modeling techniques and advanced analytical and computational techniques, all aimed at strengthening and enhancing the technology base which supports industrial design of helicopter airframe structures. Here again, procedures for mutual critique have been established, and these procedures call for a thorough discussion among the program participants of each method prior to the applications, and of the results and experiences after the applications. The aforementioned rotorcraft structural dynamics program has been given the acronym DAMVIBS (Design Analysis Methods for VIBrationS).

Under the DAMVIBS program, each of four industry participants, consisting of Bell Helicopter Textron Inc. (BHTI), Boeing Helicopters, McDonnell-Douglas Helicoper Company, and Sikorsky Aircraft, is to apply an extant coupled-rotor-fuselage analysis to calculate vibrations of the AH-1G helicopter and to correlate predictions with measurements derived from an Operational Load Survey (OLS) flight test program (references 1 and 2). The manufacturers are to present the descriptions of the analysis and correlations for critical review by the government and other manufacturers. BHTI, the manufacturer of the AH-1G, prepared and provided to the other participants the data needed to support the application of the analysis and correlation with test data. The data supplied by BHTI consisted of a detailed description of the rotor system including blade weight, material, structural, and aerodynamic properties and a description of the NASTRAN model of the fuselage (reference 3). Flight conditions were derived from data for the AH-1G Operational Load Survey aircraft (reference 4).

This report describes the analysis used by Sikorsky for the correlation study, the specifics of the application of the analysis to the AH-1G, and the correlation of theory and test. Sections 3 to 9 describe Sikorsky's RDYNE Rotorcraft Dynamics Analysis, Sikorsky's analytical tool. The method utilizes component mode synthesis to combine a modal model of the rotor with a modal model of the fuselage to represent the coupled-rotor fuselage system (reference 5). Aerodynamic loads acting on the rotor are derived from application of blade element theory and a quasisteady aerodynamic assumption. The nonlinear equations for the coupled rotor-fuselage system are integrated with respect to time to calculate blade loads, hub loads, and vibratory responses in the fuselage. Time histories are harmonically analyzed to calculated the harmonic coefficients of the responses at six flight speeds for comparison with flight test data. An unconstrained optimization method is used to calculate the trim state (reference 5). Sections 10 to 15 describe the application of RDYNE to the coupled rotor-fuselage system and compare the predictions of the method with flight vibration data for the AH-1G.

2. REQUIREMENTS FOR VIBRATION PREDICTION

REQUIREMENTS FOR ACCURATE VIBRATION PREDICTION

Research studies based on simplified models have shown the importance to vibration prediction of the simulation of dynamical couplings between the rotor and airframe. References 6 to 8 are samples from recent published literature justifying these findings. It is generally acknowledged that the rotor as the major excitation source should be modeled as accurately as possible. Established practice in loads and vibration prediction is to utilize elastic blades with several blade modes, variable rotor induced flow, and realistic aerodynamic data derived from airfoils tested in both unstalled and stalled regimes (Reference 9). Airframe modeling should strive to approximate the actual airframe as accurately as possible through modal or other representations.

REQUIREMENTS FOR ACCURATE VIBRATION PREDICTION

- Comprehensive dynamical system
  - Coupled rotor/airframe model
- Rotor
  - Elastic blades with several modes
  - Realistic aerodynamic representation
- Airframe
  - Simulation of practical system

3. OVERVIEW OF ANALYSIS

OVERVIEW OF VIBRATION PREDICTION METHODOLOGY

The tool used to predict vibrations on the AH-1G by Sikorsky Aircraft is the Rotorcraft Dynamics Analysis, referred to as RDYNE. The methodology is a component modes synthesis method and embodies the main ingredients which are assumed to be required for accurate vibration prediction, such as discussed in the preceding text. The equations of motion are solved by a time-marching procedure which utilizes a recursion formula. This formula expresses the response at each value of time as a function of previous responses, the dynamical properties of the coupled system, and the forces acting on the system. The RDYNE analysis is described in Ref. 5. (A decision was made not to use the alternative coupled rotor-fuselage Simplified Vibration Analysis (SIMVIB, reference 10), developed by Sikorsky for the Structures Laboratory, AVRADCOM Research and Technology Laboratories, and the NASA Langley Research Center under Contract NAS1-16058, because the G400-code supplying the rotor hub load excitation vector and rotor impedance matrix to SIMVIB does not work for teetering rotors. Since the completion of the work described in this report, Sikorsky has modified RDYNE using company funds to supply rotor impedance data to SIMVIB).

OVERVIEW OF VIBRATION PREDICTION METHODOLOGY

- RDYNE - Rotorcraft Dynamics Analysis
- Couples dynamical components
  - Rotor
  - Airframe
- Utilizes state-of-art aerodynamics
  - Tabulated airfoil data
  - Uniform or variable inflow
- Time-history solution

PROCESSES AND DATA FLOWS IN VIBRATION PREDICTION METHODOLOGY

In RDYNE, the properties of the rotor and airframe, and parameters defining the flight state, are supplied as input to the analysis to define the attributes and state of the helicopter, and the output from the analysis is the vibratory response of the helicopter. A given flight condition is described by airspeed, rotor shaft inclination, orientation of the rotor tip path plane, and rotor lift. The analysis adjusts rotor collective and cyclic pitch angles to match the specified flight condition in the applications of the analysis to the AH-1G performed for the study. Airframe properties consist of generalized masses, frequencies, modal dampings, and mode shapes for the normal modes calculated from a finite element representation. The mode shapes are defined at the point of connection of the rotor to the airframe, and at other points, such as the pilot's position.

PROCESSES AND DATA FLOWS IN VIBRATION PREDICTION METHODOLOGY

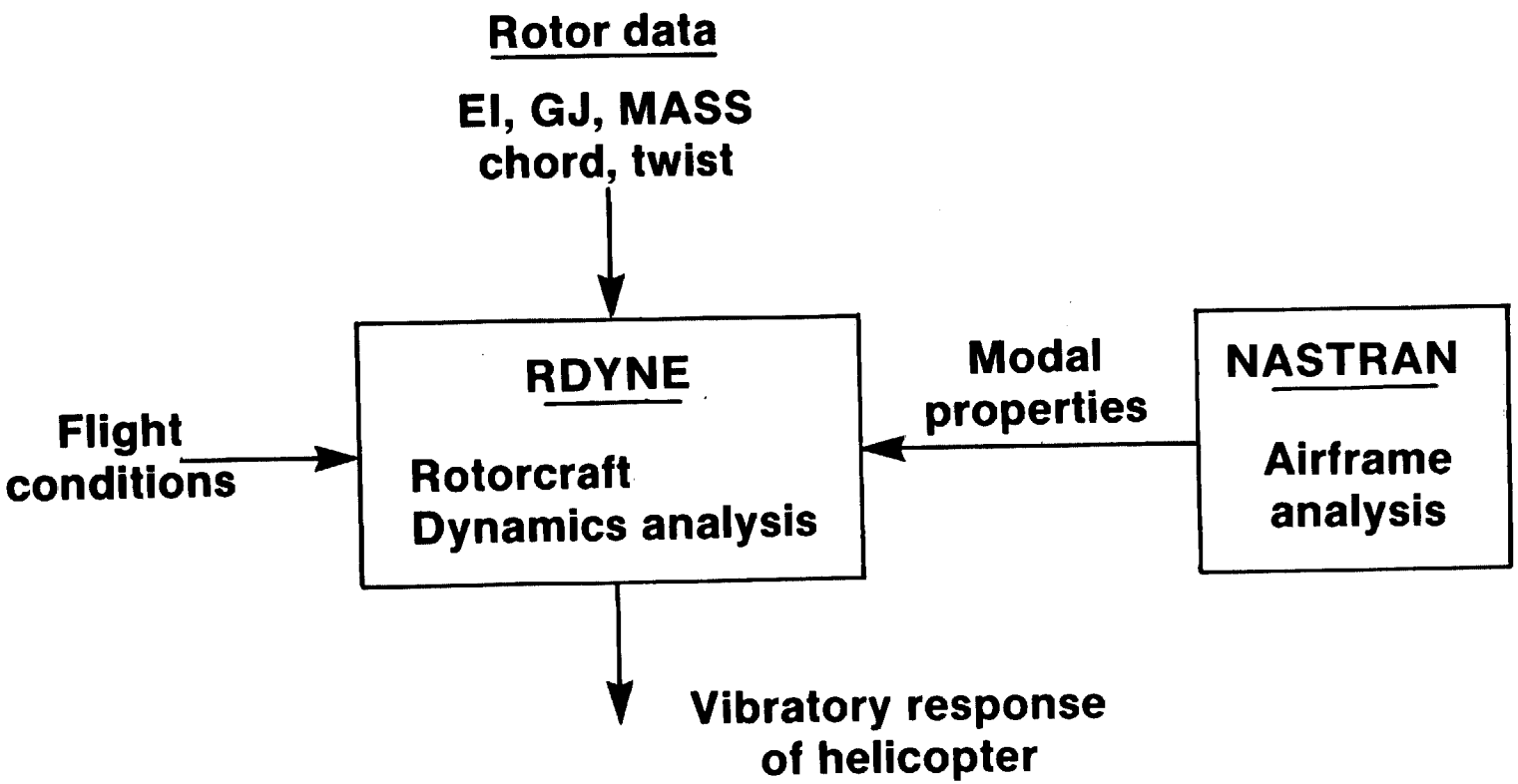

OVERVIEW OF DYNAMICAL COMPONENTS IN RDYNE

The helicopter dynamical system is assumed to be made up of dynamical substructures which are automatically assembled into a coupled system represented by a second order differential matrix equation. The figure shows a typical substructure breakdown of a helicopter. Components represented are a) elastic blades, b) articulated rigid blades, c) modal structures, d) a component that is defined as a general second order matrix equation, e) a prescribed force component, and f) a simple vibration absorber. The dynamical components invoked for the prediction of vibrations on the AH-1G are elastic blades to represent the rotor, and the modal structure to represent the airframe. Dynamical components are identified through distinct element numbers, and are coupled to other dynamical components by defining points at which the components are connected. Euler angles define the orientations of the components and provide the analysis with a versatile capability for modeling coupled dynamical systems. The figure illustrates typical element numbers and connection node numbers.

OVERVIEW OF DYNAMICAL COMPONENTS IN RDYNE

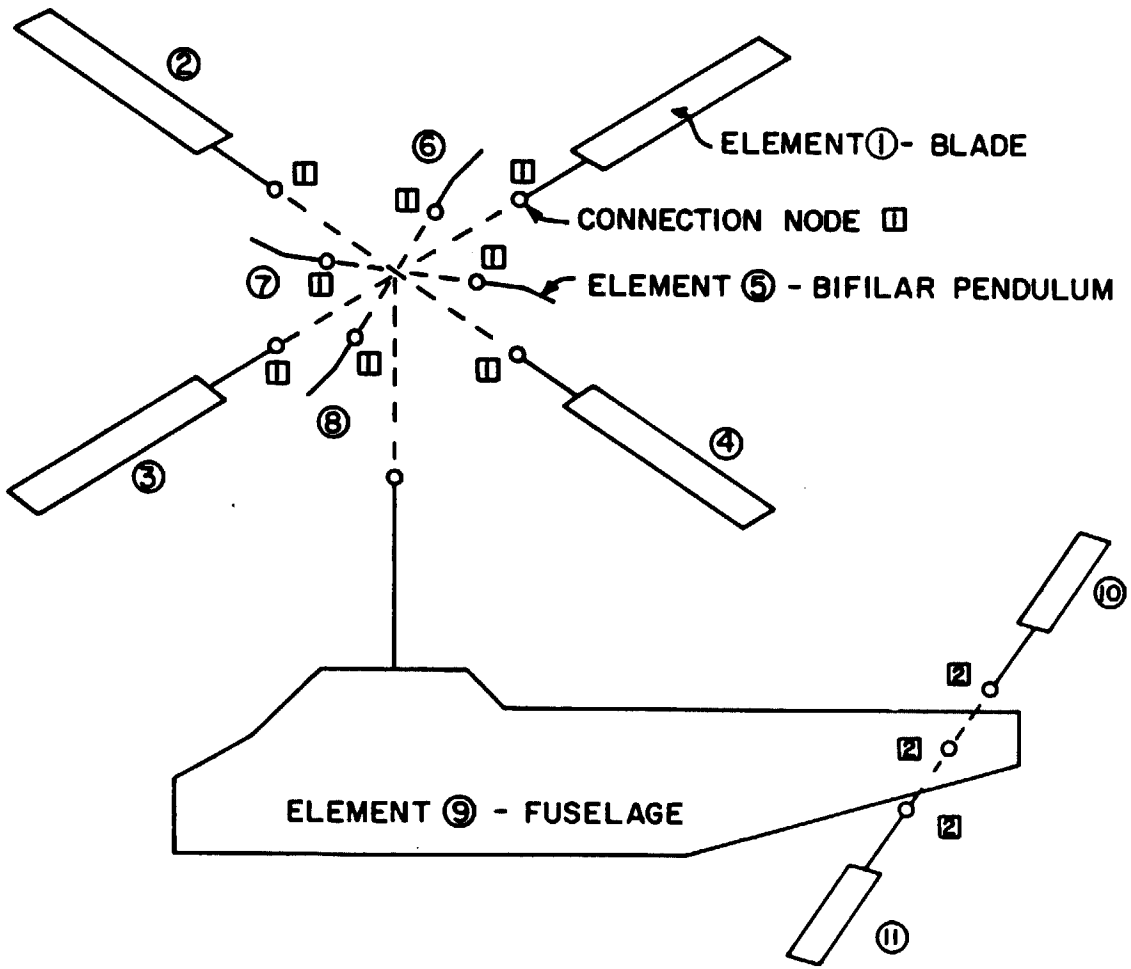

EXPANDED VIEW OF PROCESSES IN RDYNE

RDYNE forms the mass, damping, and stiffness matrices, and forcing function vectors for each dynamical component, and then assemblies these matrices to define the second-order matrix differential equation for the coupled system. The solution to this equation is the vibratory response for the system. The figure depicts processes required for the representation of a helicopter with a teetering rotor. Two components are utilized, consisting of an elastic blade and a modal representation of an airframe.

The normal modes for each blade of the teetering rotor are calculated in RDYNE by the Myklestad method, and these modes are used to reduce the basis of blade representation to normal mode coordinates. Expressing blade displacements in terms of modal coordinates transforms the partial differential beam equations for each blade to a set of ordinary differential equations which are functions of time. The blade equations are converted to equations for the teetering rotor by coupling one blade of the teetering rotor to the other blade through the application of the boundary conditions at the hinge and by utilizing relationships between the normal modes of the individual blades and the teetering rotor. This is followed by assembly of the rotor equations with the equations for the airframe, which is achieved by expressing the rotor displacements at the hub in terms of the normal modes of the airframe. The formation of the equations for each component and the assembly of the equations into the equations for the coupled system are performed at each time step and the resulting system equation is solved to obtain the vibratory response of the helicopter as a function of time.

EXPANDED VIEW OF PROCESSES IN RDYNE

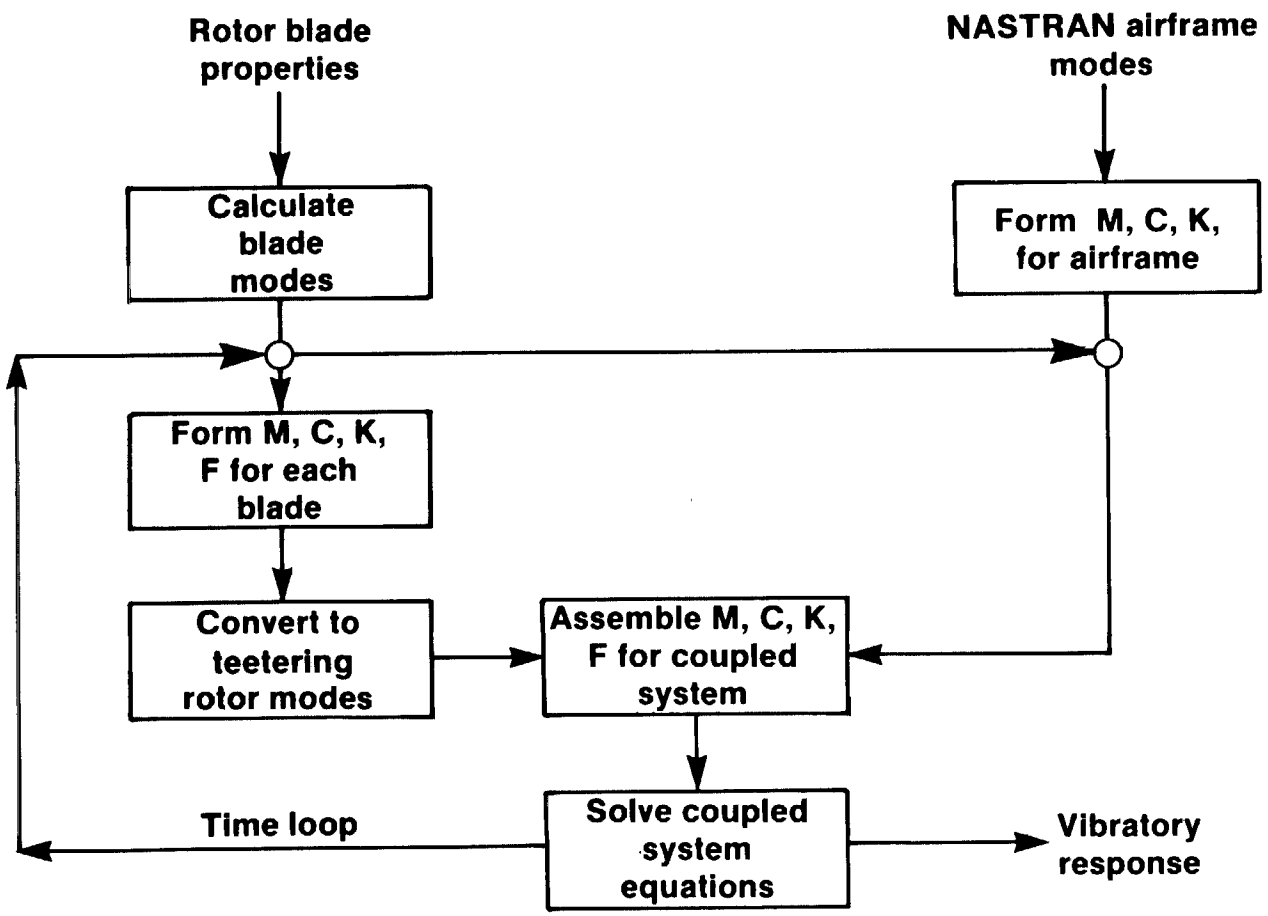

4. ROTOR REPRESENTATION

SCHEMATIC OF ELASTIC BLADE

The general features of the blade component are that it is provided with the ability to represent flap and lead displacements about mechanical hinges, blade feathering, and elastic bending and torsion displacements. The hub to which the blade is attached is assumed to rotate with constant angular speed. The hub is assumed to have three translational and three rotational displacements. These coordinates enable the blade to be coupled to another component such as another blade, an airframe, or a combination of these components, through the equating of the displacements at the hub. The blade therefore possesses the internal and connection node degrees of freedom assumed to be necessary for a state-of-the-art vibration prediction method.

The equations in Ref. 11 are used as the basis of the elastic blade. The equations were augmented with six hub equilibrium equations, corresponding to the hub connection node coordinates identified above.

SCHEMATIC OF ELASTIC BLADE

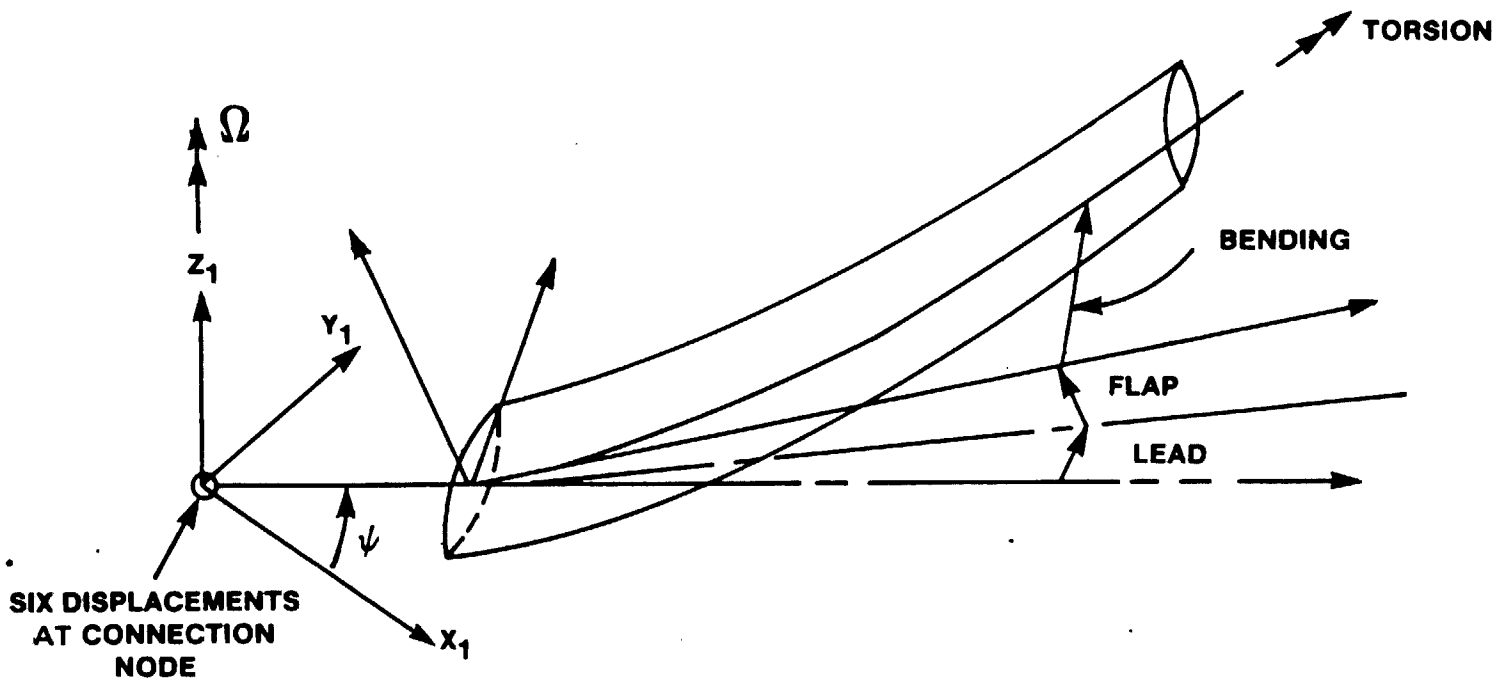

ATTRIBUTES OF ROTOR

The attributes of the rotor enable it to be used to model practical rotor systems with nonuniform properties. The aerodynamic representation is based on blade element theory and enables nonlinear airfoil data to be inserted into RDYNE in the form of tables. There is no provision for an unsteady airfoil model, except for the inclusion of a pitch damping term of noncirculatory origin derived from linear incompressible theory. Variable inflow is based on the use of a skewed helical wake, and is represented mathematically by aerodynamic influence coefficients relating blade circulation and rotor induced inflow.

ATTRIBUTES OF ROTOR

- Elastic displacements are represented
  - Bending and torsion
- Articulated, hingeless, or teetering
- Nonuniform properties
  - Chord, twist, mass, c.g., torsional inertias
- Blade element aerodynamic representation
  - Quasi-steady aerodynamics
  - Pitch damping from linear theory
- Rotor induced inflow
  - Uniform inflow from momentum theory
  - Prescribed wake variable inflow

MAJOR ASSUMPTIONS OF THE BLADE MODEL

The equations of motion are based on a set of assumptions which indicate the scope and limitations of the blade model.

1. In general, the rotor hub may be in accelerated motion. This state includes uniform motion as a special case.

2. The blade elastic axis is straight before elastic deformation has occurred, and coincides with the feathering axis before elastic deformation.

3. The blade is assumed to have structural and inertial symmetry about a major principal axis located on the aerodynamic chord.

4. Blade flap and lag hinges and feathering bearing are coincident. The hinge sequence is lag-flap pitch.

5. The blade may have a built-in aerodynamic twist of arbitrary magnitude and distribution along the blade span.

6. The blade angle of impressed collective pitch may have an arbitrary magnitude.

7. Control system flexibility and blade root restraints are represented by root springs.

8. Blade element theory describes the aerodynamic forces, and radial flow effects are neglected.

Assumption 1 follows from assuming that the hub can have six displacements relative to an inertial system. Assumption 2 restricts the analysis to systems with zero (or small) elastic axis offsets from the feathering axis which is thought to be a good approximation for the AH-1G. Assumptions 3 to 6 do not introduce restrictions in the case of the AH-1G. Assumption 7 reflects the application of the analysis in this contract, because RDYNE has the capability to enable a blade to be coupled to more complex dynamical systems than root springs. Assumption 8 similarly reflects the present application, because the analysis has a general capability to model radial flow effects.

MAJOR ASSUMPTIONS OF THE BLADE MODEL

The following major assumptions are made to derive the equations of motion.

1. In general, the rotor hub may be in accelerated motion. This state includes uniform motion as a special case.
2. The blade elastic axis is straight before elastic deformation has occurred, and coincides with the feathering axis before elastic deformation.
3. The blade is assumed to have structural and inertial symmetry about a major principal axis located on the aerodynamic chord.
4. Blade flap and lag hinges and feathering bearing are coincident. Lag-flap-pitch sequence.
5. The blade may have a built-in aerodynamic twist of arbitrary magnitude and distribution along the blade span.
6. The blade angle of impressed collective pitch may have an arbitrary magnitude.
7. Control system flexibility and blade root restraints are represented by root springs.
8. Blade element theory describes the aerodynamic forces, and radial flow effects are neglected.

SMALL QUANTITIES IN THE BLADE EQUATIONS

As a first step in the process of deriving the blade equations, small terms are identified which enable products of terms to be neglected from the equations subsequently derived, and which yield simplifications in the equations.

The following quantities and their derivatives, where applicable, are assumed to be small in comparison to unity.

1. Flap and lead angles, in radians

2. Ratios to rotor radius of translational elastic displacements, and torsional displacement in radians

3. Ratios to rotor radius of chord, center of gravity, hinge offset, mass and structural radii of gyration, and elastic centroid

4. Ratio of hub linear accelerations to $\Omega^2 R$, hub angular accelerations to Ω^2

5. Ratio of gravity acceleration to $\Omega^2 R$

6. Time-dependent component of pitch angle, in radians, induced by cyclic control inputs and pitch-lag couplings.

SMALL QUANTITIES IN THE BLADE EQUATIONS

The following quantities and their derivatives, where applicable, are assumed to be small in comparison to unity.

1. Flap and lead angles, in radians
2. Ratios of translational elastic displacements to radius, and torsional displacement in radians
3. Ratios to rotor radius of chord, center of gravity, hinge offset, mass and structural radii of gyration, and elastic centroid
4. Ratio of hub linear accelerations to $\Omega^2 R$, hub angular accelerations to Ω^2
5. Ratio of gravity acceleration to $\Omega^2 R$
6. Time-dependent component of pitch angle, in radians, induced by cyclic control inputs and pitch-lag couplings.

TERMS NEGLECTED AS HIGHER ORDER TERMS IN THE BLADE EQUATIONS

The orders of approximations in the bending and torsion equations are sufficiently accurate to enable the equations to be used for teetering and articulated rotor representations. The bending equations omit second and higher order products of elastic displacements which are known to be important for hingeless rotor stability prediction, a subject which is however beyond the scope of the present study. Hingeless rotor loads prediction is adequate, however.

Listed below are products of terms neglected as higher order in the bending equilibrium and section velocity equations. Small quantities considered in these products comprise translational elastic displacements, torsional displacement, chordwise distances, flap angle, lead angle, time-dependent component of pitch angle, hinge offset, hub accelerations and angular velocities, and gravity acceleration.

a) Flatwise and edgewise bending equations

   (1) Second and higher order products of elastic displacements

   (2) Third and higher order products of small quantities

b) Torsional equation

   (1) Third and higher order products of elastic displacements

   (2) Fourth and higher order products of small quantities

c) Section velocity equations

   (1) Second and higher order products of elastic displacements

   (2) Third and higher order products of small quantities

TERMS NEGLECTED AS HIGHER ORDER TERMS IN THE BLADE EQUATIONS

a) Flatwise and edgewise bending equations

- (1) Second and higher order products of elastic displacements
- (2) Third and higher order products of small quanities

(b) Torsional equation

- (1) Third and higher order products of elastic displacement
- (2) Fourth and higher order products of small quanities

(c) Section velocity equations

- (1) Second and higher order products of elastic displacements
- (2) Third and higher order products of small quantities

ASSUMPTIONS USED TO CALCULATE UNCOUPLED NORMAL MODES OF FREE VIBRATION OF THE BLADE

The normal modes of free vibration which are used to reduce the blade equations to ordinary differential equations expressed in terms of normal mode coordinates are derived from a subset of the blade equations.

The following assumptions are utilized to calculate the normal modes of free vibration of the blade.

1. There is no mass unbalance.

2. The elastic centroidal axis coincides with the elastic axis.

3. Coriolis terms are neglected.

4. Free vibrations occur about a position of zero steady displacement.

The assumptions used to derive the normal modes of free vibration affect only the modal calculation and are made to simplify the free vibration equations. The complete blade equations account properly for the terms neglected from the free vibration equations after the modal substitutions are made (see Ref. 11). As a consequence of the assumptions, the modes are uncoupled in the sense that the components of motion are confined solely to one direction for any mode. Flatwise modes yield displacements in the flatwise direction only and no edgewise or torsion displacements occur. Edgewise and torsion modes are uncoupled in an analogous way.

ASSUMPTIONS USED TO CALCULATE UNCOUPLED NORMAL MODES OF FREE VIBRATION OF THE BLADE

The following assumptions are utilized to calculate the normal modes of free vibration of the blade.

a) **There is no mass unbalance**

b) **The centroidal axis coincides with the elastic axis**

c) **Coriolis terms are neglected**

d) **Free vibrations occur about a position of zero steady displacement.**

FLATWISE ROTOR MODES ASSUMED FOR TEETERING ROTOR REPRESENTATION

The uncoupled flatwise normal modes for a teetering rotor are shown in the sketches. The rotor modes consist of a set of pinned and cantilever modes such as those schematically illustrated. The modes for the complete teetering rotor are constructed from the modes for two articulated blades by relating the modes for one blade to the modes for the other blade in the manner portrayed in the sketches. Pinned blade modes become rotor cyclic modes, and cantilevered blade modes become rotor collective modes.

The figure introduces the notation for identifying the variables for each rotor blade. Subscripts 1 and 2 applied to the blade coordinates denote coordinates for the first and second blades, respectively. This convention is followed consistently in the subsequent text to identify blade properties and coordinates.

FLATWISE ROTOR MODES ASSUMED FOR TEETERING ROTOR REPRESENTATION

Rotor mode	Boundary condition
Cyclic	Pinned
Collective	Cantilever
Cyclic	Pinned
Collective	Cantilever

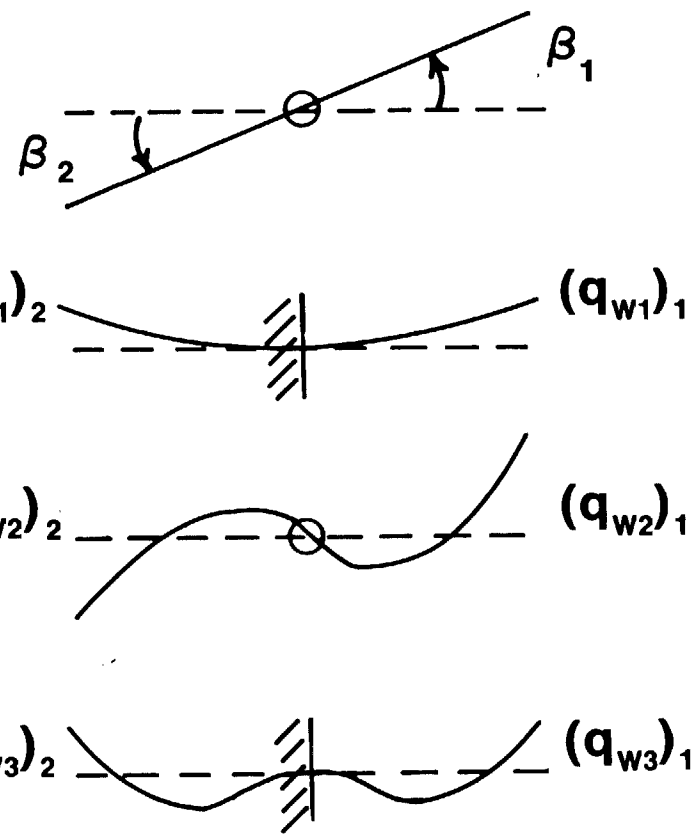

EDGEWISE ROTOR MODES ASSUMED FOR TEETERING ROTOR REPRESENTATION

A set of modes similar to that used for the uncoupled flatwise modes is used as the set of edgewise uncoupled modes, except that the lead displacement of the blade is asumed to be identically zero because the blade is cantilevered to the shaft. Consequently, the first mode, which is a pinned lead-lag mode, is not included in the set of edgewise uncoupled modes.

The selection of the edgewise modes introduces the degrees of freedom required to simulate the couplings in the rotor/airframe system. Insight into the effects of these modes is seen from the following considerations. The edgewise cyclic rotor modes couple dynamically with hub inplane translational displacements and hub pitch and roll, and do not couple with hub yaw. The edgewise collective modes couple dynamically with hub yaw, and do not couple with hub inplane translational and rotational displacements. Thus, when these two types of modes are included in the rotor mode set, couplings with both inplane translational, inplane rotational, and hub yaw motions occur, and all couplings associated with the edgewise rotor modes are accounted for.

EDGEWISE ROTOR MODES ASSUMED FOR TEETERING ROTOR REPRESENTATION

Rotor mode	Boundary condition	
Cyclic	Cantilever	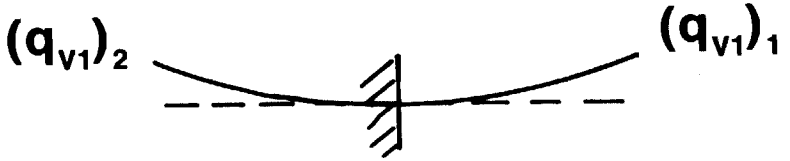
Collective	Pinned	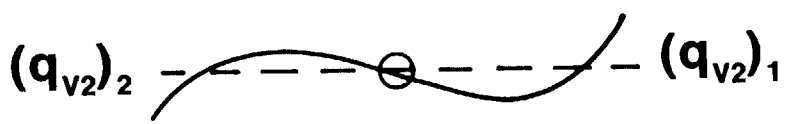
Cyclic	Cantilever	

TORSIONAL ROTOR MODES ASSUMED FOR TEETERING ROTOR REPRESENTATION

Uncoupled blade torsional modes are calculated by means of a Myklestad program for a blade restrained by a spring, representing the control system. The individual blades of the teetering rotor are assumed to be unconnected.

TORSIONAL ROTOR MODES ASSUMED FOR TEETERING ROTOR REPRESENTATION

Rotor mode	Boundary condition
Independent blade modes	Spring restrained

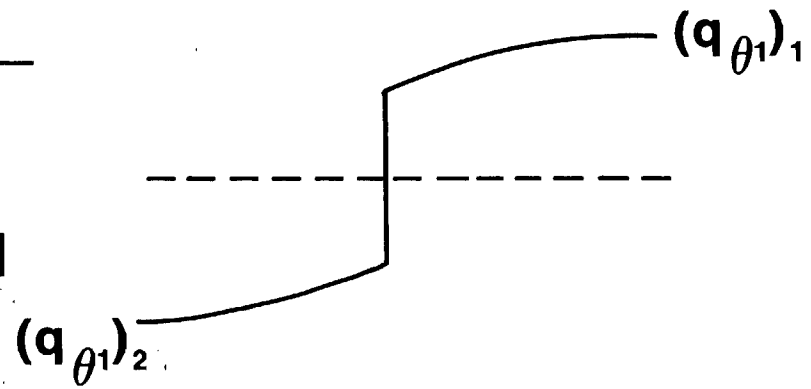

BLADE HUB DISPLACEMENTS ASSUMED

The motions of the blade are assumed to be referred to a frame fixed to the hub which is allowed to displace translationally and rotationally relative to an inertial frame. The displacements provide the blade with the degrees of freedom required to simulate arbitrary hub displacements, subject to the size restrictions listed previously, and enable the hub to be coupled to an airframe.

BLADE HUB DISPLACEMENTS ASSUMED

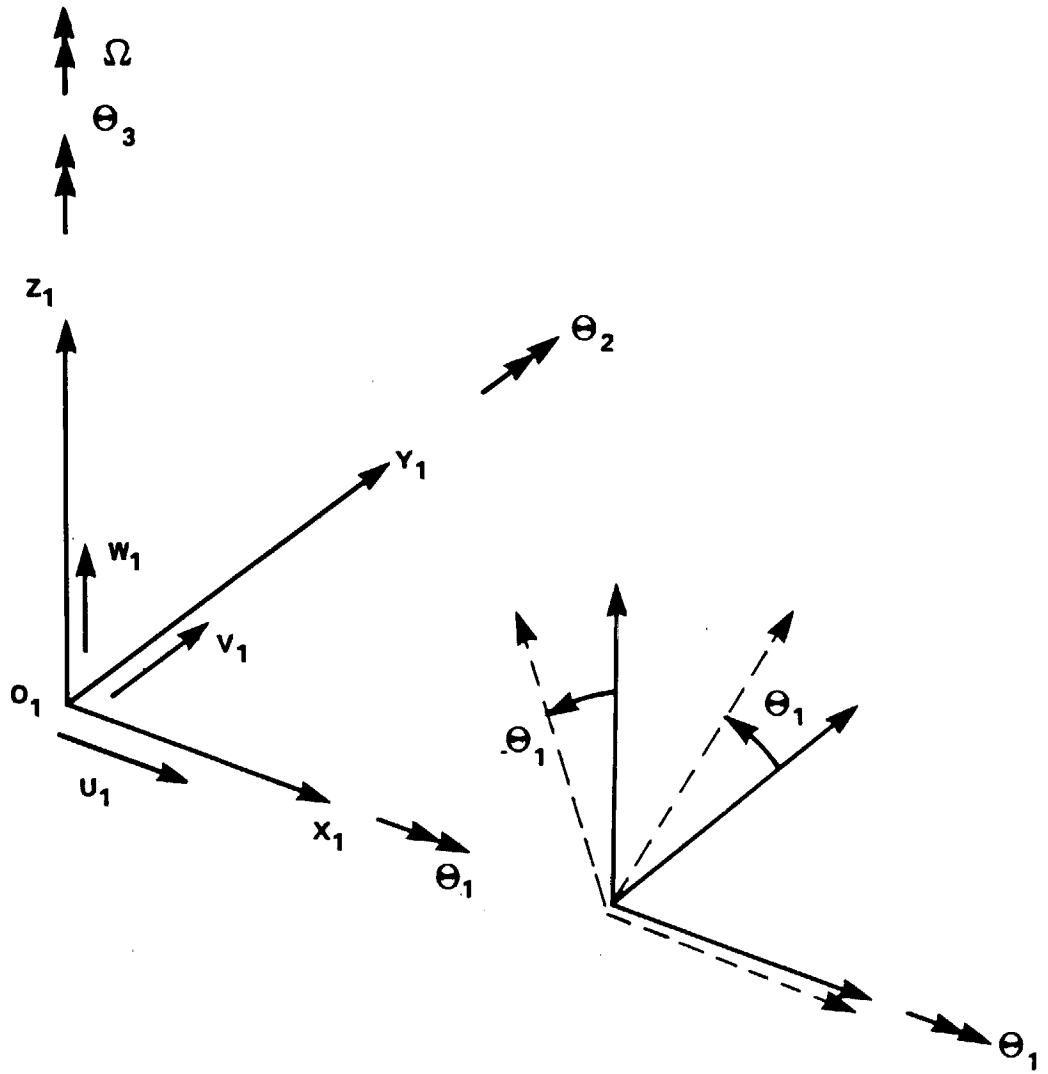

DISPLACEMENTS AND FORCES ACTING ON A CONNECTION NODE

A connection node is a point on a dynamical component, such as a blade or an airframe, which allows it to be coupled to another component. Three translational and three rotational displacements are assumed at each node. Six external loads are defined to be applied at the node, and consist of three forces (f_{x_1}, f_{y_1}, f_{z_1}) and three moments (m_{x1}, m_{y1}, m_{z1}). These loads may be induced by aerodynamic, gravitational, or steady forces (such as steady centrifugal tension) in the case of a blade, or may be zero in the case of an airframe. Reaction forces (r_{x_1}, r_{y_1}, r_{z1}) and moments (r_{mx1}, r_{my1}, r_{mz1}) are applied at the node by other components to which a component is joined. These reaction loads balance the external and inertial loads acting at the node. The condition that the sum of the reaction loads from all components connected to a node is zero and the equating of displacements at the node are used to couple components into a system. After the solution to the system equations is found, reaction loads may be calculated from the component equilibrium equations at the node.

DISPLACEMENTS AND FORCES ACTING ON A CONNECTION MODE

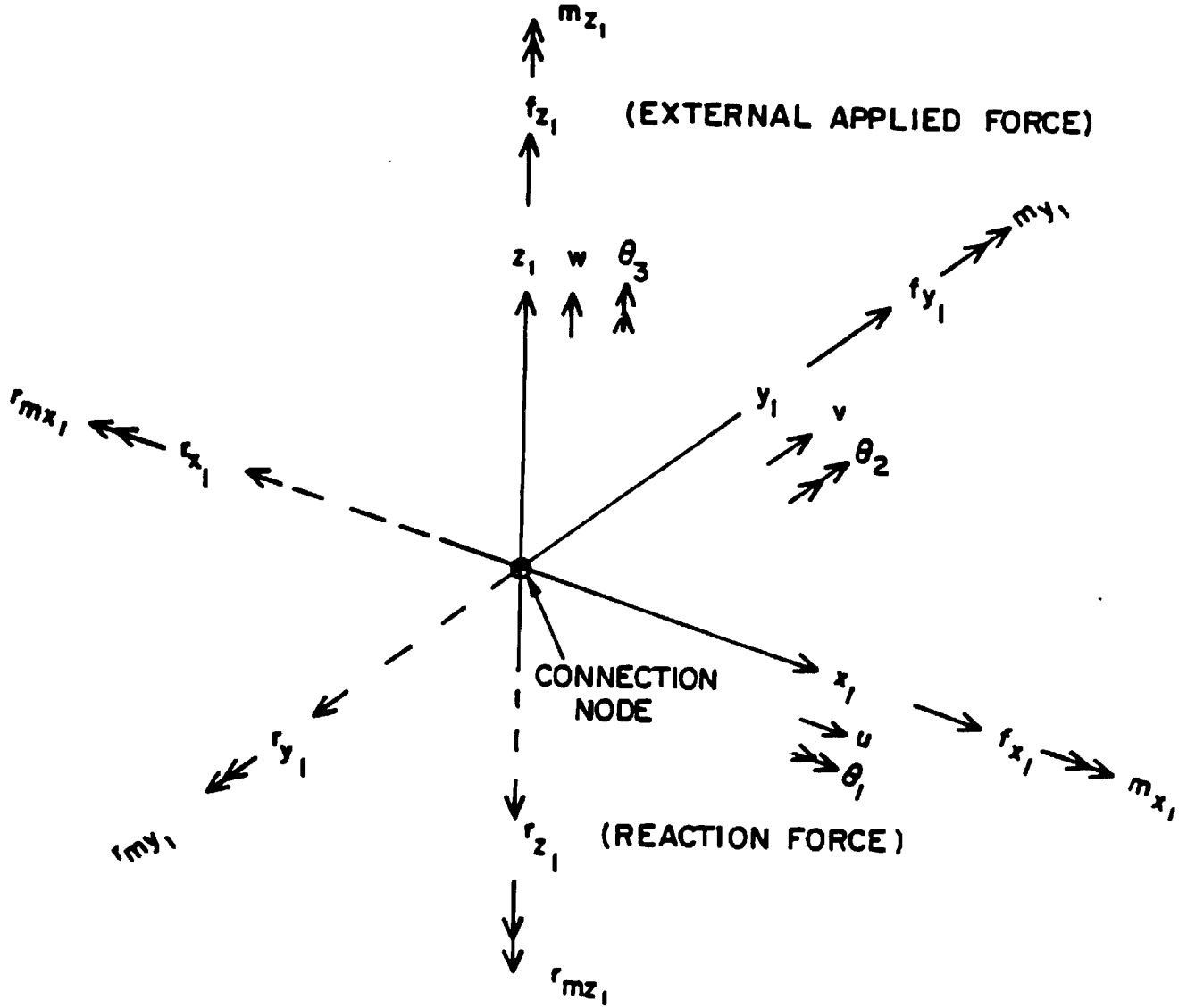

BLADE COORDINATES

Blade coordinates are defined as the first step to illustrate the process of deriving the equations of motion for the teetering rotor and the coupled rotor/airframe system. The coordinates for blade 1 consist of a set of modal coordinates, q_{B1}, and a set of hub coordinates, q_{H1}. The modal coordinates, q_{B1}, are referred to as internal coordinates, to indicate that they are not subsequently eliminated by being expressed in terms of airframe coordinates. The hub coordinates are referred to as connection node coordinates because they are subsequently expressed in terms of airframe coordinates. The entire set for blade 1 is denoted by X_{B1}. Similarly, coordinates for blade 2 are q_{B2}, q_{H2}, and X_{B2}. Symbol T denotes the transpose.

BLADE COORDINATES

$$X_B^T = X_{B1}^T \;\vdots\; X_{B2}^T$$

BLADE 1 BLADE 2

$$= \left\{ q_{B1}^T \quad q_{H1}^T \;\vdots\; q_{B2}^T \quad q_{H2}^T \right\}$$

$$q_{B1}^T = \left\{ \beta_1 \quad (q_{w1})_1 \quad (q_{w2})_1 \quad (q_{w3})_1 \quad (q_{v1})_1 \quad (q_{v2})_1 \quad (q_{v3})_1 \quad (q_{\theta 1})_1 \right\}$$

$$q_{B2}^T = \left\{ \beta_2 \quad (q_{w1})_2 \quad (q_{w2})_2 \quad (q_{w3})_2 \quad (q_{v1})_2 \quad (q_{v2})_1 \quad (q_{v3})_1 \quad (q_{\theta 1})_2 \right\}$$

$$q_{H1}^T = \left\{ u \quad v \quad w \quad \theta_1 \quad \theta_2 \quad \theta_3 \right\}_1$$

$$q_{H2}^T = \left\{ u \quad v \quad w \quad \theta_1 \quad \theta_2 \quad \theta_3 \right\}_2$$

REACTION LOADS

The sketch defines the symbols for the reaction load vectors acting on the blades on a teetering rotor. The reaction load vectors reacting blades 1 and 2 are denoted by R_{H1} and R_{H2}, respectively.

REACTION LOADS

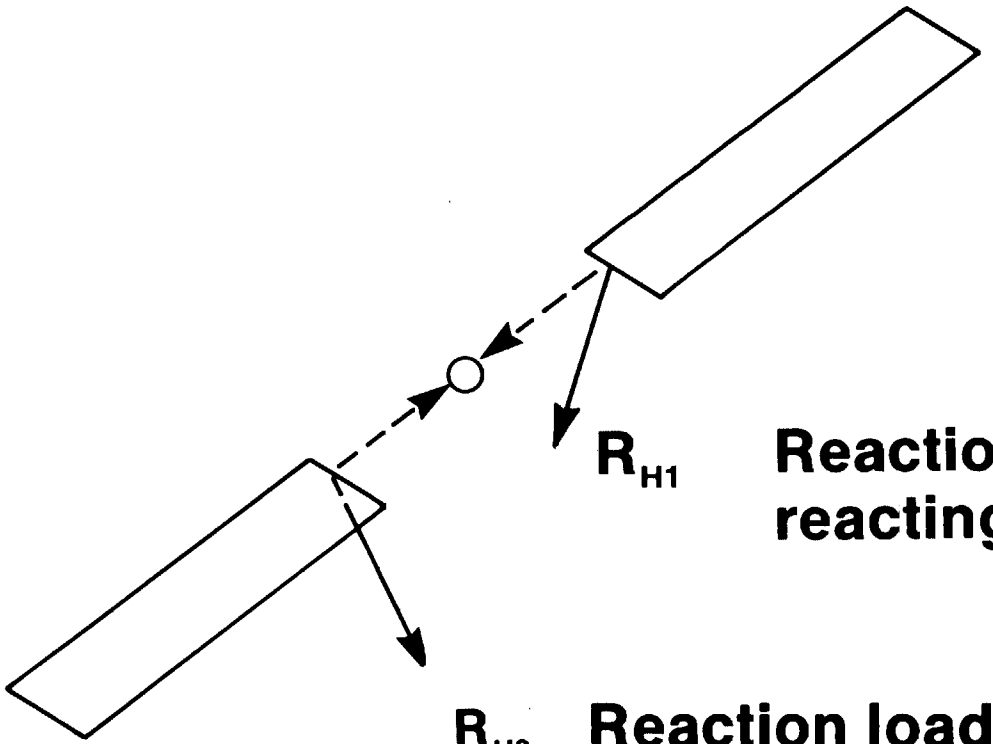

R_{H1} **Reaction load vector reacting blade 1**

R_{H2} **Reaction load vector reacting blade 2**

PARTITIONED BLADE EQUATIONS

The matrix equations for the blades of the rotor are collected into a partitioned second-order matrix differential equation, with a vector of coordinates X_B consisting of the coordinates for the separate blades. Diagonal submatrices in the mass matrix are M_{B1}, M_{H1}, M_{B2}, and M_{H2} and correspond to blade coordinates q_{B1}, q_{H1}, q_{B2}, and q_{H2}, respectively. Similar relationships hold for the damping and stiffness matrices. External aerodynamic, steady centrifugal, and gravitational generalized force vectors applied by other components to nodes at which blades 1 and 2 are connected are denoted by R_{H1} and R_{H2}. The negative signs on the reaction loads occur because these loads are defined oppositely to the applied loads.

PARTITIONED BLADE EQUATIONS

$$\begin{bmatrix} M_{B1} & (M_{12})_1 & & \\ (M_{21})_1 & M_{H1} & 0 & \\ & 0 & M_{B2} & (M_{12})_2 \\ & & (M_{21})_2 & M_{H2} \end{bmatrix} \begin{Bmatrix} \ddot{X}_B \end{Bmatrix} + \begin{bmatrix} C_{B1} & (C_{12})_1 & & \\ (C_{21})_1 & C_{H1} & 0 & \\ & 0 & C_{B2} & (C_{21})_2 \\ & & (C_{12})_2 & C_{H2} \end{bmatrix} \begin{Bmatrix} \dot{X}_B \end{Bmatrix}$$

$$\begin{bmatrix} K_{B1} & (K_{12})_1 & & \\ (K_{21})_2 & K_{H1} & 0 & \\ & 0 & K_{B2} & (K_{12})_2 \\ & & (K_{21})_2 & K_{H2} \end{bmatrix} \begin{Bmatrix} X_B \end{Bmatrix} = \begin{Bmatrix} F_{B1} \\ F_{H1} - R_{H1} \\ F_{B2} \\ F_{H2} - R_{H2} \end{Bmatrix}$$

RELATIONS BETWEEN BLADE COORDINATES FOR TEETERING ROTOR

The relationships between the internal coordinates for the blades of the teetering rotor are defined mathematically. These relationships correspond to the cyclic and collective rotor modes sketched previously. The hub displacements for the individual blades are equated to each other to make the blade displacements identical at the hub. After this is done the rotor coordinates retained to represent the teetering rotor reduce to the coordinates for the first blade, q_{B1} and q_{H1}. The relationships between coordinates may be defined by a matrix equation expressing the transformation from the rotor coordinates, q_{B1} and q_{H1}, to the blade coordinates X_B.

RELATIONS BETWEEN BLADE COORDINATES FOR TEETERING ROTOR

$$\beta_2 = -\beta_1$$

$$(q_{W1})_2 = (q_{W1})_1$$

$$(q_{W2})_2 = -(q_{W2})_1$$

$$(q_{W3})_2 = (q_{W3})_1$$

$$(q_{V1})_2 = -(q_{V1})_1$$

$$(q_{V2})_2 = (q_{V2})_1$$

$$(q_{V3})_2 = -(q_{V3})_1$$

$$q_{H2} = q_{H1} = \{u \quad v \quad w \quad \theta_1 \quad \theta_2 \quad \theta_3\}_1$$

RELATIONS BETWEEN BLADE COORDINATES FOR TEETERING ROTOR (CONT'D)

$$X_B = \begin{Bmatrix} X_{B1} \\ \hline \\ X_{B2} \end{Bmatrix} = \begin{Bmatrix} q_{B1} \\ q_{H1} \\ q_{B2} \\ q_{H2} \end{Bmatrix}$$

$$= \begin{bmatrix} I & 0 \\ 0 & I \\ \beta_2 & 0 \\ 0 & I \end{bmatrix} \times \begin{Bmatrix} q_{BI} \\ q_{HI} \end{Bmatrix} \quad ; \quad \beta_2 = \begin{bmatrix} -1 & 1 & & & 0 \\ & & -1 & 1 & \\ & & & -1 & \\ 0 & & & & 1 \\ & & & & -1 \end{bmatrix}$$

EQUATIONS FOR TEETERING ROTOR

The equation for the teetering rotor is derived from the equations for the rotor blades by expressing the blade coordinates in terms of rotor coordinates, utilizing the transformation defined previously, and premultiplying the blade equations by the transpose of the transformation matrix. The process of premultiplication corresponds to deriving the generalized process for the rotor by considering the work done by the forces of the individual blades acting through a virtual displacement of a coordinate for the rotor. The resulting equations apply to a teetering rotor and do not yet apply to the coupled rotor/airframe system. The effects of the airframe are contained in the reaction loads, R_{H1} and R_{H2}, exerted by the airframe on the rotor.

EQUATIONS FOR TEETERING ROTOR

$$\begin{bmatrix} M_{B1} + \beta_2^T M_{B2} \beta_2 , (M_{12})_1 + \beta_2^T (M_{21})_2 \\ (M_{21})_1 + (M_{21})_2 \beta_2 , M_{H1} + M_{H2} \end{bmatrix} \begin{Bmatrix} \ddot{q}_{B1} \\ \ddot{q}_{H1} \end{Bmatrix}$$

$$+ \begin{bmatrix} C_{B1} + \beta_2^T C_{B2} \beta_2 , (C_{12})_1 + \beta_2^T (C_{12})_2 \\ (C_{21})_1 + (C_{21})_2 \beta_2 , C_{H1} + C_{H2} \end{bmatrix} \begin{Bmatrix} \dot{q}_{B1} \\ \dot{q}_{H1} \end{Bmatrix}$$

$$+ \begin{bmatrix} K_{B1} + \beta_2^T K_{B2} \beta_2 , (K_{12})_1 + \beta_2^T (K_{12})_2 \\ (K_{21})_1 + (K_{21})_2 \beta_2 , K_{H1} + K_{H2} \end{bmatrix} \begin{Bmatrix} q_{B1} \\ q_{H1} \end{Bmatrix} = \begin{Bmatrix} F_{B1} + \beta_2^T F_{B2} \\ F_{H1} - R_{H1} + F_{H2} - R_{H2} \end{Bmatrix}$$

5. FUSELAGE REPRESENTATION

EQUATIONS FOR AIRFRAME

A normal mode representation of the airframe is used. Modal properties are calculated from a finite element model of the airframe, as represented in the NASTRAN computer program. Mass (M_q) and stiffness (K_q) matrices are calculated for the free vibration modes of the airframe and are therefore diagonal for the modal coordinates. A stiffness matrix element is proportional to the frequency squared ω_q^2, of the mode, multiplied by the generalized mass element of the mode, M_q. The elements of the diagonal modal damping matrix are $2\zeta\ \omega_q\ M_q$, where ζ is the damping ratio. The elements of the modal matrix ϕ are defined at the point of application of the reaction loads at the hub of the rotor. These reaction loads R_H are the only loads assumed to be applied to the airframe. The generalized forces exciting the mode are $\phi^T\ R_H$. The number of modes assumed is M and the dimensions of any of the matrices from among mass, or stiffness matrices is M x M, and of the modal matrix, ϕ, is 6 x M.

EQUATIONS FOR AIRFRAME

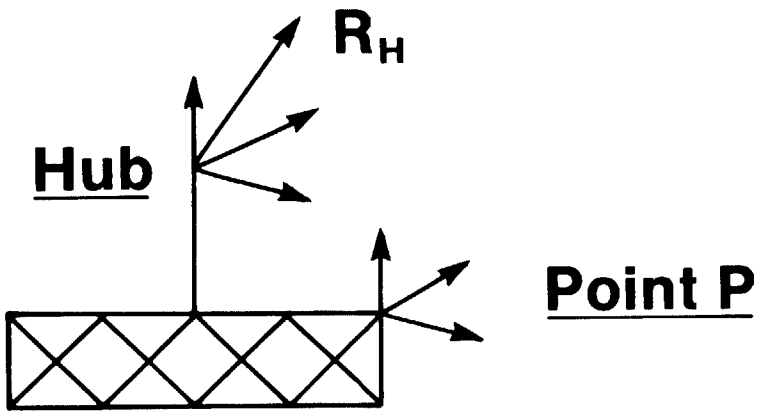

$$M_q \ddot{q} + C_q \dot{q} + K_q q = \phi^T R_H$$

$q^T = q_1 \; q_2 \; q_3 \cdots q_M$, M = Number of Airframe modes

6. SYSTEM EQUATIONS

PARTITIONED EQUATIONS FOR ROTOR AND AIRFRAME

The matrix equation for the teetering rotor derived previously and the normal mode equation for the airframe are collected into a partitioned second-order matrix differential equation with a vector of coordinates consisting of rotor coordinates, q_{B1}, and q_{H1}, and airframe coordinates, q. This step is made in anticipation of the derivation of the equations for the coupled system. At this point, the equations are fewer in number than the number of unknowns, which include the reactions among the variables, and cannot be solved to obtain the system response. These equations are also described as the dependent rotor and airframe equations.

PARTITIONED EQUATIONS FOR ROTOR AND AIRFRAME

$$\left[\begin{array}{cc|c} M_{B1} + \beta_2^T M_{B2} \beta_2 & (M_{12})_1 + \beta_2^T (M_{12})_2 & 0 \\ (M_{21})_1 + (M_{21})_2 \beta_2 & M_{H1} + M_{H2} & 0 \\ \hline 0 & 0 & M_q \end{array}\right] \left\{\begin{array}{c} \ddot{q}_{B1} \\ \ddot{q}_{H1} \\ \hline \ddot{q} \end{array}\right\}$$

$$\left[\begin{array}{cc|c} C_{B1} + \beta_2^T C_{B2} \beta_2 & (C_{12})_1 + \beta_2^T (C_{12})_2 & 0 \\ (C_{21})_1 + (C_{21})_2 \beta_2 & C_{H1} + C_{H2} & 0 \\ \hline 0 & 0 & C_q \end{array}\right] \left\{\begin{array}{c} \dot{q}_{B1} \\ \dot{q}_{H1} \\ \hline \dot{q} \end{array}\right\}$$

$$\left[\begin{array}{cc|c} K_{B1} + \beta_2^T K_{B1} \beta_2 & (K_{12})_1 + \beta_2^T (K_{12})_2 & 0 \\ (K_{21})_1 + (K_{21})_2 \beta_2 & K_{H1} + K_{H2} & 0 \\ \hline 0 & 0 & K_q \end{array}\right] \left\{\begin{array}{c} q_{B1} \\ q_{H1} \\ \hline q \end{array}\right\} = \left\{\begin{array}{c} F_{B1} + \beta_2^T F_{B2} \\ \hline F_{H1} - R_{H1} + F_{H2} - R_{H2} \\ \hline \phi^T R_H \end{array}\right\}$$

RELATIONS BETWEEN HUB DISPLACEMENTS AND AIRFRAME MODES

The determination of the frequencies and mode shapes of the normal modes in NASTRAN enables the physical displacements at the rotor hub attachment to the airframe to be expressed as summations of products of mode shapes and modal amplitudes. The expressions for each displacement are defined in the figure. The relationship between physical displacements at the hub and modal coordinates is contracted into the matrix equation shown, with ϕ representing the 6 x M modal matrix.

RELATIONS BETWEEN HUB DISPLACEMENTS AND AIRFRAME MODES

$$u = (\phi_{x1})_i \, q_i \quad \text{(SUM ON REPEATED SUFFIX)}$$

$$v = (\phi_{y1})_i \, q_i$$

$$w = (\phi_{z1})_i \, q_i$$

$$\theta_1 = (\phi_{\theta 1})_i \, q_i$$

$$\theta_2 = (\phi_{\theta 2})_i \, q_i$$

$$\theta_3 = (\phi_{\theta 3})_i \, q_i$$

$$q_{H1} = \phi \, q$$

RELATIONS BETWEEN COORDINATES FOR ROTOR AND AIRFRAME AND INDEPENDENT COORDINATES

The relations between the coordinates for the rotor and airframe and the independent coordinates for the coupled system, consisting of rotor internal coordinates and airframe modes only, is expressed as a matrix equation. The submatrices in the transformation matrix are the identity matrix I with the same dimensions as the vector q_{Bl}, and the 6 x M modal matrix ϕ. The transformation equation is derived by utilizing the relations between the hub displacements and airframe modes discussed previously.

RELATIONS BETWEEN COORDINATES FOR ROTOR AND AIRFRAME AND INDEPENDENT COORDINATES

$$\begin{Bmatrix} q_{B1} \\ q_{H1} \\ q \end{Bmatrix} = \begin{bmatrix} I & O \\ O & \phi \\ O & I \end{bmatrix} \times \begin{Bmatrix} q_{B1} \\ q \end{Bmatrix}$$

EQUATIONS FOR THE COUPLED ROTOR/AIRFRAME SYSTEM

The independent equation for the coupled rotor and airframe is derived from the dependent equations for rotor and airframe by expressing rotor and airframe coordinates in terms of independent coordinates, utilizing the transformation defined previously, and premultiplying the dependent equations by the transformation matrix. At this point the condition is used that the sum of the reactions at the hub introduced by the teetering rotor and airframe is zero, and this condition eliminates these variables. The data and approach used to define the aerodynamic generalized force acting on the rotor equations and exemplified by F_{B1}, + β_2^T F_{B2} are discussed in a later section. A similar approach is used to define the generalized force F_{H1} + β_2 F_{H2}. As a result of these steps, the number of equations is equal to the number of unknowns and the equations may be solved for the response of the coupled system.

EQUATIONS FOR COUPLED ROTOR/AIRFRAME SYSTEM

$$\begin{bmatrix} M_{B1} + \beta_2^T M_{B2} \beta_2 & , ((M_{12})_1 + \beta_2^T (M_{12})_2)\phi \\ \phi^T((M_{21})_1 + (M_{21})_2\beta_2) & , \phi^T(M_{H1} + M_{H2})\phi + M_q \end{bmatrix} \begin{Bmatrix} \ddot{q}_{B1} \\ \ddot{q} \end{Bmatrix}$$

$$+ \begin{bmatrix} C_{B1} + \beta_2^T C_{B2} \beta_2 & , ((C_{12})_1 + \beta_2^T (C_{12})_2)\phi \\ \phi^T((C_{21})_1 + (C_{21})_2\beta_2 & , \phi^T(C_{H1} + C_{H2})\phi + C_q \end{bmatrix} \begin{Bmatrix} \dot{q}_{B1} \\ \dot{q} \end{Bmatrix}$$

$$+ \begin{bmatrix} K_{B1} + \beta_2^T K_{B2} \beta_2 & , ((K_{12})_1 + \beta_2^T (K_{12})_2)\phi \\ \phi^T((K_{21})_1 + (K_{21})_2\beta_2) & , \phi^T(K_{B1} + K_{B2})\phi + K_q \end{bmatrix} \begin{Bmatrix} q_{B1} \\ q \end{Bmatrix} = \begin{Bmatrix} F_{B1} + \beta_2^T F_{B_2} \\ \phi^T(F_{H1} + F_{H2}) \end{Bmatrix}$$

HUB REACTIONS SUM TO ZERO

$$-\phi^T (R_{H1} + R_{H2}) + \phi^T R_H = 0$$

7. SOLUTION TO SYSTEM EQUATIONS

TIME HISTORY SOLUTION

The second order matrix differential equation of motion for the coupled system, expressed in terms of independent coordinates, is solved by means of the Newmark-Beta method (Ref. 12). The implementation of the method is described in Ref. 5). First and second time derivatives of the vectors of coordinates are expressed as functions of the displacements of the system at successive time intervals. The variation of acceleration within the time step is controlled by the user by specifying the value of the Newmark-Beta factor. A value of 1/4 for the factor corresponds to assuming a constant acceleration during the interval, and 1/6 corresponds to a linear variation. A value of zero yields formulas which are similar to the formulas in a second order finite difference method. (A value of 1/4 was used in the applications made to the teetering rotor). The resulting formulas express the magnitudes of the coordinates at previous times, and are a function of the mass, damping, and stiffness properties, and the forces acting on the system. After a solution is calculated, the value of time is increased and the calculations are repeated until a steady vibratory state is reached. The results, consisting of airframe vibrations, rotor hub loads, and blade bending moments, are then harmonically analyzed.

TIME HISTORY SOLUTION

- **System equation**

$$M\ddot{X} + C\dot{X} + KX = F$$

- **Newmark - Beta method**
  - Obtains solution to system equation by a time-marching procedure
  - Recursion formula relates displacement vector at a current time to previous displacements and forces

8. AERODYNAMIC LOADS

DEFINITIONS OF AERODYNAMIC SECTION VARIABLES

Variables are defined which are required for the calculation of the aerodynamic lift, drag, and moment coefficients acting on each section of the rotor blade. The angle of attack α consists of the local pitch angle θ, and a component ϕ arising from the motion of the blade and the rotor induced inflow. The angle ϕ is = $\tan^{-1}$ (U_P/U_T), wher U_P and U_T are components of relative airflow velocity perpendicular to the plane of rotation and lying in the plane of rotation, respectively. The local Mach number is $M = U/a_\infty$ where a_∞ is the speed of sound in the undisturbed flow.

DEFINITIONS OF AERODYNAMIC SECTION VARIABLES

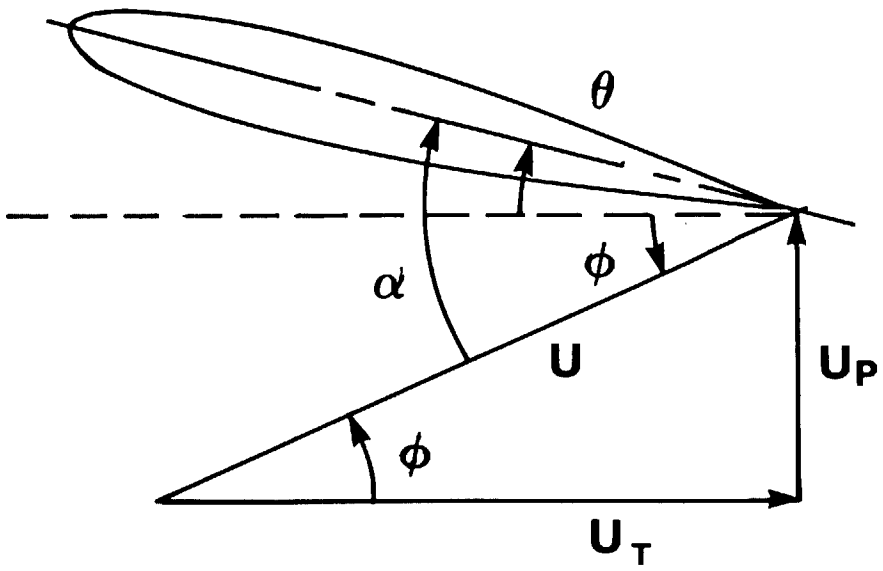

BLADE ELEMENT THEORY YIELDS AERODYNAMIC COEFFICIENTS

Blade element theory assumes that the flow affecting each section of the blade is two dimensional. A quasi-steady assumption is made in RDYNE which assumes that airfoil coefficients are calculated from steady-state data and are functions only of the instantaneous angle of attack and Mach number. Airfoil coefficients do not depend on variables of unsteady motion. The only unsteady affect included is a pitch damping term of noncirculatory origin derived from linear incompressible flow theory.

As a result of these assumptions, aerodynamic coefficients may be derived from tables which express aerodynamic coefficients as functions of section angle of attack and Mach number. Blade element theory enables real airfoil behavior to be modeled through the use of the test data and thereby accounts for viscous, transonic, and stall phenomena.

The relative airflow velocity components are determined from kinematic relations which relate U_P and U_T to the blade coordinate values and their time derivatives, and the rotor induced inflow. The relative airflow angle ϕ and the section angle of attack α are calculated from U_P and U_T. The section angle of attack is consequently a function of the coupled system response because blade responses are functions of system responses. The mathematical expressions for the functional dependencies between coordinate systems are the transformations between the blade and system coordinates. The Mach number is also a function of system coordinate values and their time derivatives.

BLADE ELEMENT THEORY YIELDS AERODYNAMIC COEFFICIENTS

$\alpha\ (q_{B1}, \dot{q}_{B1}, q_{H1}, \dot{q}_{H1})$

$M\ (q_{B1}, \dot{q}_{B1}, q_{H1}, \dot{q}_{H1})$

Blade responses from previous time step

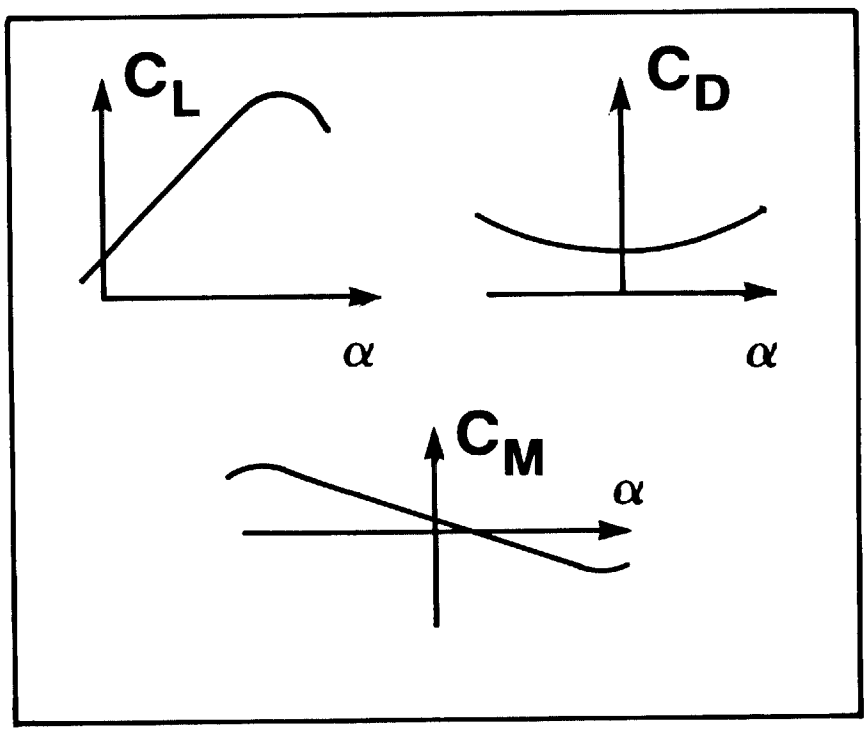

C_L C_D C_M

GENERALIZED AERODYNAMIC FORCES APPLIED TO TEETERING ROTOR

After the values of the aerodynamic coefficients are determined, generalized aerodynamic forces affecting the teetering rotor may be calculated. The formulas for these forces are derived from the work done on the teetering rotor by the aerodynamic loads acting through a virtual displacement of a coordinate. The figure depicts the elements in the vector of generalized aerodynamic forces affecting the equations for the blade coordinates. Subscripts 1 and 2 refer to blades 1 and 2, respectively. New variables introduced are ρ = density, c = chord, r = radial distance along the blade from the center of rotation, c_ϕ = $\cos\phi$, and s_ϕ = $\sin\phi$.

GENERALIZED AERODYNAMIC FORCES APPLIED TO TEETERING ROTOR

$$F_{B1} + \beta_2^T F_{B2} = \int_0^R \frac{1}{2} \rho c r \left[U_1^2 \left(C_L C_\phi + C_D S_\phi \right)_1 - U_2^2 \left(C_L C_\phi + C_D S_\phi \right)_2 \right] dr$$

$$+ \int_0^R \frac{1}{2} \rho c \gamma_{w1} \left[U_1^2 \left(C_L C_\phi + C_D S_\phi \right)_1 + U_2^2 \left(C_L C_\phi + C_D S_\phi \right)_2 \right] dr$$

$$+ \int_0^R \frac{1}{2} \rho c \gamma_{v1} \left[U_1^2 \left(C_L S_\phi - C_D C_\phi \right)_1 - U_2^2 \left(C_L S_\phi - C_D C_\phi \right)_2 \right] dr$$

SEQUENCE OF CALCULATIONS FOR AERODYNAMIC LOADS

Section angle of attack and Mach number are calculated from blade responses at previous time steps. Blade responses are derived from coupled system responses by application of the transformations between component responses and coupled system responses identified previously. The relative airflow angle ϕ includes the effects of the motions of the coupled rotor and airframe and the contribution of rotor induced inflow. Inflow is calculated from a momentum theory based uniform inflow analysis which derives inflow from rotor thrust, or from a prescribed wake variable inflow analysis. When variable inflow is calculated, there is an iteration between blade responses and the calculation of inflow until the values of inflow and blade circulation are consistent in both processes. The variable inflow field is based on equation of aerodynamic influence coefficients which relates radial and azimuthal distributions of blade circulations and inflow in the plane of rotation. The influence coefficient matrix is a function of advance ratio.

Generalized aerodynamic forces are calculated from the section aerodynamic coefficients and the formulas for generalized forces defined previously. After these forces are calculated, the value of time is incremented, the coupled system response is calculated, and the sequence of calculations described above is repeated.

SEQUENCE OF CALCULATIONS FOR AERODYNAMIC LOADS

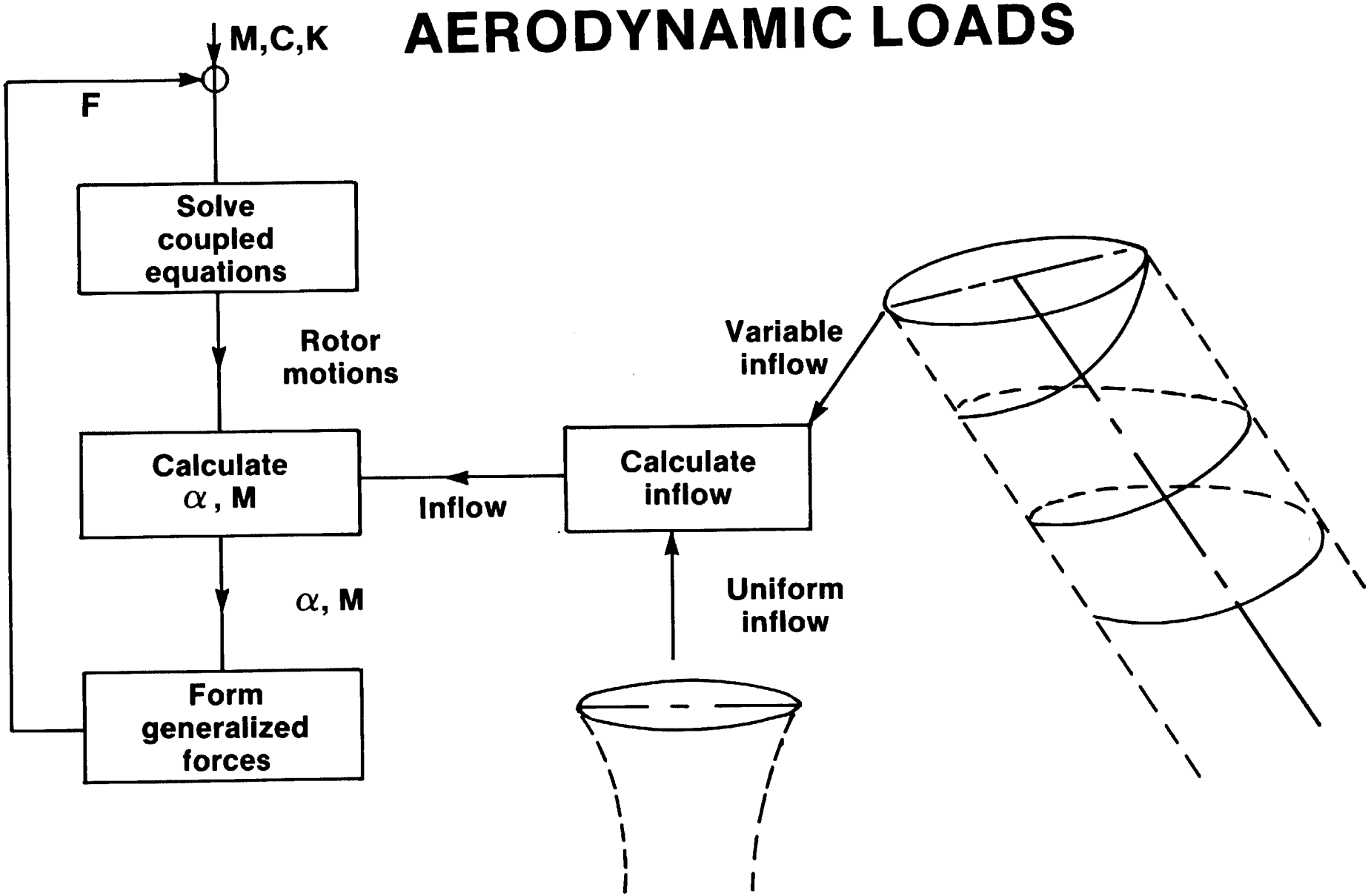

9. RECOVERY OF RESPONSES

TRANSFORMATION TO COMPONENT RESPONSES

Blade responses are required to define section angle of attack and Mach number and generalized forces affecting the rotor airframe, as well as bending moments in the blades. Airframe responses include the vibrations in the airframe. Responses for these components are derived from the responses for the coordinates used in the system equations of motion by successively applying transformations between coordinate systems. The figure shows the transformation for the teetering rotor which is derived by successive multiplication of transformations first from blade to rotor coordinates, and second from dependent to independent coordinates for rotor and airframe. The same transformation applies to first and second derivatives of the coordinates with respect to time. The transformation does not show the effects of rotations through Euler angles that one component may have relative to another in RDYNE. These effects are accounted for by multiplying the coordinate transformations described above by matrices of direction cosines defining the transformations through Euler angles.

TRANSFORMATION TO COMPONENT RESPONSES

$$\begin{Bmatrix} q_{B1} \\ q_{H1} \\ q_{B2} \\ q_{H2} \\ q \end{Bmatrix} = \begin{bmatrix} I & O \\ O & \phi \\ \beta_2 & O \\ O & \phi \\ O & I \end{bmatrix} \begin{Bmatrix} q_{B1} \\ q \end{Bmatrix}$$

BLADE BENDING MOMENTS ARE DERIVED FROM INTERNAL MOMENT EXPRESSIONS

Bending moments in the blade are calculated by application of the formulas for the elastic bending and torsion moments internal to the beam which react the externally applied moments. These moments are calculated from the radial derivatives of mode shapes derived from the Myklestad calculation, denoted by primed variables, and the known amplitudes of the coordinates for bending and torsion. The double subscript convention is used and indicates summation on the number of modes. Symbol θ is the local pitch angle resulting from built-in twist and control inputs. Symbol θ_e denotes a torsional displacement. The other symbols follow standard convention, with F and E denoting flatwise and edgewise bending, respectively.

BLADE BENDING MOMENTS ARE DERIVED FROM INTERNAL MOMENT EXPRESSIONS

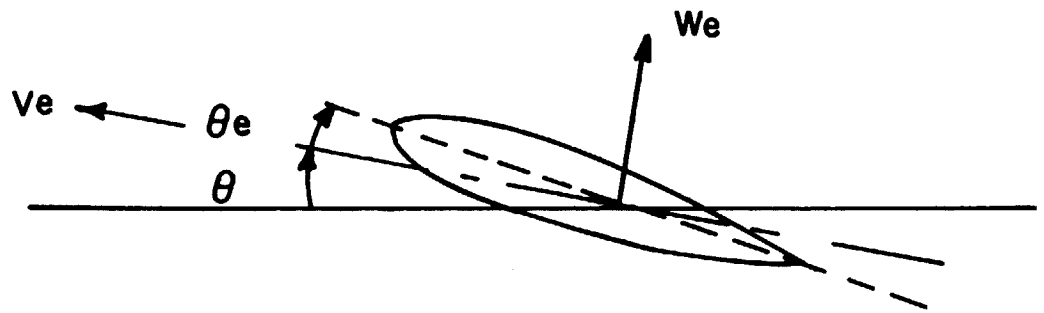

$$M_F = E\,I_F\,W_e'' = E\,I_F\,\gamma_{W_i}''\,q_{W_i}$$

$$M_E = E\,I_E\,V_e'' = E\,I_E\,\gamma_{V_j}''\,q_{V_j}$$

$$M\theta_e = G\,J\,\theta_e' = G\,J\,\gamma_{\theta_K}'\,q_K$$

RECOVERY OF HUB REACTION LOADS

Reaction loads exerted on a blade may be recovered from the equation of equilibrium for the blade component defined previously, after component responses are recovered from coupled system responses. The hub loads are calculated from a formula which explicitly accounts for loads which are externally applied, in contrast to the blade bending moment calculation which depends on internal moment expressions. The hub loads for each blade are referred to the nonrotating $x_1 y_1 z_1$ axes illustrated previously, which are fixed in the aircraft. The equation yields the reaction loads exerted on blade 1 by blade 2 and the airframe. Reaction loads exerted by the airframe on the rotor are calculated by summing the reaction loads for blades 1 and 2.

RECOVERY OF HUB REACTION LOADS

$$R_{HI} = F_{HI} - (M_{2I})_I \ddot{q}_{BI} - (M_{HI}) \ddot{q}_{HI}$$

$$- (C_{2I})_I \dot{q}_{BI} - (C_{HI}) \dot{q}_{HI}$$

$$- (K_{2I})_I q_{BI} - (K_{HI})_I q_{HI}$$

RECOVERY OF AIRFRAME VIBRATIONS FOR COUPLED ROTOR/AIRFRAME SYSTEM

Airframe vibrations are the final product of the application of the theory. A component of vibration is calculated by multiplying the mode shape at a point in the airframe by the modal acceleration, and forming the sum of such products for all airframe modes. Airframe accelerations are derived from coupled system vibrations by application of the transformation relating accelerations for the airframe to independent coordinates for the rotor and airframe system.

RECOVERY OF AIRFRAME VIBRATIONS FOR COUPLED ROTOR/AIRFRAME SYSTEM

$$\ddot{u}_p = (\phi_{xp})_i \ddot{q}_i$$
$$\ddot{v}_p = (\phi_{yp})_i \ddot{q}_i$$
$$\ddot{w}_p = (\phi_{zp})_i \ddot{q}_i$$

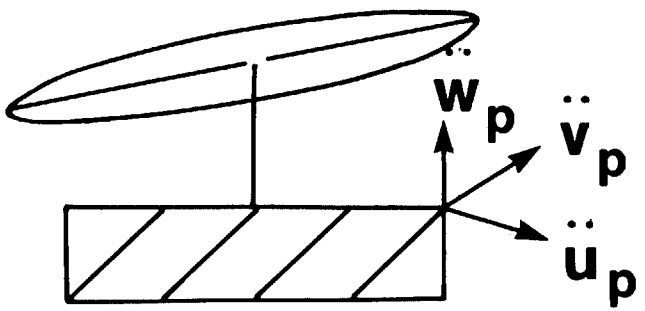

Point P

10. MODELING OF COMPONENTS

AH-1G HELICOPTER

The AH-1G uses a Model 540 two-bladed wide-chord "door hinge" 44 ft diameter main rotor rotor system similar to that of the UH-1C. The interchangeable blades are built up of extruded aluminum spars and laminates. The tail rotor is a two-bladed all-metal flex beam tractor tail rotor located on the starboard side and is of honeycomb construction. The main rotor rpm is 324 (5.4 Hz). The 44½ ft long AH-1G fuselage is a conventional all metal semimonocoque structure with low silhouette and narrow profile. The small mid-mounted stub wings carry armament and off-load the rotor in flight. The landing gear is a nonretractable tubular skid type gear.

The AH-1G maximum takeoff and landing weight is 9500 lb. The never exceed speed is 190 knots while the maximum level speed at sea level is 149 knots.

AH-1G HELICOPTER

EXPLODED VIEW

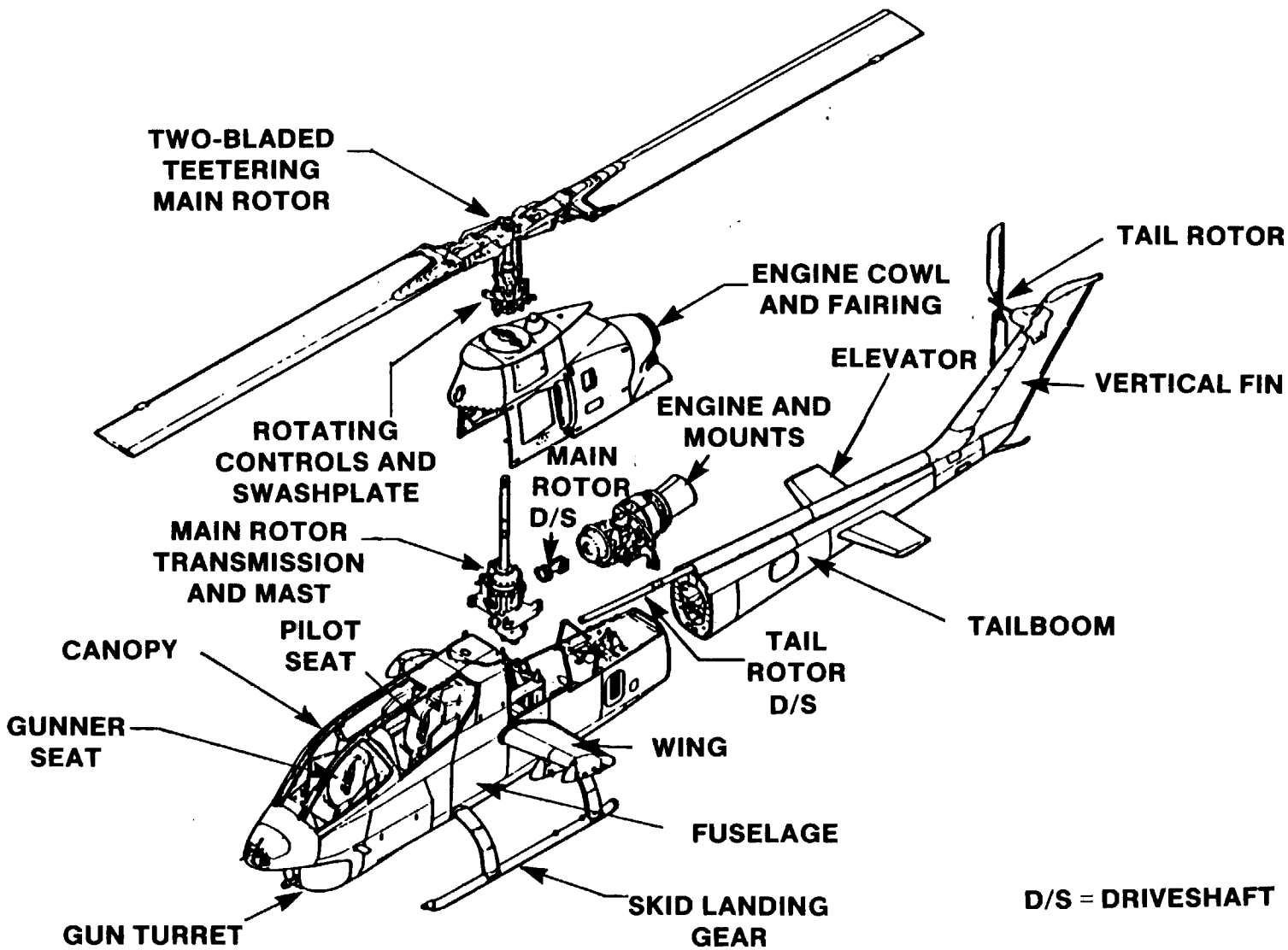

10.1 ROTOR MODEL

AH-1G OLS ROTOR SYSTEM CHARACTERISTICS

The AH-1G rotor system developed by Bell Helicopter Textron is a 540 main rotor modified for the instrumentation system for the operational loads survey. The modifications alter the blade physical characteristics as shown in this figure. The notable changes include a longer chord and shifted aerodynamic reference center.

AH-1G OLS ROTOR SYSTEM CHARACTERISTICS

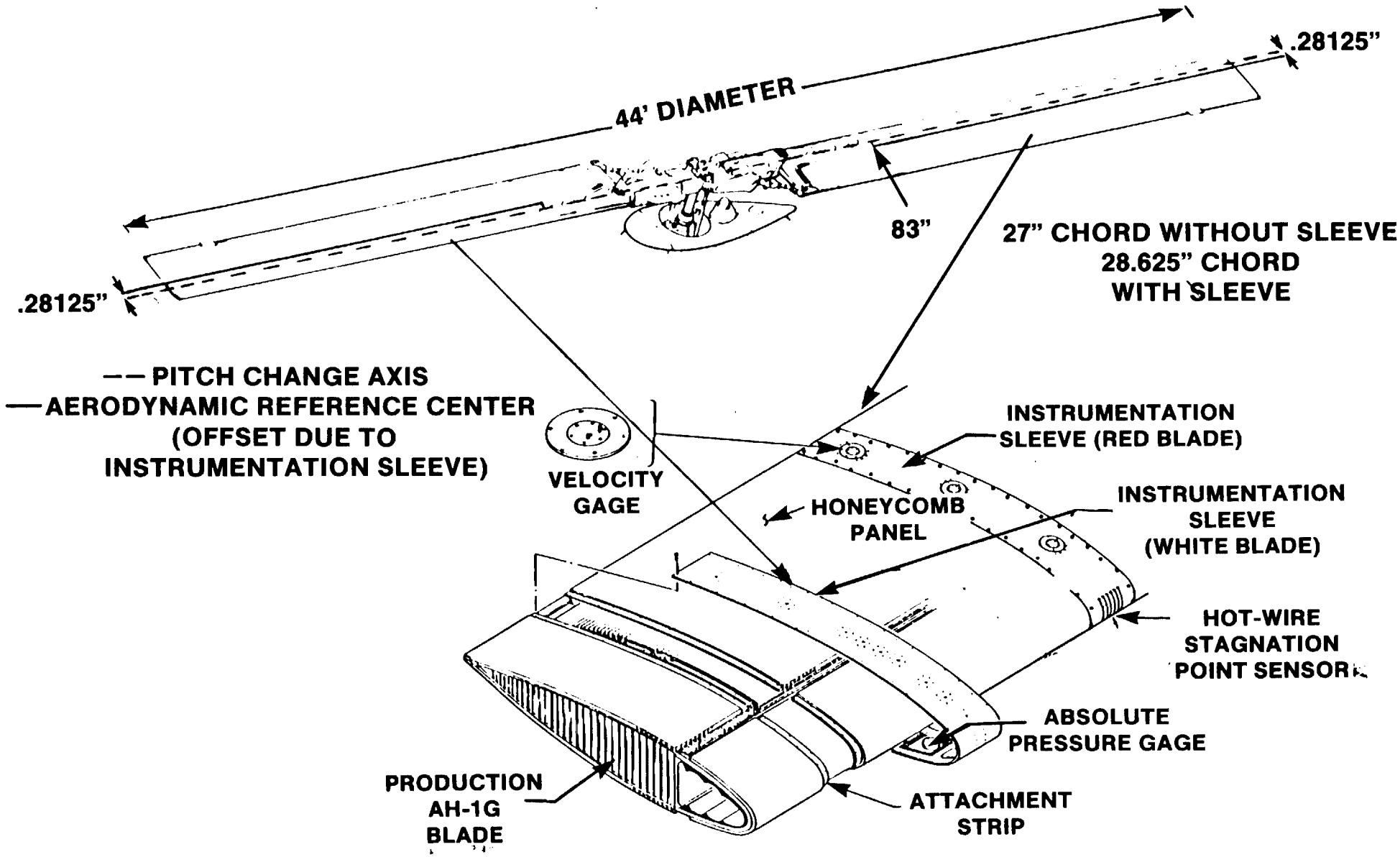

AH-1G ROTOR HUB PARAMETERS

The AH-1G utilizes a teetering rotor system. A precone angle of 2.75° is built in with an undersling of 4.5 inches. This may be seen in the following figure. The rotor has zero pitch-flap and pitch-lag coupling.

AH-1G OLS ROTOR HUB PARAMETERS

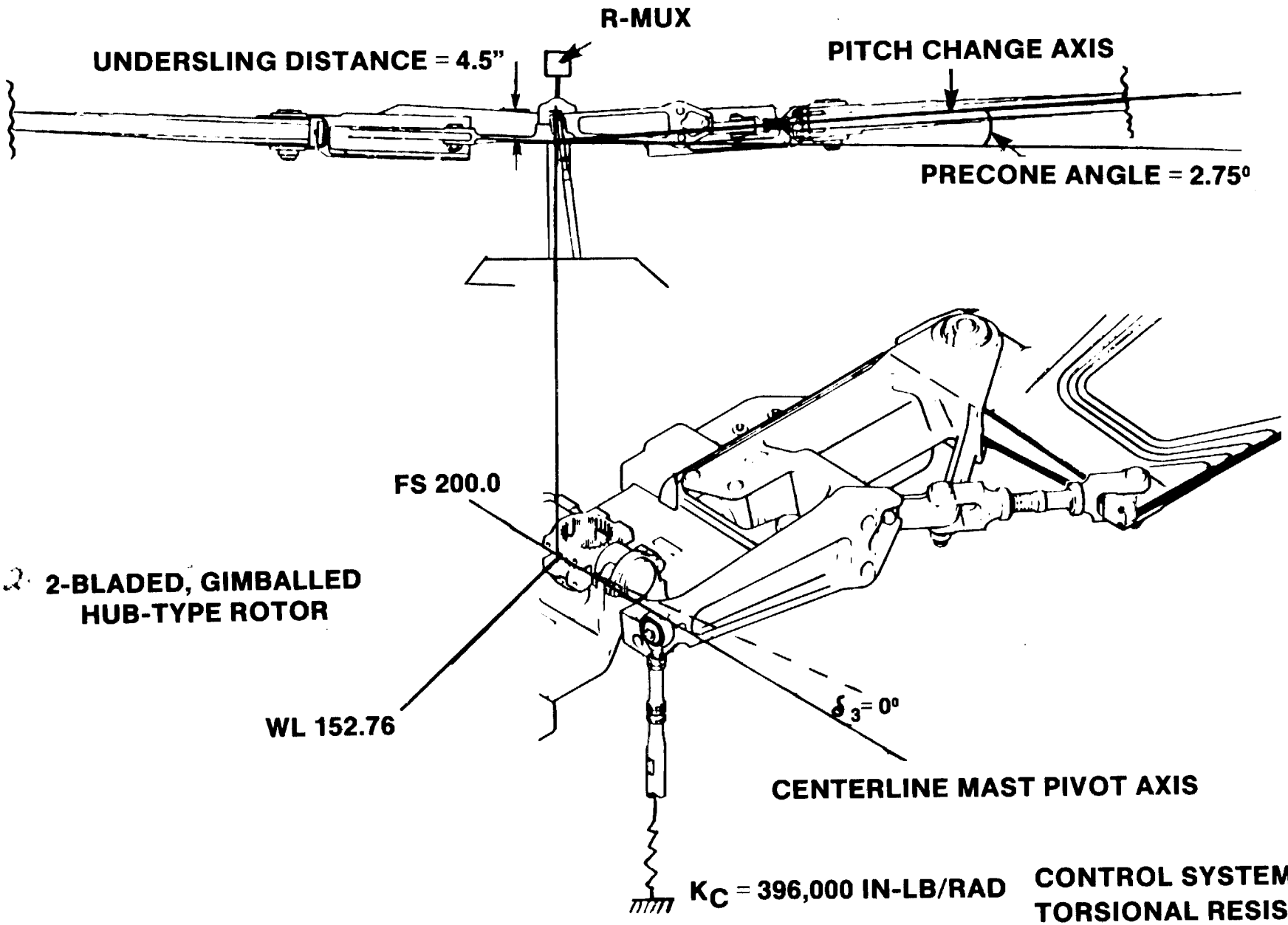

AH-1G MAIN ROTOR HUB GEOMETRY

A detailed main rotor hub geometry is shown in the following figure. Station numbers are provided to illustrate hub dimensions and location of characteristic components. Locations of pitch links, teetering axis, and feathering axis are shown. The pitch link moment arm is also illustrated in the figure.

AH-1G OLS MAIN ROTOR HUB GEOMETRY

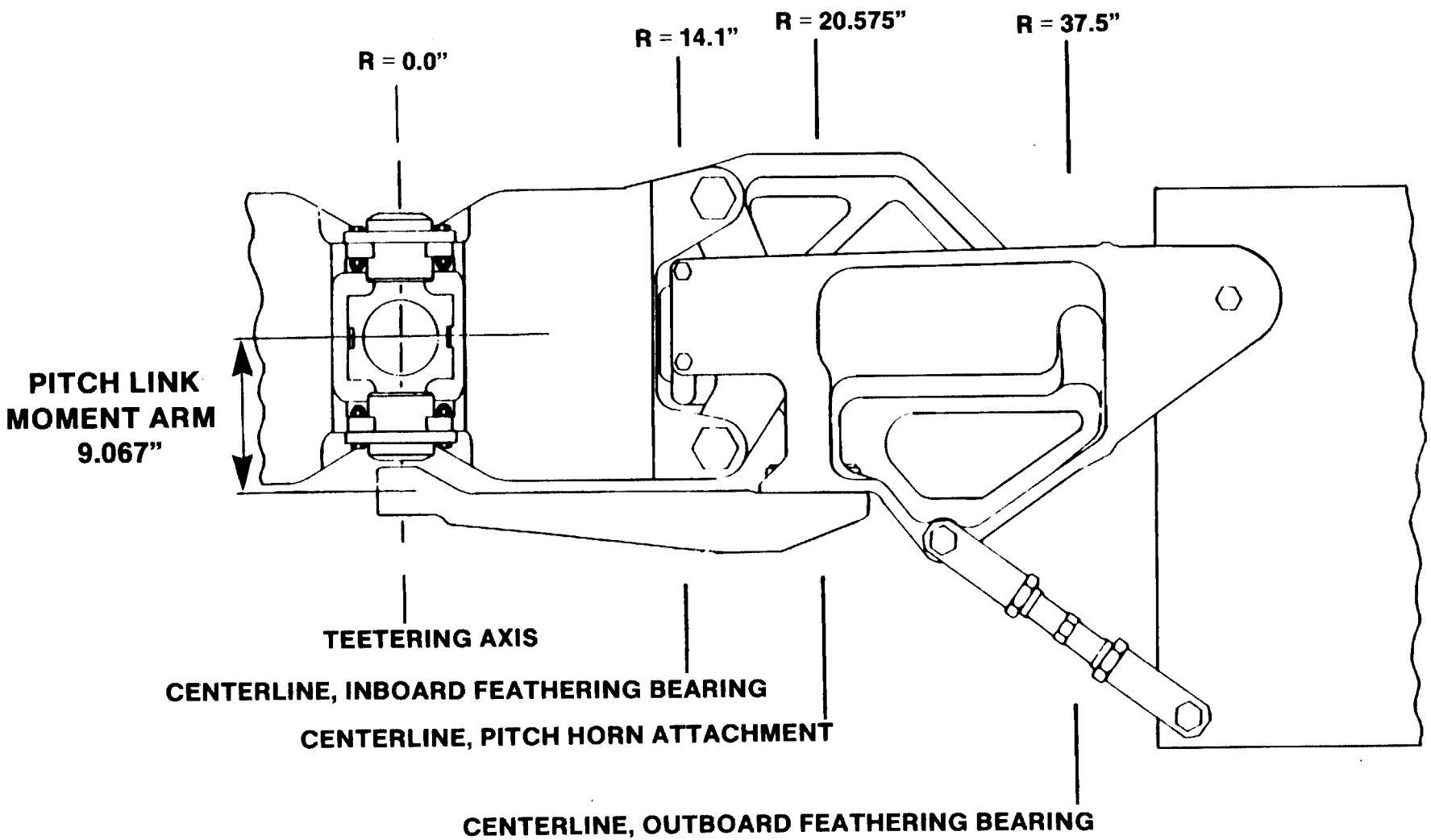

ROTOR COMPONENT MODES - FLATWISE

The basic geometric stiffness and mass characteristics of the rotor were furnished by Bell Helicopter in Reference 4. These included radial distributions of mass and flatwise and chordwise EI, GJ, and chordwise radius of gyration. These values were input into a Myklestad-analysis program which calculates the natural frequencies and mode shapes of a single rotating blade, assuming uncoupled bending and torsion motions.

Blade modes are calculated for two different root boundary conditions, cantilevered and pin-ended. These were converted, in RDYNE, into symmetric and antisymmetric modes, respectively, to represent the complete 2-bladed rotor. These rotor modes were then used as rotor component-mode degrees of freedom in the coupled rotor/fuselage RDYNE analyses.

In the flatwise direction, the blade pinned modes become rotor cyclic modes and the blade cantilever modes become rotor collective modes in the coupled analyses.

This figure shows the flatwise blade (rotor) modes which were kept as degrees of freedom in the coupled analyses.

ROTOR COMPONENT MODES - FLATWISE

MODE NO.	NATURAL FREQUENCY		BLADE MODE		CORRESPONDING ROTOR MODE	
	Hz	PER REV	ROOT BOUNDARY CONDITION	MODE SHAPE	MODE TYPE	MODE SHAPE
1	5.400	1.000	PINNED		CYCLIC	
2	5.642	1.045	CANTILEVERED		COLLECTIVE	
3	14.06	2.603	PINNED		CYCLIC	
4	15.14	2.803	CANTILEVERED		COLLECTIVE	
5	24.27	4.494	PINNED		CYCLIC	
6	26.57	4.920	CANTILEVERED		COLLECTIVE	
7	41.36	7.659	PINNED		CYCLIC	
8	45.06	8.345	CANTILEVERED		COLLECTIVE	
9	62.91	11.65	PINNED		CYCLIC	

ROTOR COMPONENT MODES - EDGEWISE

In the edgewise direction the rotor antisymmetric modes become rotor collective modes and the symmetric modes become rotor cyclic modes in the coupled analyses. This figure shows the edgewise blade (rotor) modes which were kept as degrees of freedom in the coupled analyses.

In the edgewise collective direction the situation is not as straightforward as in the edgewise cyclic direction or in the flatwise directions. In the latter directions, the backup structure in the airframe to which the rotor is attached is modeled in the NASTRAN airframe model. However,in the edgewise collective direction, the rotor is attached to a drive train, which is not modeled in the NASTRAN FEM. In the absence of a drive train model, the rotor was assumed to be unattached to the fuselage in this direction, and consequently the rotor component mode used as the rotor collective degree of freedom was calculated with the root boundary condition pinned, as shown in the figure. The effect of this assumption should be investigated, especially in light of the lack of correlation in blade edgewise moments which was found.

C.2

ROTOR COMPONENT MODES — EDGEWISE

MODE NO.	NATURAL FREQUENCY			BLADE MODE		CORRESPONDING ROTOR MODE	
	Hz	PER REV		ROOT BOUNDARY CONDITION	MODE SHAPE	MODE TYPE	MODE SHAPE
1	7.875	1.458	.01 ↓	CANTILEVERED		CYCLIC	
2	36.38	6.737		PINNED		COLLECTIVE	

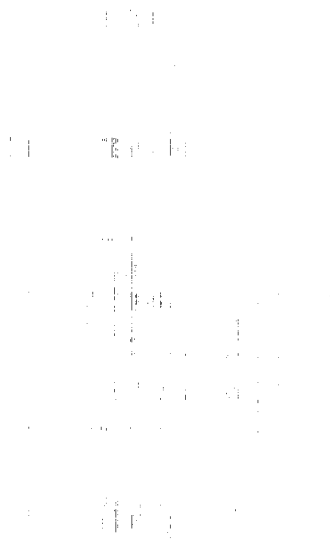

10.2 FUSELAGE MODEL

AH-1G FUSELAGE NASTRAN MODEL

The fuselage is modeled with a NASTRAN model illustrated in the following figure. Fuselage data were supplied by Bell Helicopter Textron Inc. (BHTI, reference 3).

AH-1G FUSELAGE NASTRAN MODEL

FUSELAGE

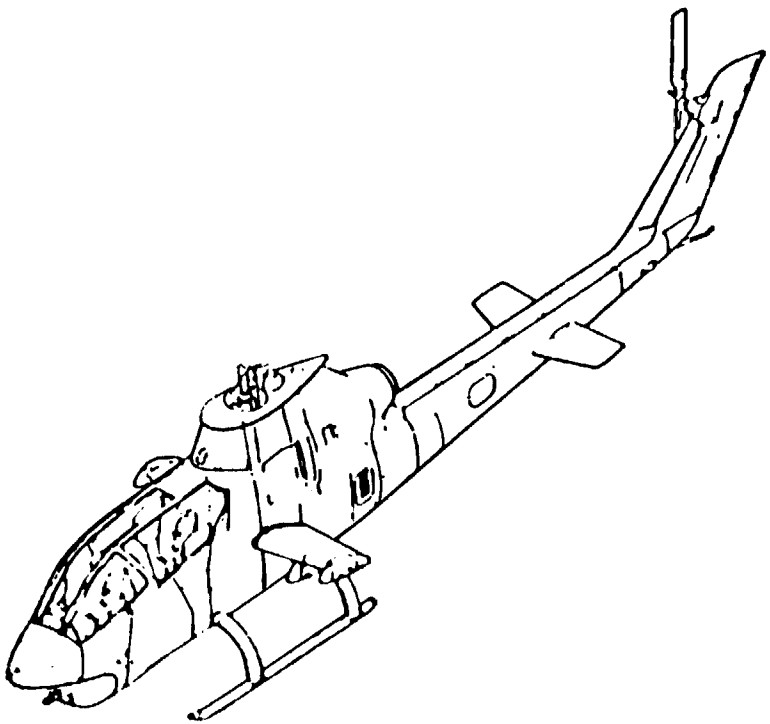

NASTRAN MODEL

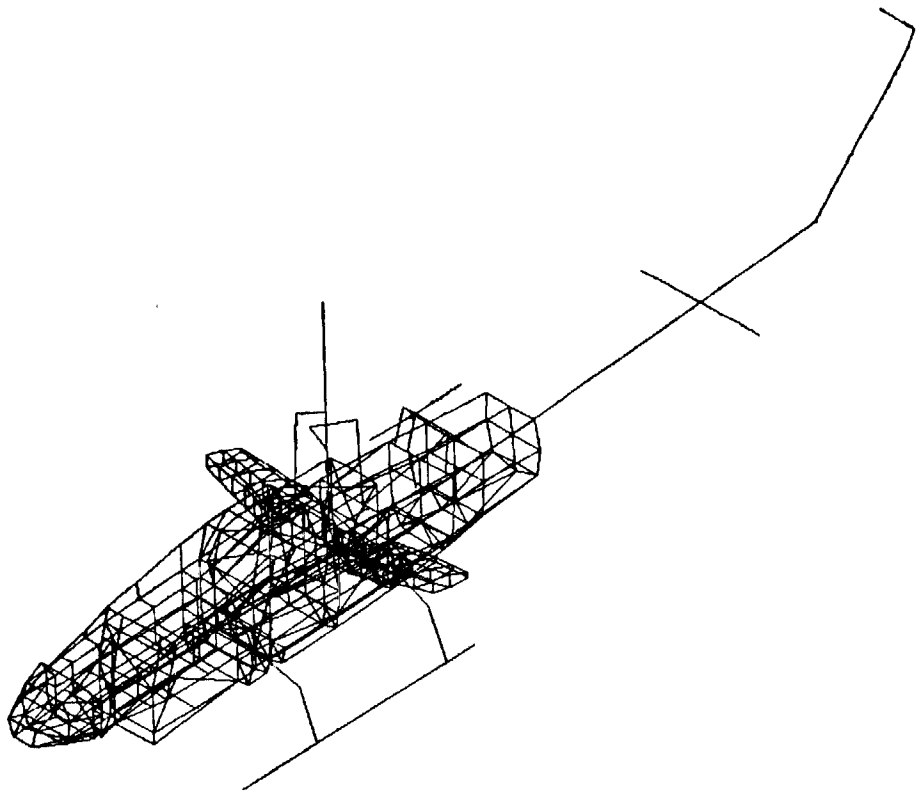

FUSELAGE MODES USED IN COUPLED ROTOR/FUSELAGE ANALYSIS

A free-free modal analysis was performed using the fuselage NASTRAN model. The resulting set of free-interface component modes are tabulated in this figure. These calculated frequencies are identical to those of Reference 3. The elastic modes selected were based on a recommendation by Bell Helicopter Textron Inc.

The full rotor mass was included as a concentrated mass in the fuselage modal analyses so that the fuselage component mode shapes be more representative of the fuselage in the final coupled analyses, especially at the critical hub interface location. To avoid double accounting of this rotor mass, negative values of the concentrated rotor mass were added to the fuselage modal model when the coupling of the flexible rotor was effected in RDYNE.

FUSELAGE MODES USED IN COUPLED ROTOR/FUSELAGE ANALYSIS

	MODE	FREQ-HZ 8320 LO-CLEAN WING-AFT	GENERALIZED MASS LB SEC²/IN
(1)*	MAIN ROTOR PYLON TORE-AND-AFT ROCKING (PYLON PITCH)	2.987	3.990
(2)*	MAIN ROTOR PYLON LATERAL ROCKING (PYLON ROLL)	3.866	3.131
(3)*	FIRST FUSELAGE LATERAL BENDING	7.121	0.438
(4)*	FIRST FUSELAGE VERTICAL BENDING	7.969	0.612
	SKID	14.572	0.272
(5)*	FIRST FUSELAGE TORSION	16.032	1.234
(6)*	SECOND FUSELAGE VERTICAL BENDING	17.221	0.842
(7)*	SECOND FUSELAGE LATERAL BENDING	17.783	0.571
(8)*	FUSELAGE ROLL/ENGINE LATERAL	19.273	0.614
	SKID	19.834	0.322
	FUSELAGE TORSION/WING YAW	21.879	1.169
	SKID	23.431	0.251
	THIRD FUSELAGE VERTICAL BENDING	25.153	0.569
(9)*	MAIN ROTOR MAST LATERAL BENDING	25.591	0.345
	THIRD FUSELAGE LATERAL BENDING	26.529	1.147
(10)*	MAIN ROTOR MAST FORE-AND-AFT BENDING	27.099	0.451
	SKID	29.104	0.221
	FOURTH FUSELAGE VERTICAL BENDING	32.264	2.858

*ONLY THE NUMBERED MODES WERE USED IN THE COUPLED ANALYSES

FUSELAGE RESPONSE LOCATIONS FOR CORRELATION

Airframe response locations were chosen to provide a distribution of points along the entire fuselage. Flight test accelerometer locations on the airframe were used to determine the locations selected for analysis. This provided a direct comparison of the calculated fuselage vibratory levels with flight test data. The fuselage locations used are shown in this table. Included are FS, BL, WL locations for each point analyzed and the corresponding NASTRAN Grid Point ID.

FUSELAGE RESPONSE LOCATIONS FOR CORRELATION

ACCELEROMETER COORDINATE LOCATIONS
OLS (AH-1G — FLIGHT 35A)

ACCELEROMETER	FS	BL	WL	CORRESPONDING NASTRAN GRID POINT ID
NOSE (LV)	46.00	-9.07	46.00	4637
PILOT (LV)	148.50	-10.00	46.00	14837
HUB (FLV)	200.00	0.00	152.76	200153
T/B JUNC (LV)	298.70	-12.29	62.80	29969
ELEVATOR (LV)	401.33	-9.68	55.91	40147
FIN (LV)	515.43	0.00	109.46	51545

23 FUSELAGE ACCELEROMETERS USED IN FLIGHT TESTS

L - LATERAL
V - VERTICAL
F - FORE AND AFT

FUSELAGE RESPONSE LOCATIONS

A pictorial view of the fuselage response locations are shown in the following figure.

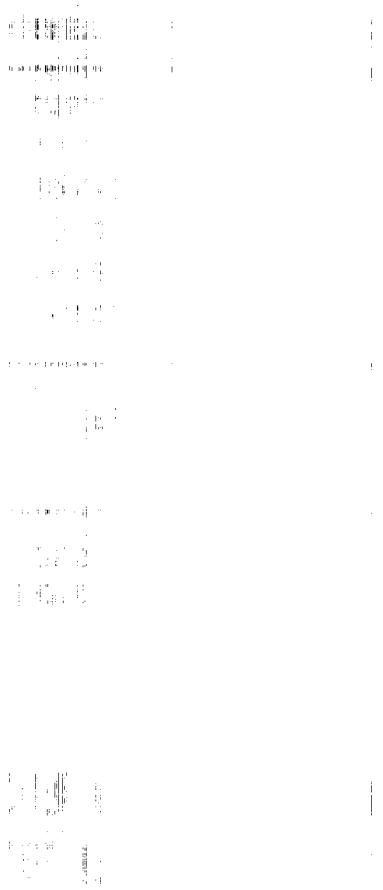

FUSELAGE RESPONSE LOCATIONS

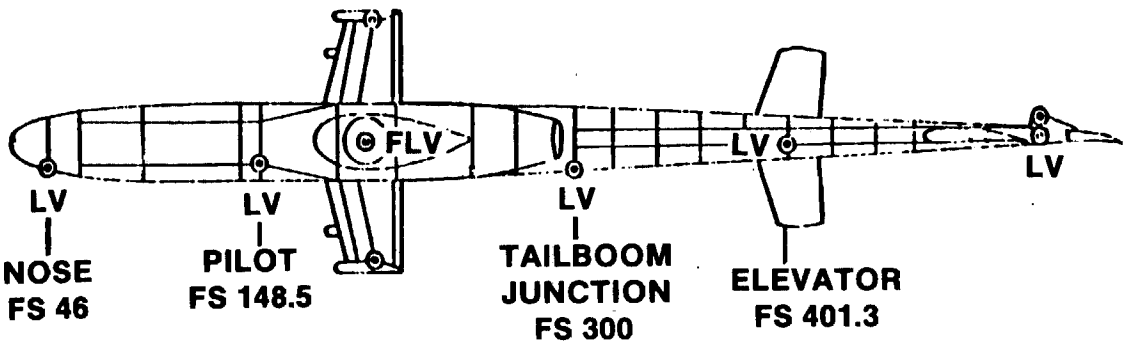

F~FORE-AND-AFT
L~LATERAL
V~VERTICAL
FS~FUSELAGE STATION
WL~WATERLINE

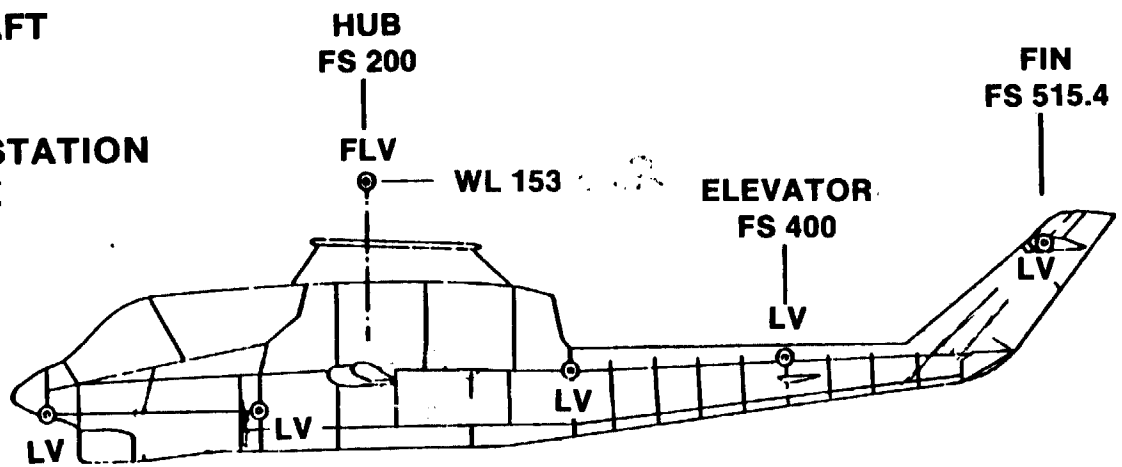

FLIGHT VIBRATION CORRELATION AIRSPEEDS

Results obtained from the RDYNE analysis were compared with flight test data from the AH-1G operational load survey, U.S. Army ATL Contract DAAJ02-73-C-0105 (Ref. 4). Level flight vibration data were selected for the clean wing aft c.g. configuration. The aircraft gross weight analyzed is 8300 lb. The six airspeeds selected are shown in this table.

The RDYNE analysis was first run with fixed hub to determine the trim values of the rotor system. A detailed discussion of the trimming procedure and trimming variables is given in the subsequent text. The trimming process was conducted for the six airspeeds listed in the figure. The trimmed rotor was then coupled with the ten important fuselage modes and the response of the coupled system calculated. All rotor and fuselage response characteristics may be determined from the RDYNE computer analysis. Blade bending moments and fuselage vibration levels are illustrated in this report.

Problems were encountered when the trimmed rotor characteristics at 142 knots were coupled with the fuselage. Numerical instabilities were encountered, therefore, no results were obtained for the 142 knot condition.

FLIGHT VIBRATION CORRELATION AIRSPEEDS

	AIRSPEED (KNOTS)					
CONFIGURATION	1	2	3	4	5	6
35A CLEAN WING AT AFT CG	67	85	101	114	128	142

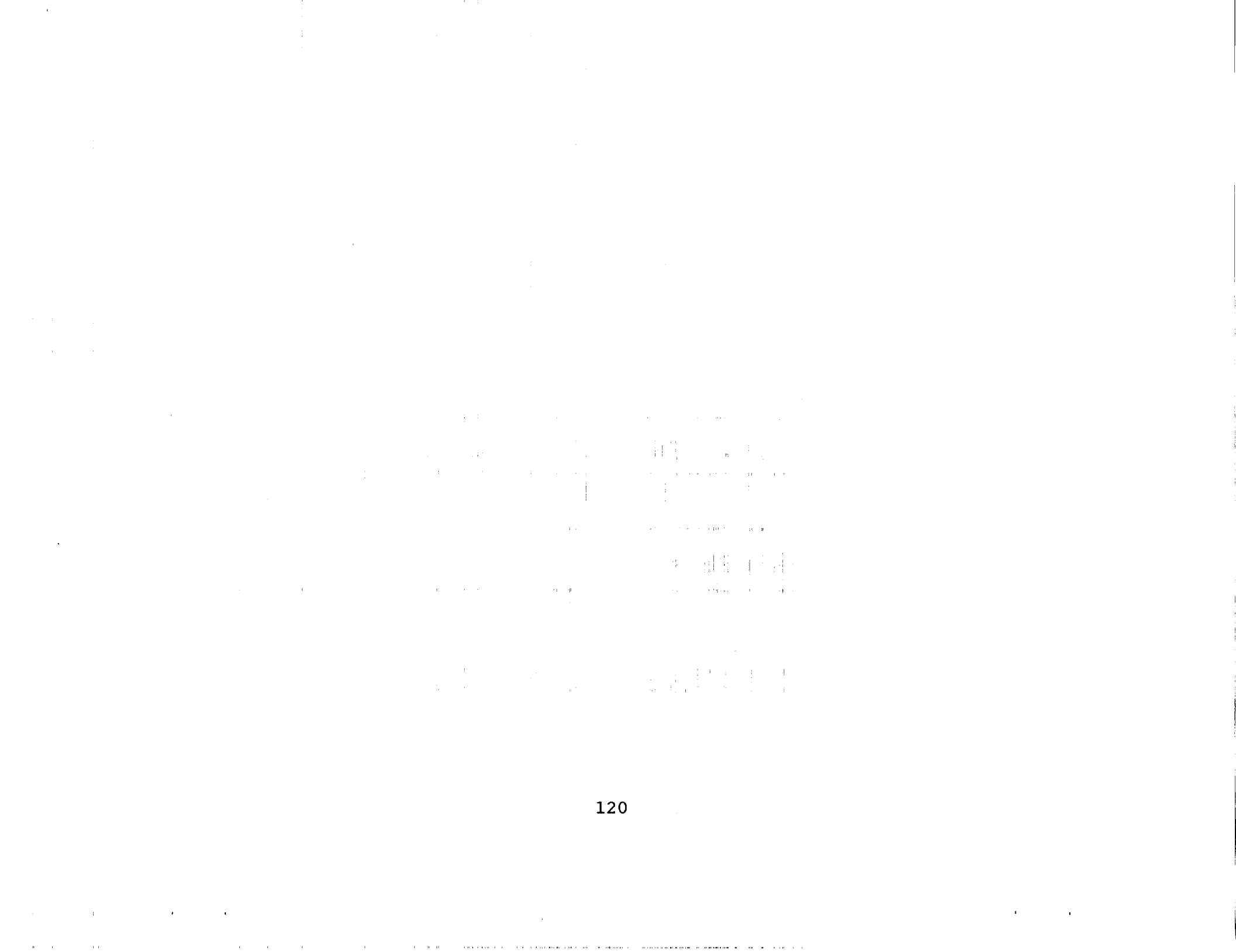

11. STEPS FOLLOWED IN CALCULATING IN-FLIGHT RESPONSE

IN-FLIGHT RESPONSE ANALYSIS OF ROTOR WITH HUB FIXED

To calculate the control inputs required to trim the rotor, in-flight response runs were made in RDYNE, at each forward speed, with the rotating rotor attached to a fixed hub. Starting values for these time-history runs were taken from flight test. They included the following variables:

T	Thrust
α_s	shaft angle
a_{1s}	longitudinal flapping angle
b_{1s}	lateral flapping angle
θ_{75}	collective pitch
A_{1s}	lateral cyclic pitch angle
B_{1s}	longitudinal cyclic pitch angle

During these runs the automatic trimming feature of RDYNE was turned on. In this procedure, certain variables are held constant and others are allowed to vary, in an iterative fashion, until a steady-state equillibrium ("trim") state is reached. In the present correlation study, the first four of these variables were held constant, they being considered the most important to match from a vibration-prediction standpoint. The last three were allowed to vary, and thus their final equilibrium values differed, in general, from flight test.

IN-FLIGHT RESPONSE ANALYSIS OF ROTOR WITH HUB FIXED

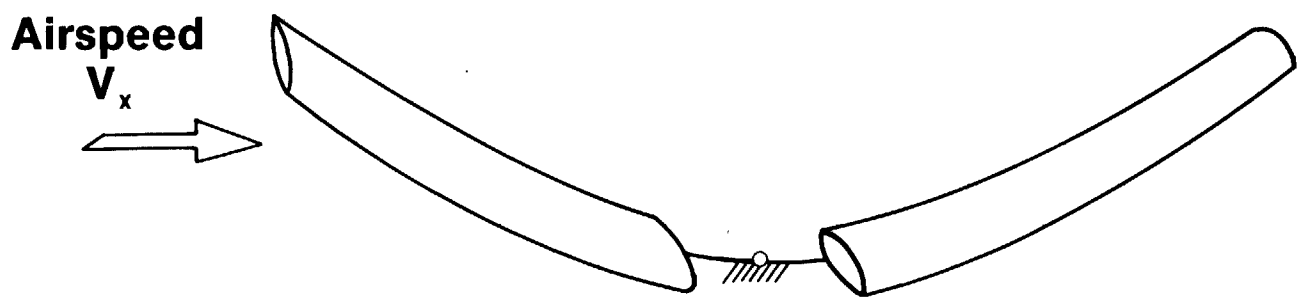

IN-FLIGHT RESPONSE ANALYSIS OF COUPLED ROTOR/FUSELAGE SYSTEM

The next and final step in calculating fuselage vibration was to make in-flight response runs, using RDYNE, with the rotor coupled to the flexible fuselage. Trim values from the hub-fixed runs were used as starting values for these runs. These included values for the seven variables listed on page 122 as well as two additional variables, blade flapping angle and flapping velocity, at zero azimuth, which were also found to be necessary to specify in order to achieve convergence.

During this run the trimming feature was turned off so as not to interact with the vibration calculations. This meant that the response was calculated for fixed values of control inputs. Fortunately, in practice, they changed little from the hub-fixed values, as will be seen.

IN-FLIGHT RESPONSE ANALYSIS OF COUPLED ROTOR/FUSELAGE SYSTEM

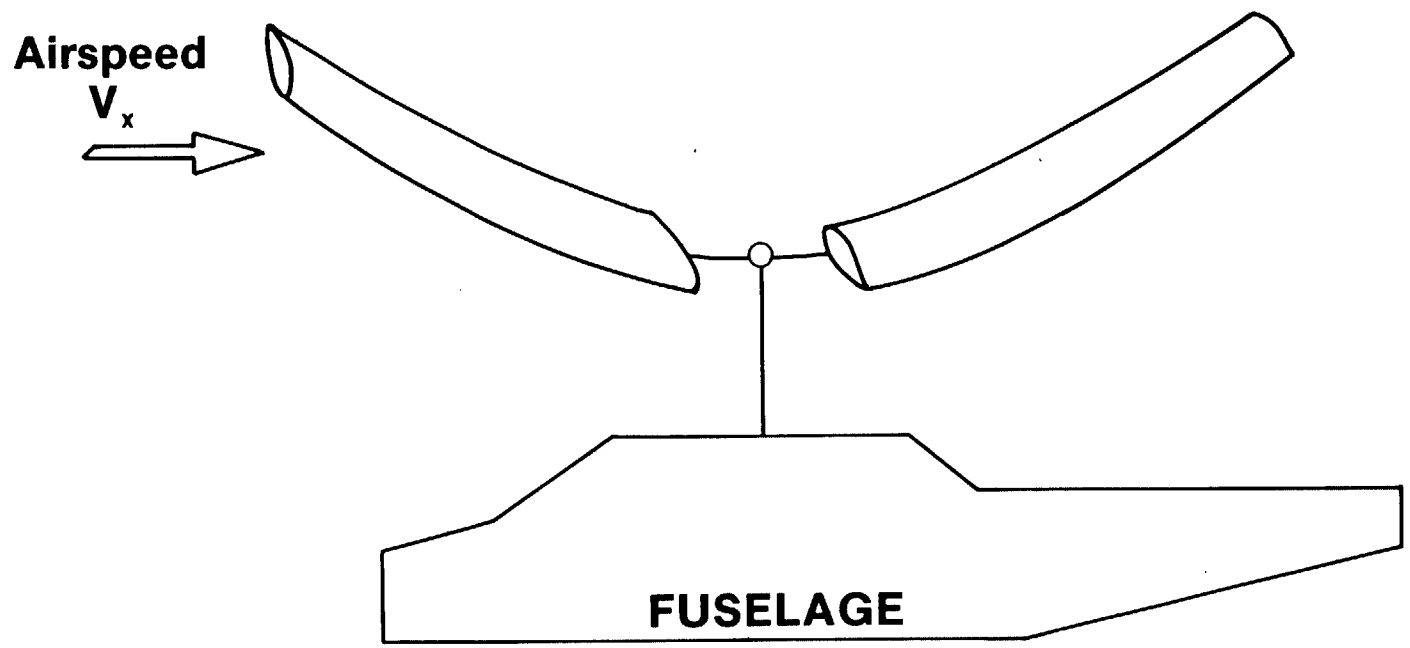

PROCESSING THE TIME HISTORY DATA FROM A RESPONSE RUN

The first figure shows a time history response from a typical coupled rotor/fuselage run in RDYNE for the acceleration response at the pilot's location. Initial transients are observed following the application, at time = 0, of hub-fixed rotor conditions to the now-coupled rotor/fuselage system. New steady-state response conditions are seen to be reached after two seconds.

The second figure is a time history of a continuous 2/rev Fourier analysis of this response. The final steady-state level of this curve furnishes the calculated 2/rev vibration level, in this case 5.5 ft/sec^2 or 0.17 g's, which is then compared to the flight test value.

PROCESSING THE TIME-HISTORY DATA FROM A RESPONSE RUN

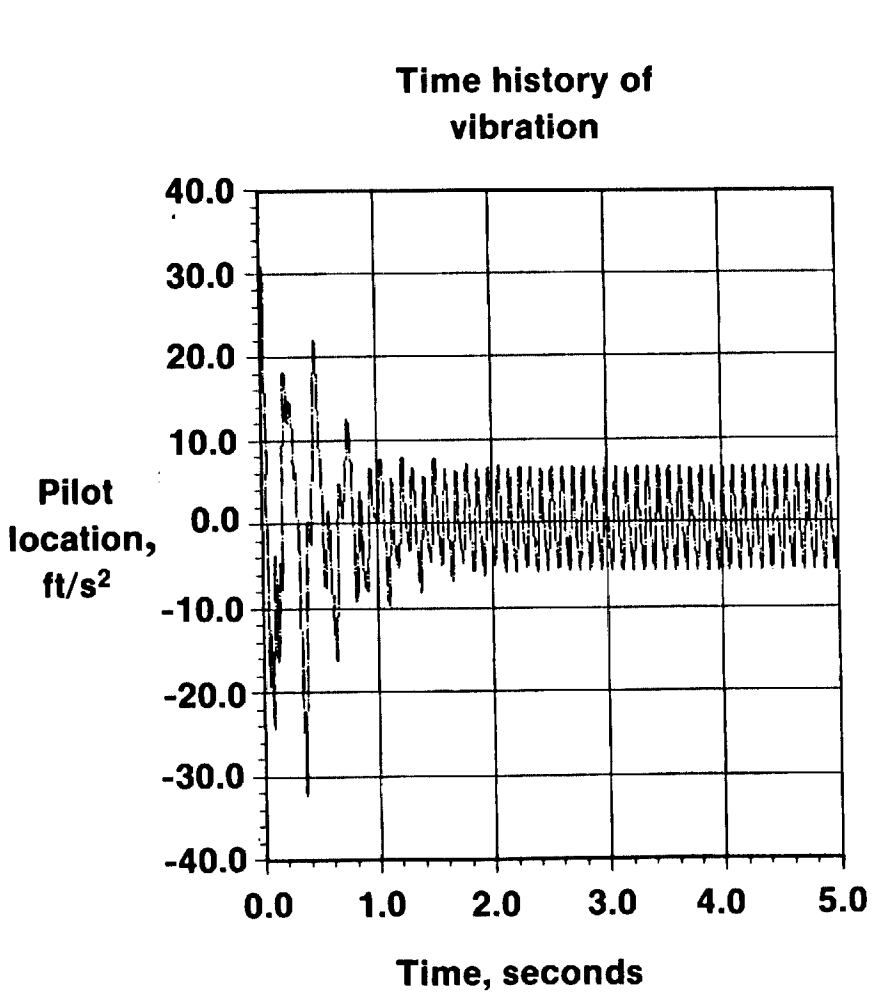

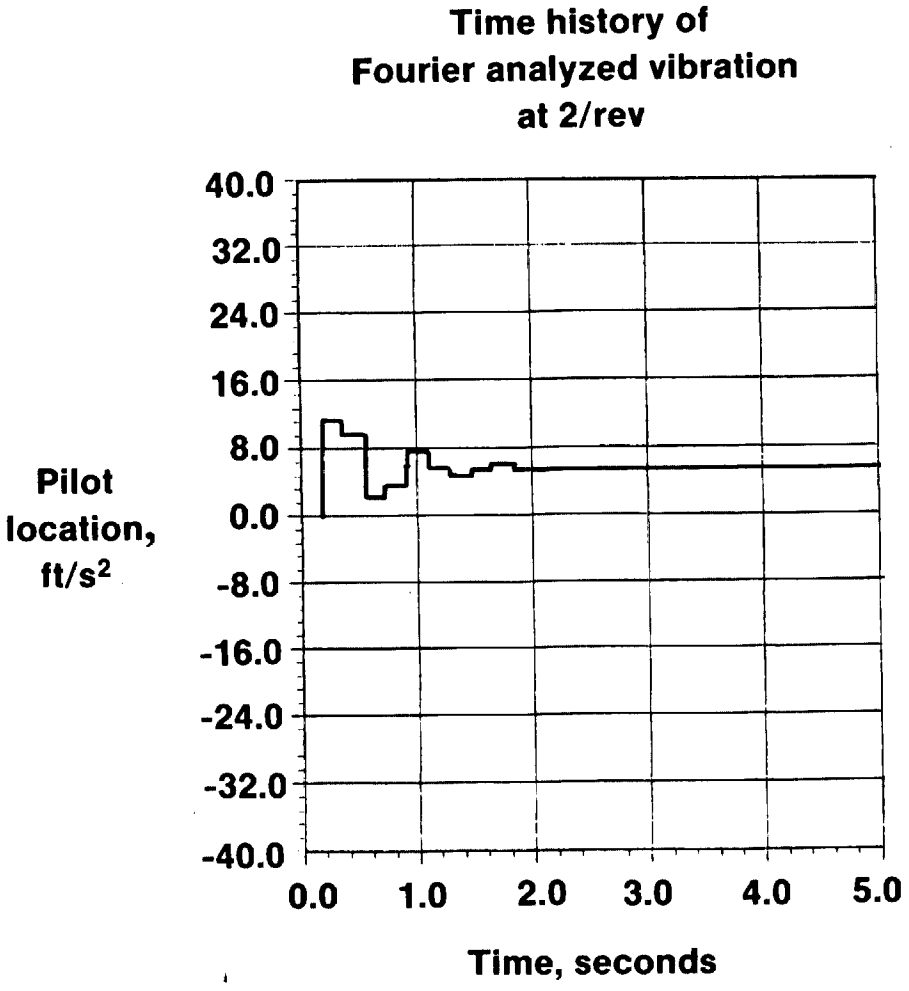

SIGN CONVENTION

The sign convention used throughout the presented text is described in the following table.

SIGN CONVENTION

PARAMETER	SYMBOL	SIGN CONVENTION
1. Rotor lift	—	Positive up perpendicular to airflow
2. Shaft angle	α_s	Negative shaft angle pitch forward
3. Cosine component of flapping angle	a_{1s}	Negative angle flapping up
4. Sine component of flapping angle	b_{1s}	Negative angle flapping up
5. Collective pitch	θ_{75}	Increasing pitch
6. Lateral cyclic pitch angle	A_{1s}	Negative angle increasing pitch
7. Longitudinal cyclic pitch angle	B_{1s}	Negative angle increasing pitch
8. Hub longitudinal reaction	F_x	Force aft
9. Hub lateral reaction	F_y	Force right
10. Hub vertical reaction	F_z	Force up

SIGN CONVENTION (CONCLUDED)

PARAMETER	SYMBOL	SIGN CONVENTION
11. Hub moment about longitudinal axis	M_x	Right hand rule about longitudinal axis
12. Hub moment about lateral axis	M_y	Right hand rule about lateral axis
13. Hub moment about vertical axis	M_z	Right hand rule about vertical axis
14. Flatwise blade bending moment	—	Lower side in tension
15. Edgewise blade bending moment	—	Leading edge in tension
16. Acceleration longitudinal	—	Ship accelerates aft
17. Acceleration lateral	—	Ship accelerates right
18. Acceleration vertical	—	Ship accelerates up

ASSUMPTIONS IN THE BASELINE MODEL

In the course of obtaining the present analytical results, difficulties were encountered in converging to a steady-state vibration solution, especially at the higher forward speeds. To overcome these difficulties, some deviations from the orginally-intended model were made in the course of arriving at a baseline model for which results could be obtained throughout the speed range. These assumptions in the baseline model include:

a) Uniform inflow

b) Damping in the fuselage modes = 10%

c) Rigid torsion - blade torsion modes were not included as rotor d.o.f.

In addition, in order to achieve convergence at 128 knots, an additional assumption had to be made.

d) At 128 knots, the roll component of the 2nd fuselage mode was set equal to zero.

The effect of making these changes will be discussed later.

ASSUMPTIONS IN THE BASELINE MODEL

a) Uniform inflow
b) Damping in the fuselage modes = 10%
c) Rigid torsion
d) Roll component of the 2nd fuselage mode set equal to zero at V = 128 knots

12. CORRELATION OF EQUILIBRIUM VARIABLES

COMPARISON OF TEST AND ANALYSIS ROTOR LIFT AND SHAFT ANGLE

A comparison of rotor lift and shaft angle is illustrated on the following figure. Both hub fixed and cases with fuselage are compared with test data. The analysis predicts rotor lift and shaft angle very well, with the exception of rotor lift at 128 knots. An underprediction of 700 lbs of lift is calculated.

COMPARISON OF TEST AND ANALYSIS ROTOR LIFT AND SHAFT ANGLE

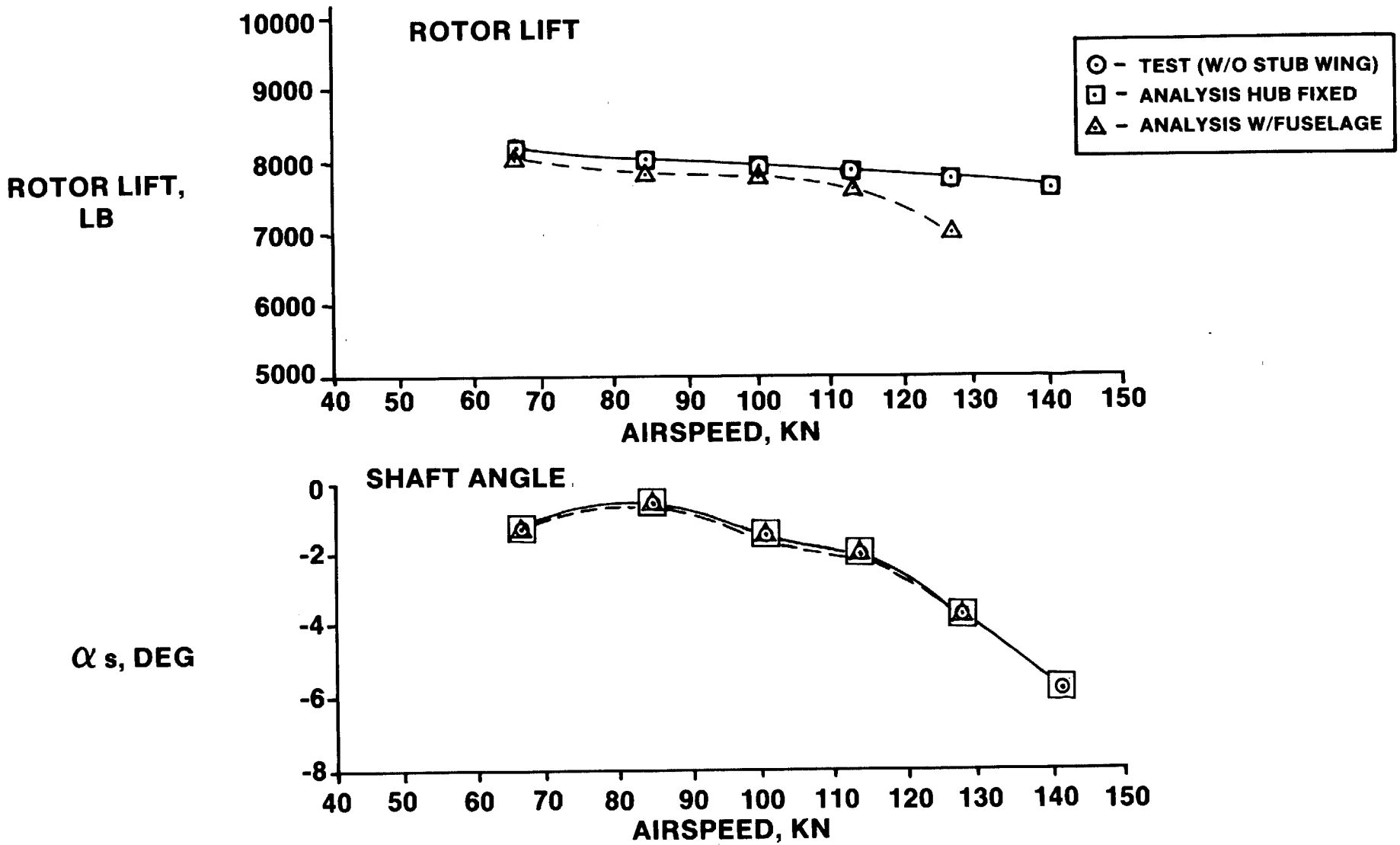

COMPARISON OF TEST AND ANALYSIS ROTOR FLAPPING ANGLE

Rotor flapping angle versus airspeed are shown in the following figure. Fixed hub flapping angles a_{1s} and b_{1s} agree well with test data because trimming control variables, consisting of θ_{75}, A_{1s}, and B_{1s}, were adjusted to yield a match between predicted and measured flappings. Flapping angles when the rotor is combined with fuselage are shown to deviate slightly from test data because the fixed hub trim control variables were derived from the hub fixed condition, and consequently the trim variables are not exactly the values required to yield flapping responses for the coupled rotor-fuselage system.

COMPARISON OF TEST AND ANALYSIS ROTOR FLAPPING ANGLE

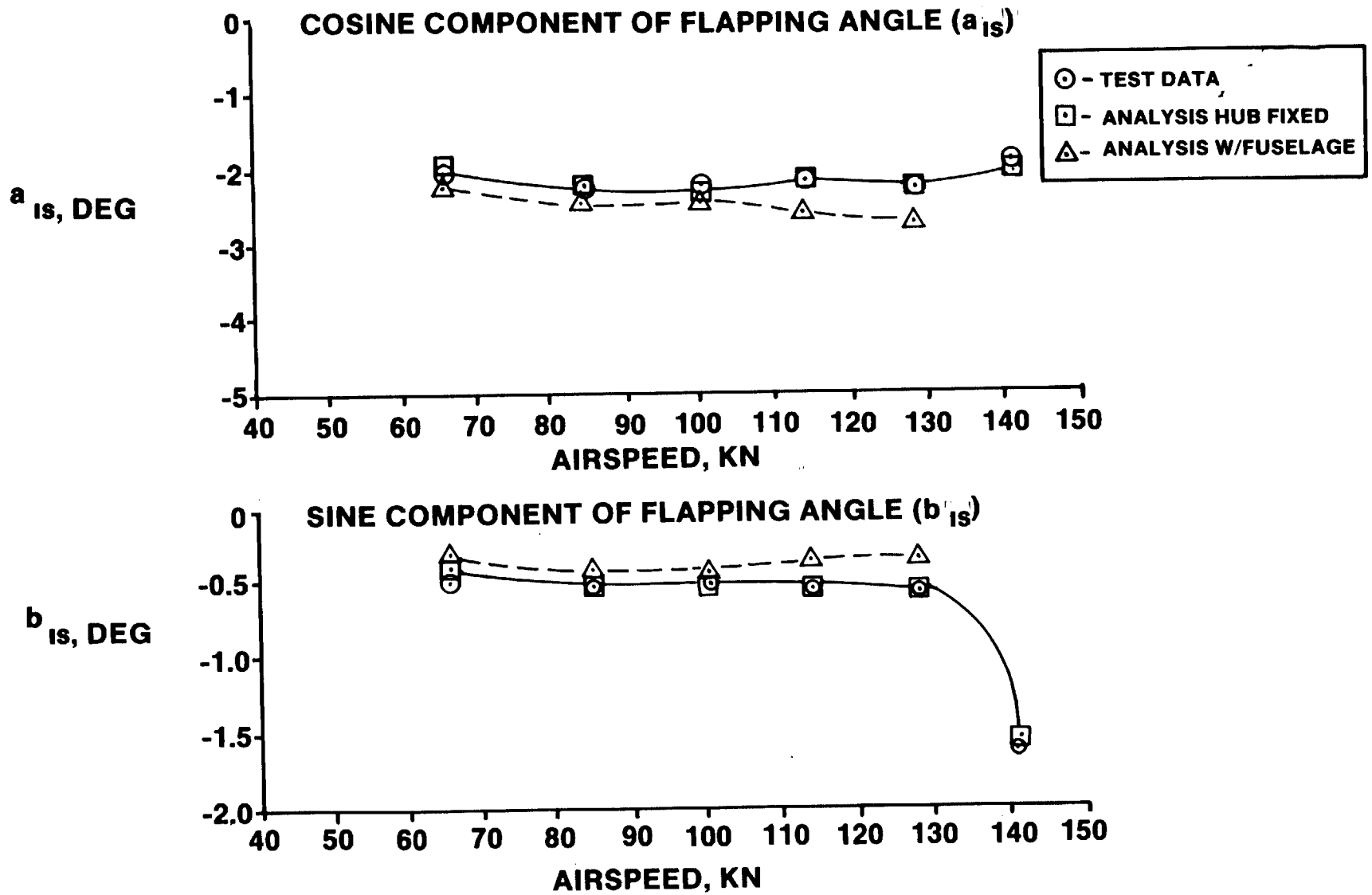

COMPARISON OF TEST AND ANALYSIS HORSEPOWER AND COLLECTIVE PITCH

Horsepower and collective pitch are in good agreement with test data. Horsepower from analysis is derived from steady shaft torque at the main rotor. Horsepower was analyzed for the hub fixed and with fuselage. Hub fixed predictions are extremely good with a slightly lower horsepower prediction at 114 knots. Horsepower predictions with fuselage are also fairly good with lower values at 101 and 114 knots.

Collective pitch was also analyzed for hub fixed and with fuselage. Good agreement is seen with the results shown in the following figure. Slightly higher collective pitch is required for the lower airspeeds, while the higher airspeeds show very good correlation. Collective pitch trends with fuselage show similar results as the hub fixed condition. Predicted values of collective pitch agree among fixed hub and rotor coupled to fuselage (free hub) cases because free hub cases utilized fixed hub values for trim variables.

COMPARISON OF TEST AND ANALYSIS HORSEPOWER AND COLLECTIVE PITCH

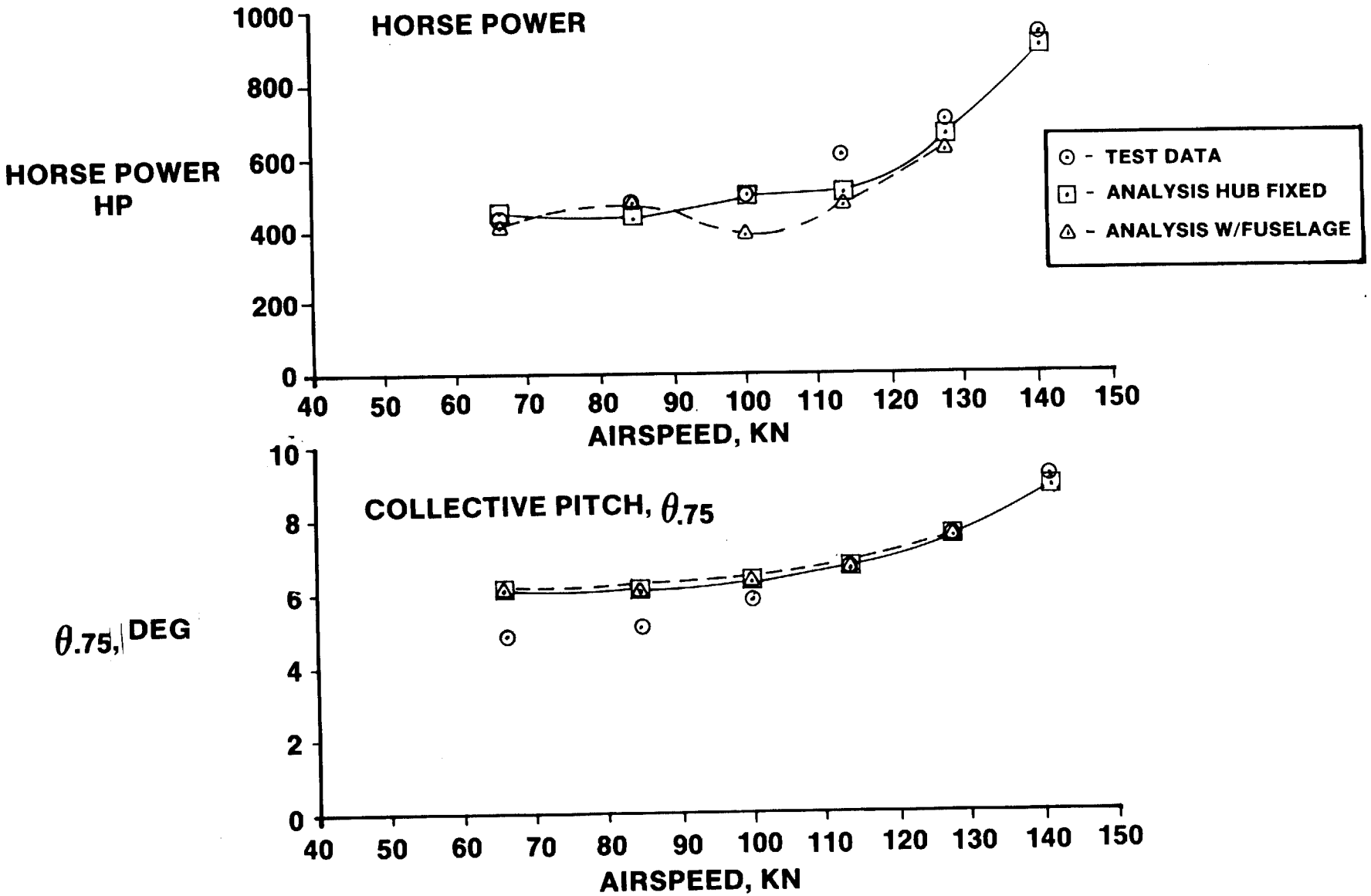

COMPARISON OF TEST AND ANALYSIS OF LATERAL AND LONGITUDINAL CYCLIC PITCH

Computed and flight test main rotor lateral and longitudinal cyclic pitch angles are shown in the following figure. The calculated lateral cyclic pitch angle (A_{1s}) is shown to be smaller for both the hub fixed and with fuselage conditions than the test data. However, the general flight test trend is followed.

The longitudinal cyclic pitch angle (B_{1s}) is also lower than test data. As airspeed is increased, deviations from test data becomes more pronounced. Hub fixed and the case with the fuselage are similar in longitudinal cyclic pitch angle.

The calculated cyclic pitch angles are in reasonable agreement with the test data.

Again, similar remarks to the remarks made previously discussing the agreement between predicted values of collective pitch for fixed and free hub cases apply here - that is, fixed and free hub values of cyclic pitch agree because free hub cases utilized fixed hub values.

COMPARISON OF TEST AND ANALYSIS OF LATERAL AND LONGITUDINAL CYCLIC PITCH

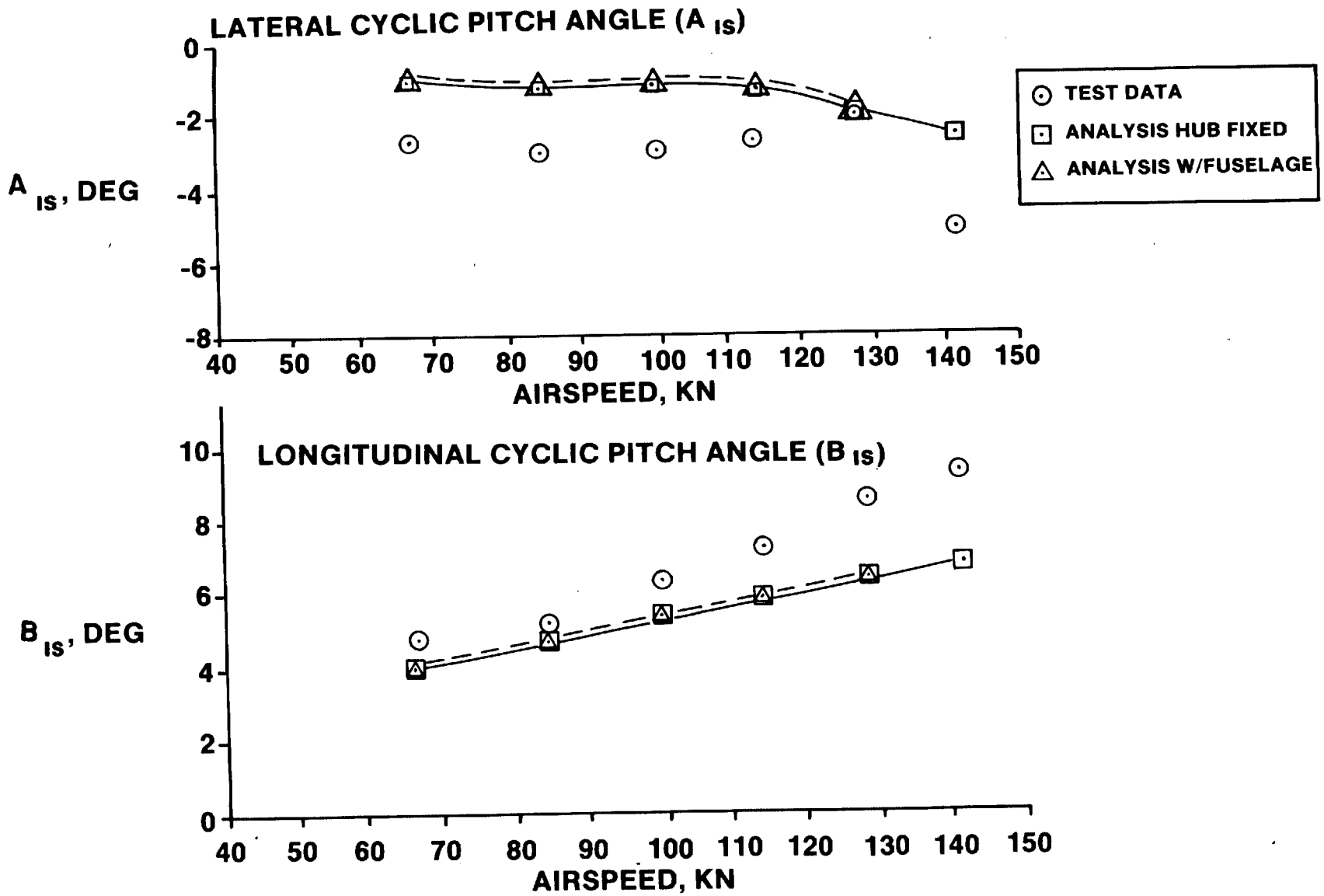

13. CORRELATION OF VIBRATORY BLADE BENDING MOMENTS

HARMONICS OF BLADE FLATWISE BENDING MOMENT AT 50% RADIUS

The blade flatwise bending moment at the 50 percent radial location was harmonically analyzed. Shown below are various harmonics of flatwise bending moment versus airspeed. The 2/rev and 3/rev flatwise bending moment show good agreement with test data. The largest constituent of the flatwise bending moment is the 1/rev component. The analysis overpredicts this component. The overprediction stays relatively constant with airspeed variation, with a slightly greater overprediction at airspeeds of 101 and 114 knots.

HARMONICS OF BLADE FLATWISE BENDING MOMENT AT 50% RADIUS

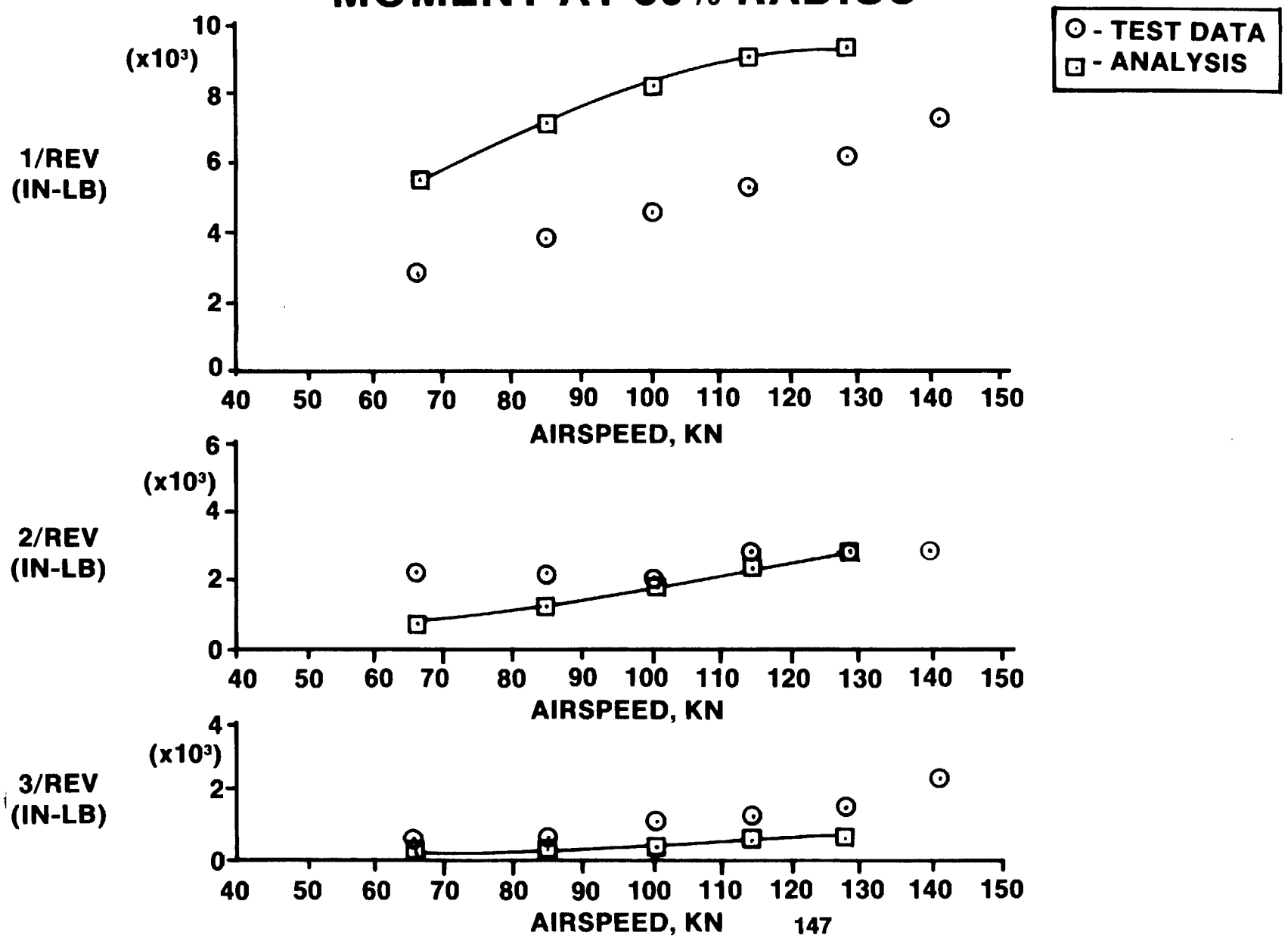

HARMONICS OF EDGEWISE BENDING MOMENT AT 50% RADIUS

The blade edgewise bending moment at the 50 percent radial location was harmonically analyzed. Shown below are various harmonics of edgewise blade bending moments versus airspeed. Overprediction was encountered for the 1/rev and 2/rev harmonics with large deviations seen in the 1/rev component. The assumption of pinned collective edgewise rotor modes, as discussed on page 106, which was made owing to a lack of information on drive train properties, is a possible cause for these large discrepancies. The discrepancies are more pronounced at lower harmonics (i.e., 1/rev), and slightly lower than test data at 3/rev. As a result of the large deviations in edgewise blade bending moments, vibration responses are likely to be directly affected.

HARMONICS OF EDGEWISE BENDING MOMENT AT 50% RADIUS

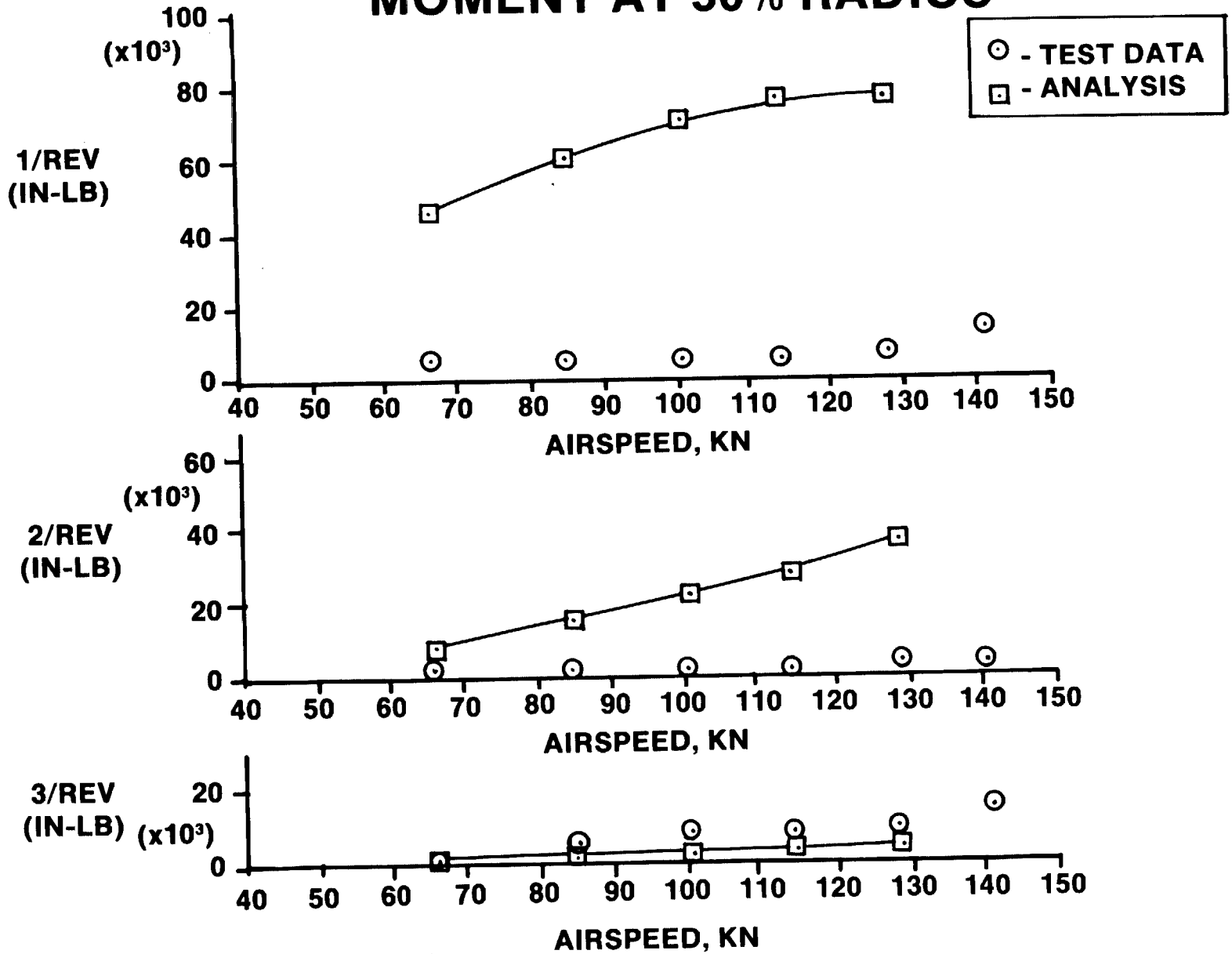

RADIAL DISTRIBUTION OF BLADE FLATWISE BENDING MOMENT

Plots at the selected correlation airspeeds are presented showing blade flatwise bending moment versus blade radius. The following five pages illustrate the effects of airspeed on flatwise bending moments. The flatwise bending moments for 2/rev and 3/rev demonstrate good agreement with flight test data. The 1/rev flatwise bending moment shows consistently higher values.

The airspeeds represented are:

1. V = 67 knots
2. V = 85 knots
3. V = 101 knots
4. V = 114 knots
5. V = 128 knots

RADIAL DISTRIBUTION OF BLADE FLATWISE BENDING MOMENT (V = 67 KN)

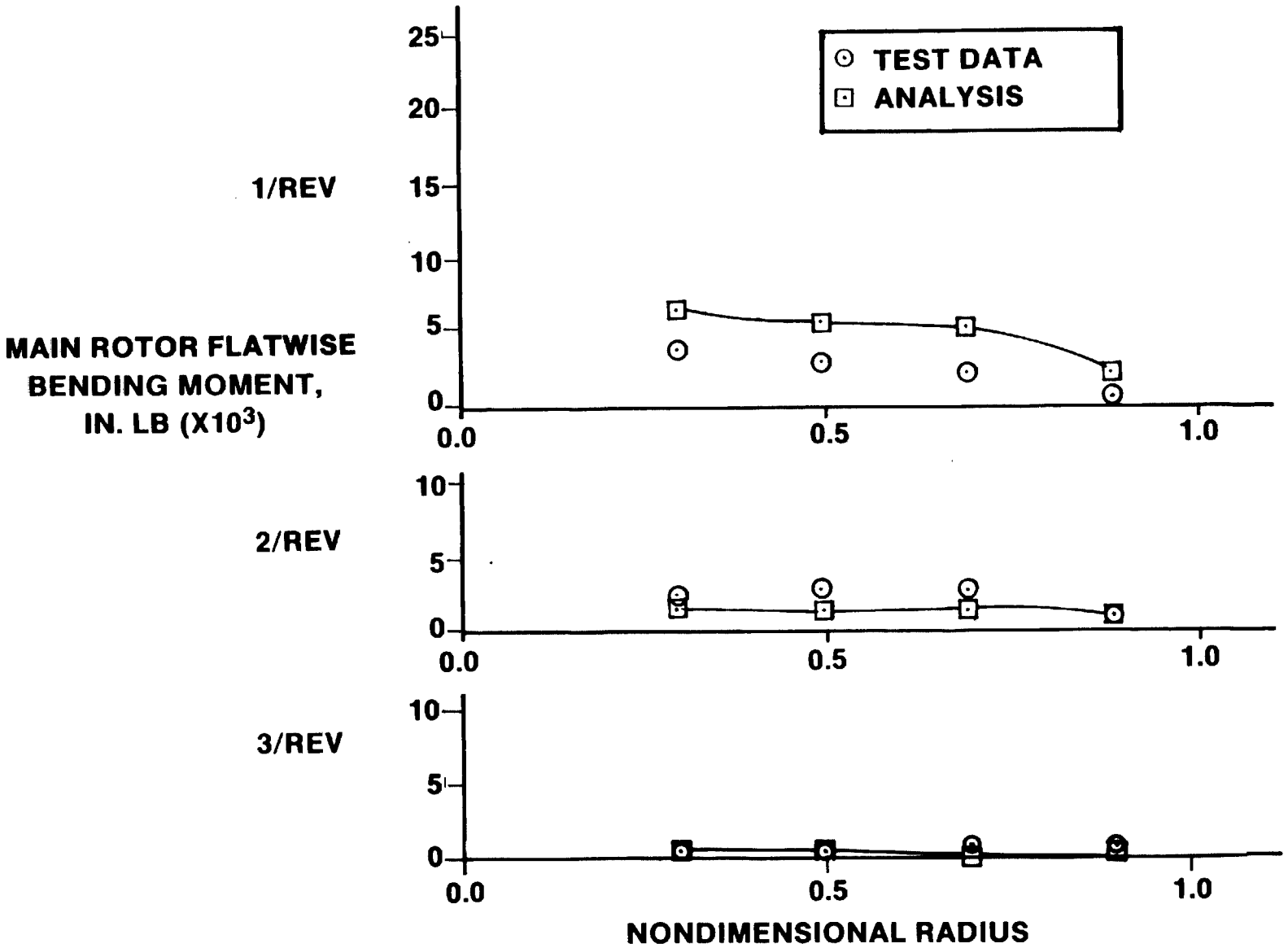

RADIAL DISTRIBUTION OF BLADE FLATWISE BENDING MOMENT (V = 85 KN)

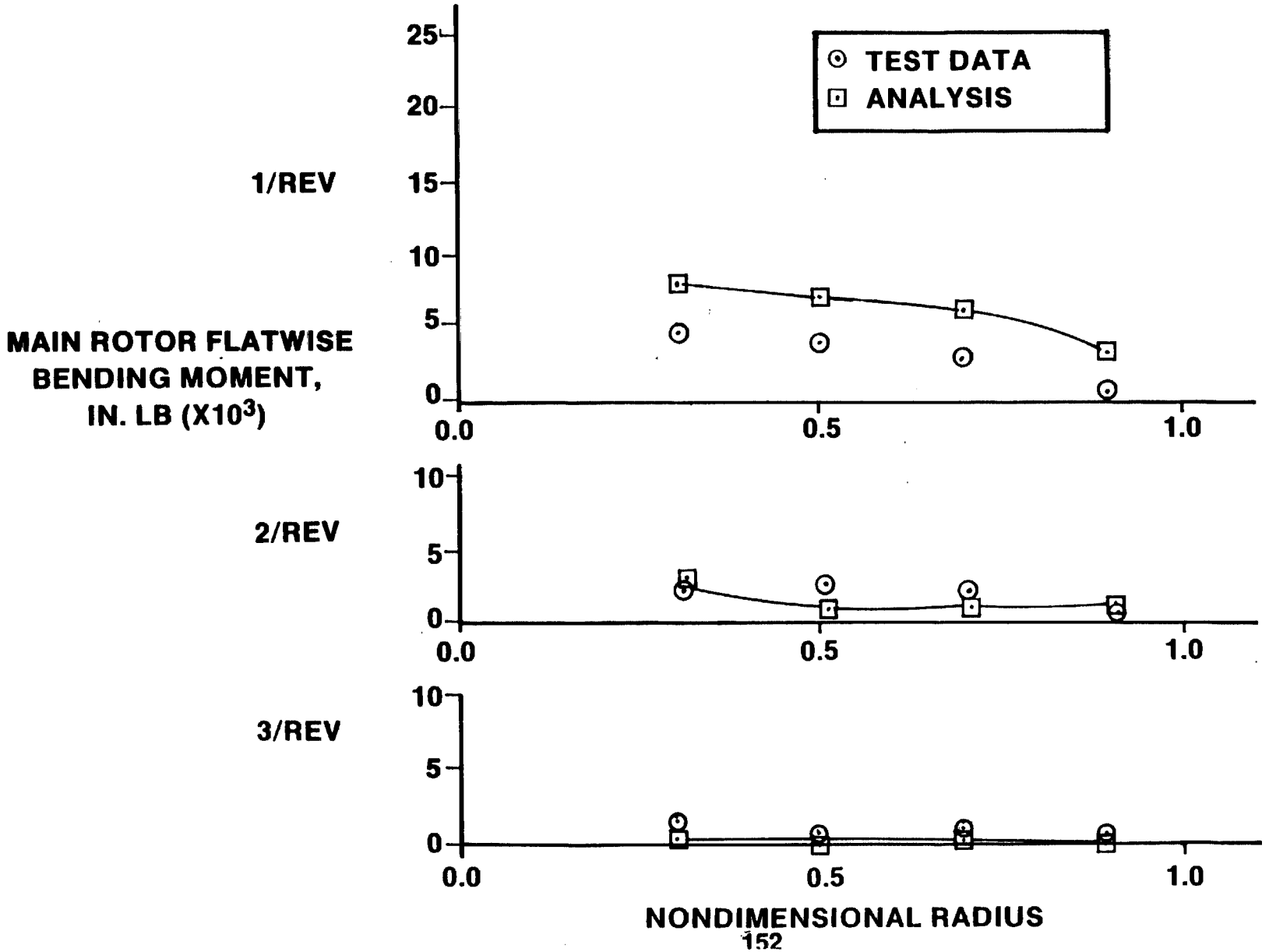

RADIAL DISTRIBUTION OF BLADE FLATWISE BENDING MOMENT (V = 101 KN)

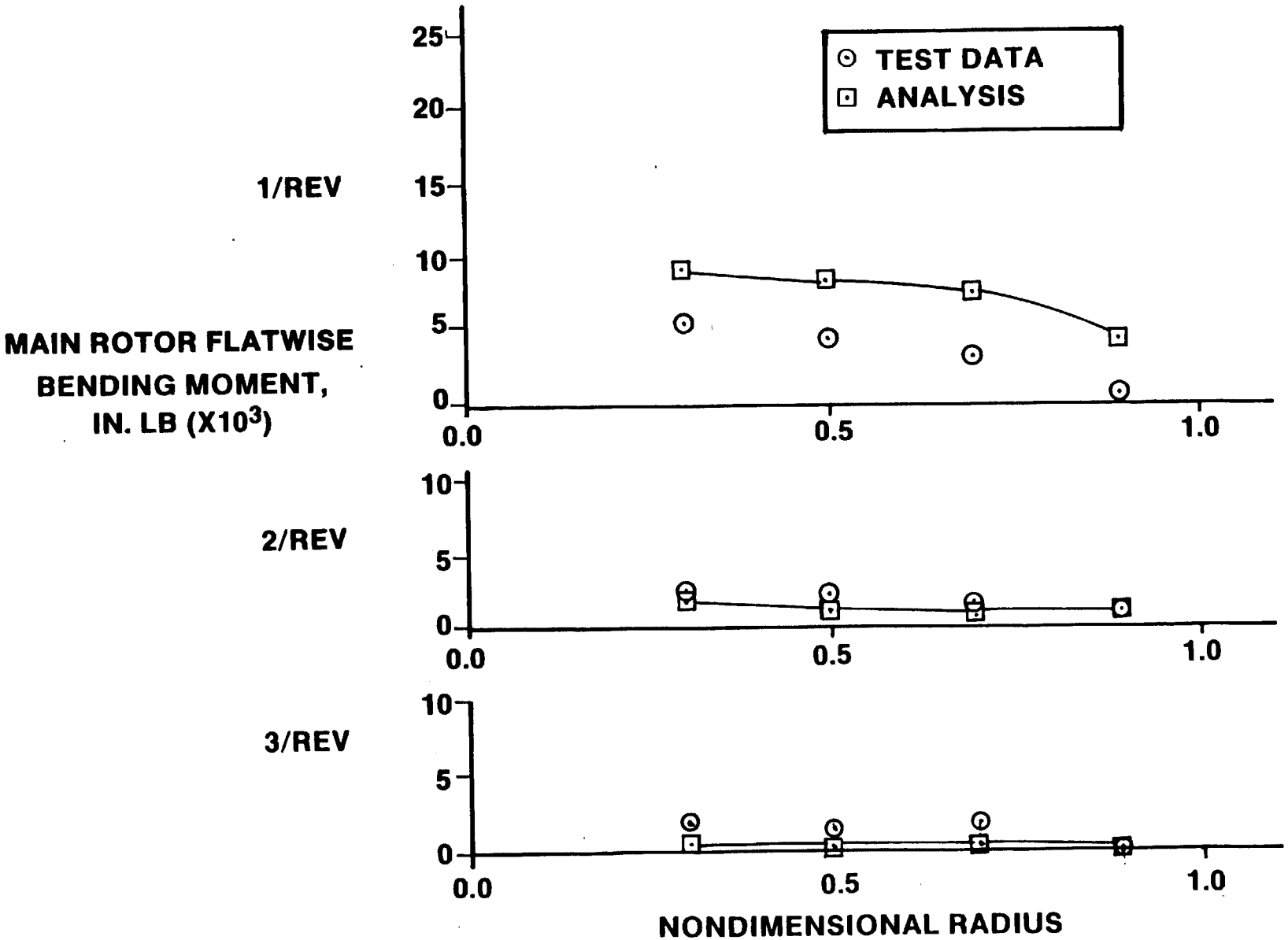

RADIAL DISTRIBUTION OF BLADE FLATWISE BENDING MOMENT (V = 114 KN)

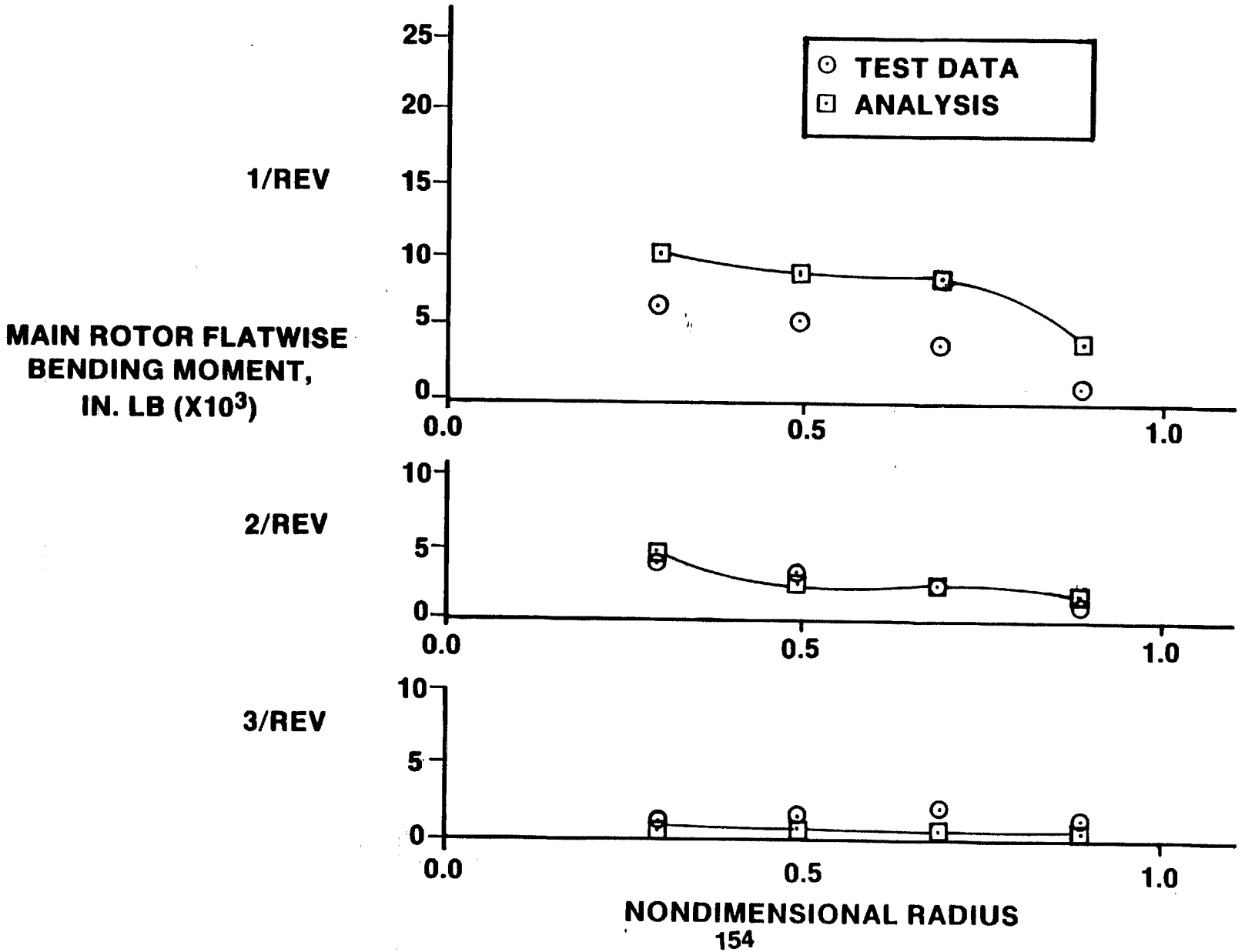

RADIAL DISTRIBUTION OF BLADE FLATWISE BENDING MOMENT (V = 128 KN)

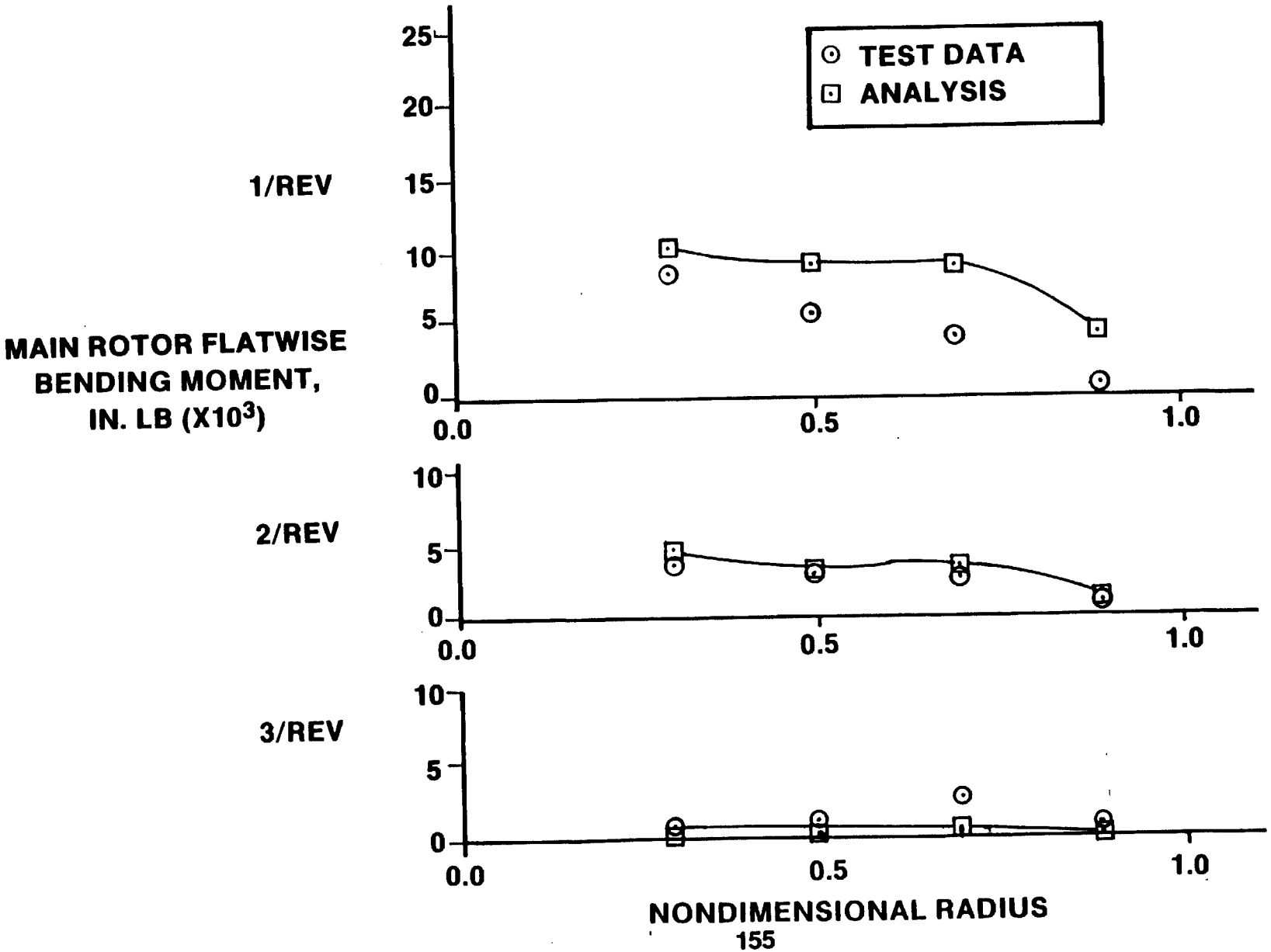

RADIAL DISTRIBUTION OF BLADE EDGEWISE BENDING MOMENT

Plots at the selected correlation airspeeds are presented showing blade edgewise bending moment versus blade radius. The following five pages illustrate the effects of airspeed on edgewise bending moments. Overprediction is observed for the 1/rev and 2/rev harmonics with the 1/rev edgewise moments overpredicted by a factor of seven.

The airspeeds represented are:

1. V = 67 knots
2. V = 85 knots
3. V = 101 knots
4. V = 114 knots
5. V = 128 knots

RADIAL DISTRIBUTION OF BLADE EDGEWISE BENDING MOMENT (V = 67 KN)

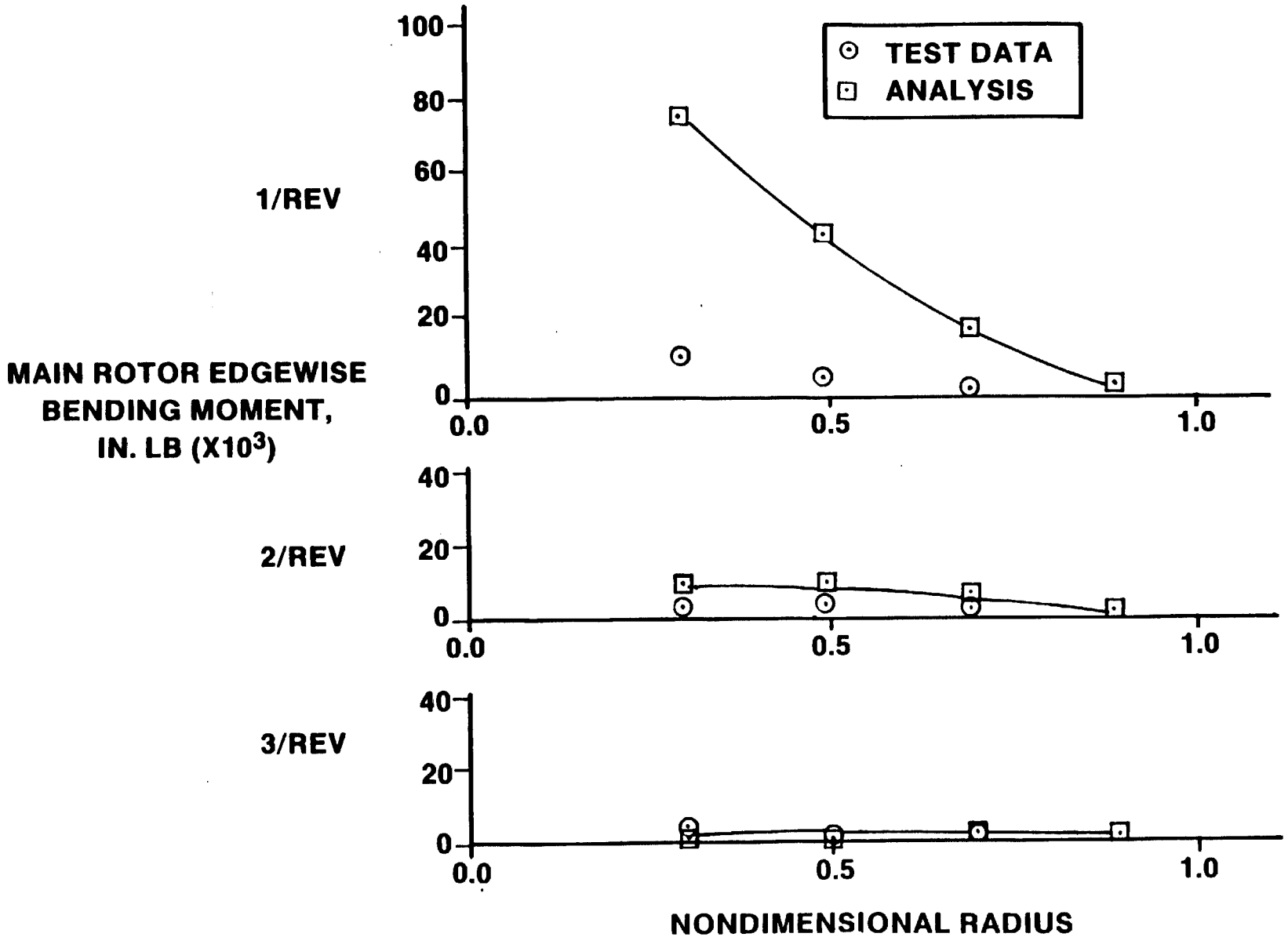

RADIAL DISTRIBUTION OF BLADE EDGEWISE BENDING MOMENT (V = 85 KN)

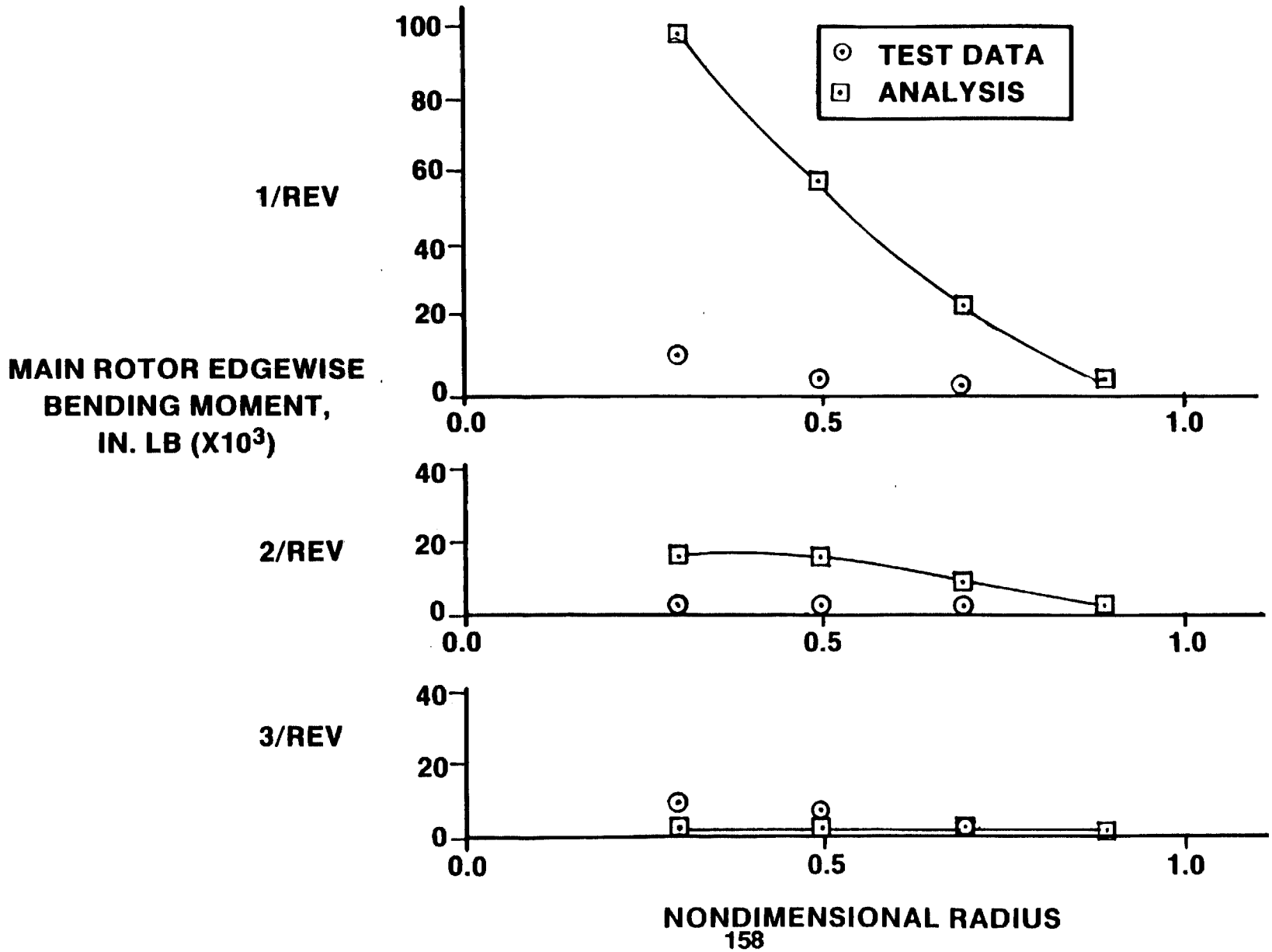

RADIAL DISTRIBUTION OF BLADE EDGEWISE BENDING MOMENT (V = 101 KN)

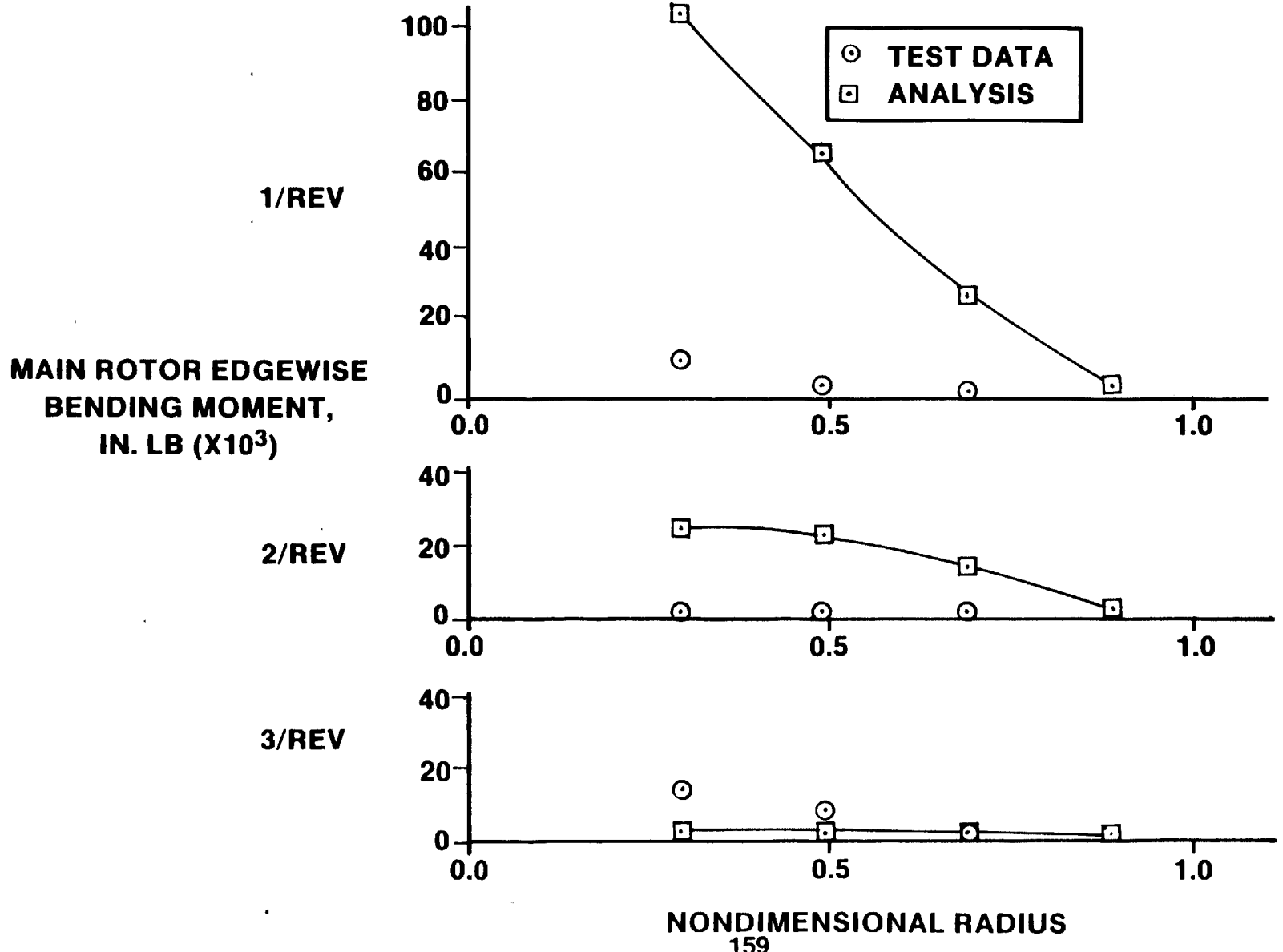

RADIAL DISTRIBUTION OF BLADE EDGEWISE BENDING MOMENT (V = 114 KN)

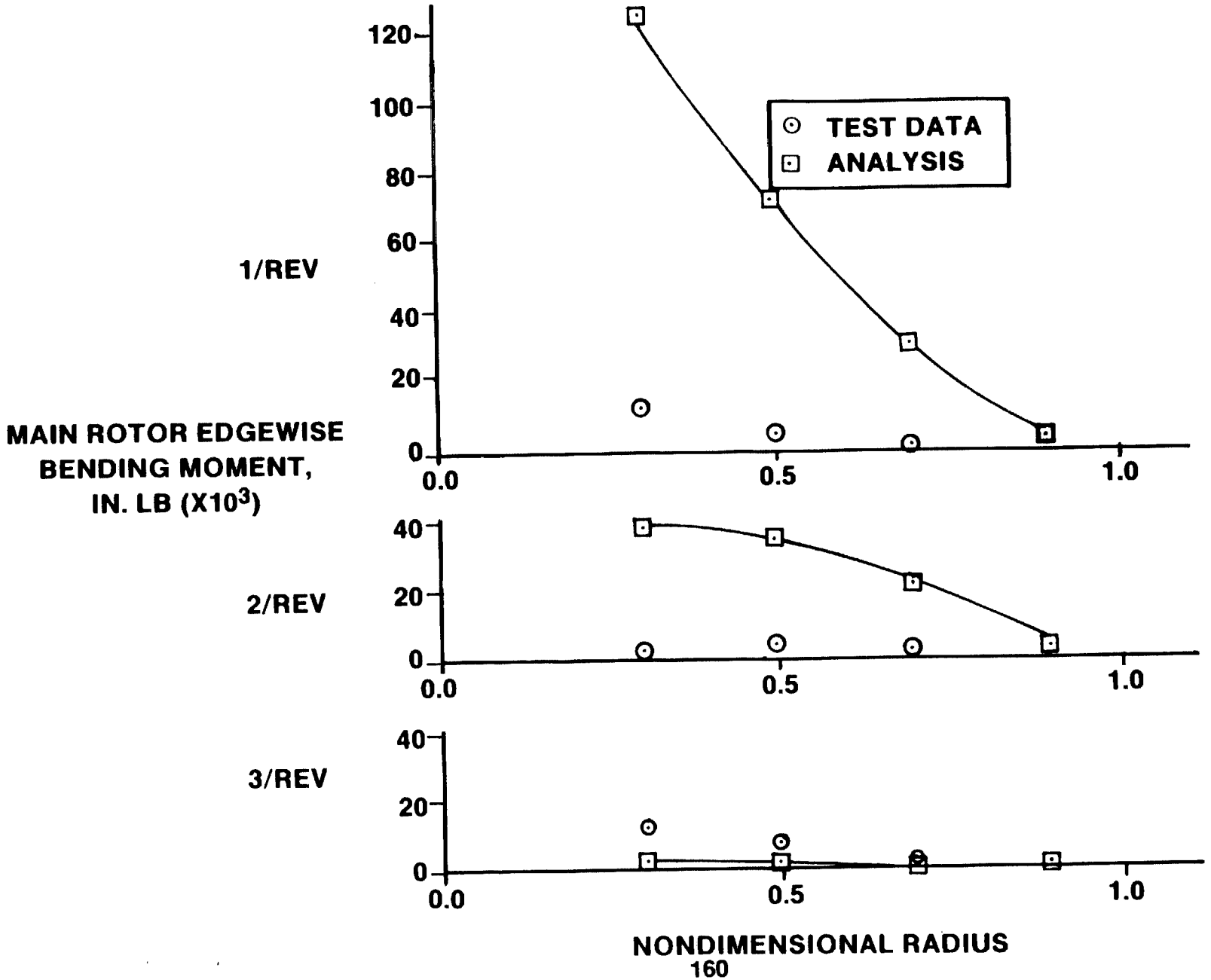

RADIAL DISTRIBUTION OF BLADE EDGEWISE BENDING MOMENT (V = 128 KN)

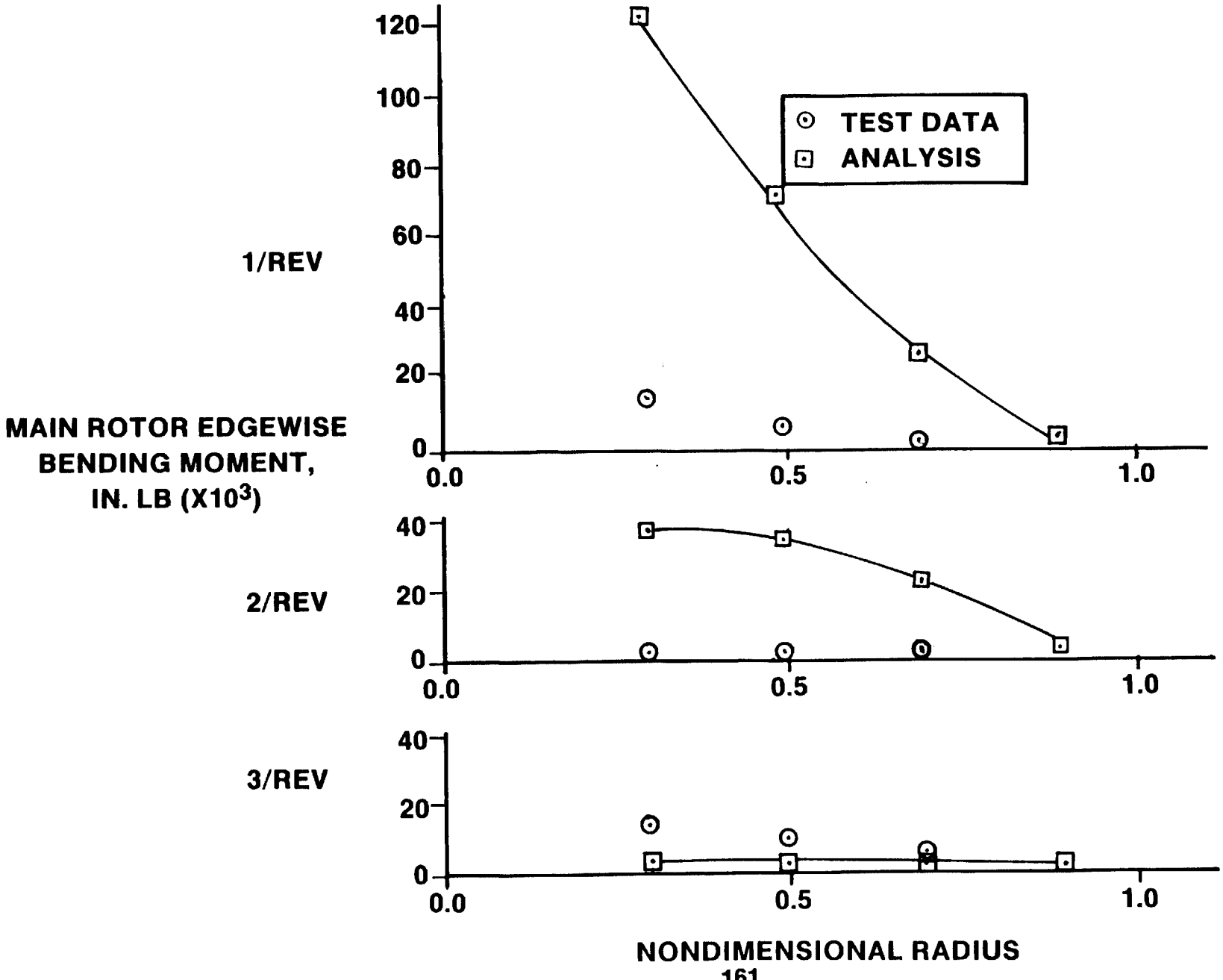

BLADE FLATWISE BENDING MOMENT TIME HISTORIES AT V = 67 KNOTS

The blade flatwise bending moment time histories are compared in the next two figures for radial stations of 30, 50, and 70 percent radius at 67 knots. The blade flatwise bending moment signatures compare fairly well with flight test data at the 50 and 70 percent radial stations, however some phase shifts are observed. Inboard at 30 percent radius, larger deviations are seen, with analysis overpredicting test data.

BLADE FLATWISE BENDING MOMENT TIME HISTORIES (V = 67 KN)

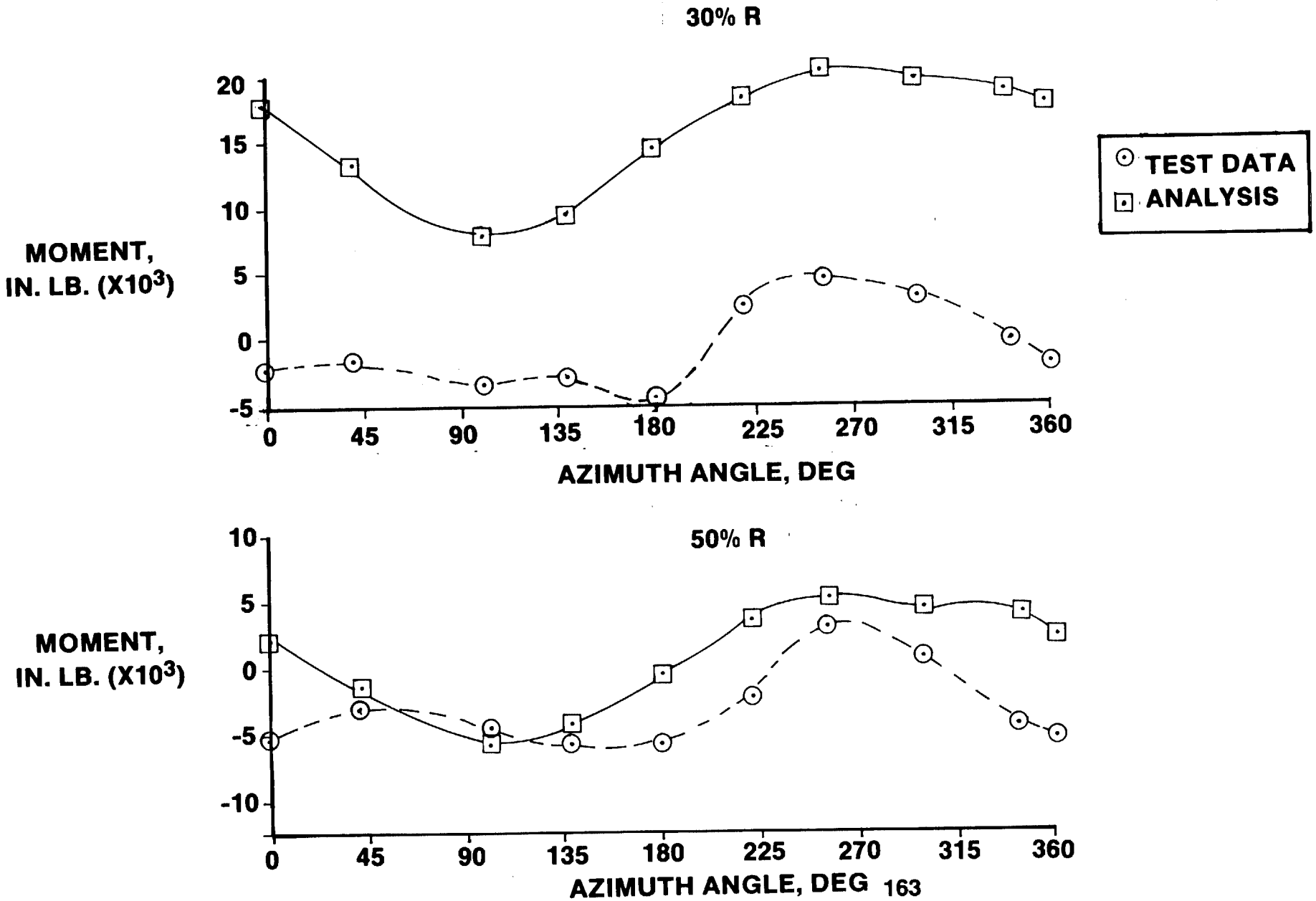

BLADE FLATWISE BENDING MOMENT TIME HISTORIES (V = 67 KN)

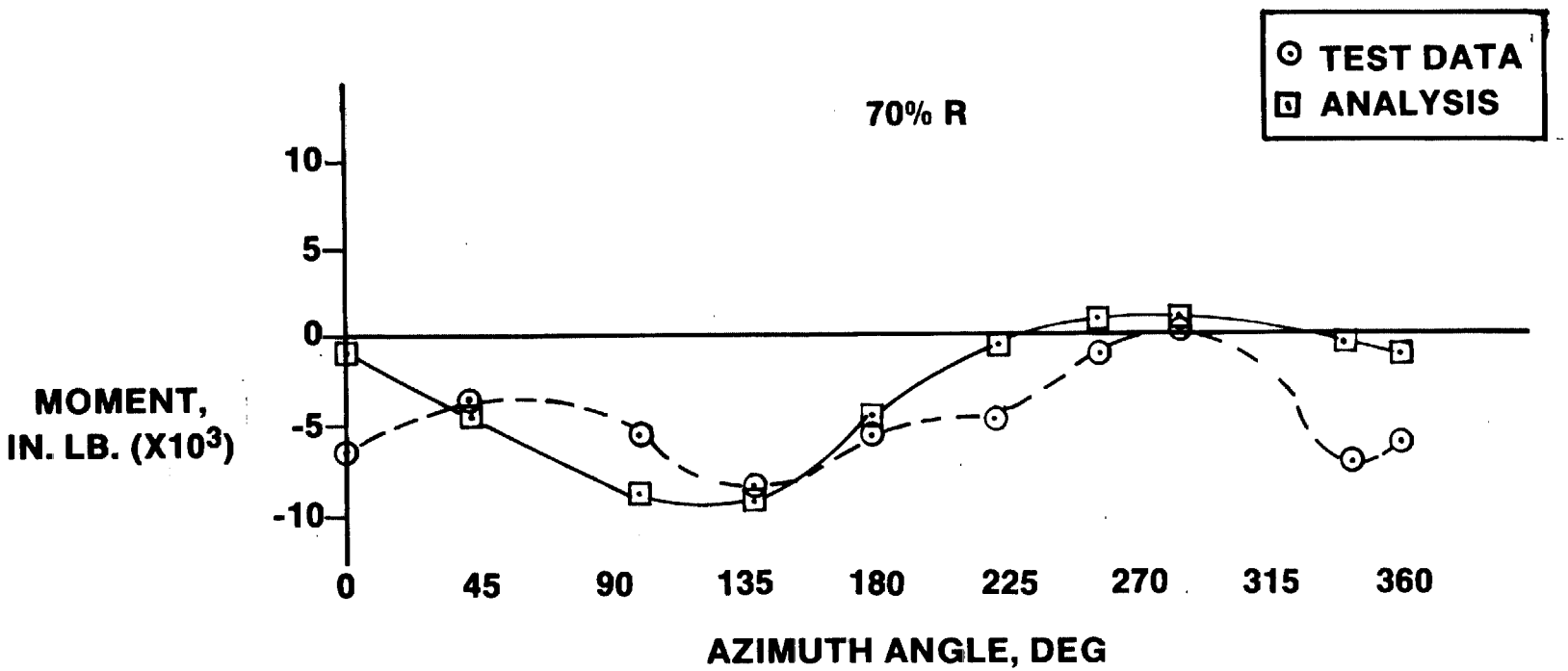

BLADE EDGEWISE BENDING MOMENT TIME HISTORIES AT V = 67 KNOTS

The blade edgewise bending moment time histories are compared for radial stations of 30, 50, and 70 percent radius at 67 knots. The blade edgewise bending moments are seen to be overpredicted by a factor of two over flight test data. The figures on the following two pages illustrate the correlation between analysis and test data.

BLADE EDGEWISE BENDING MOMENT TIME HISTORIES
V = 67 KN

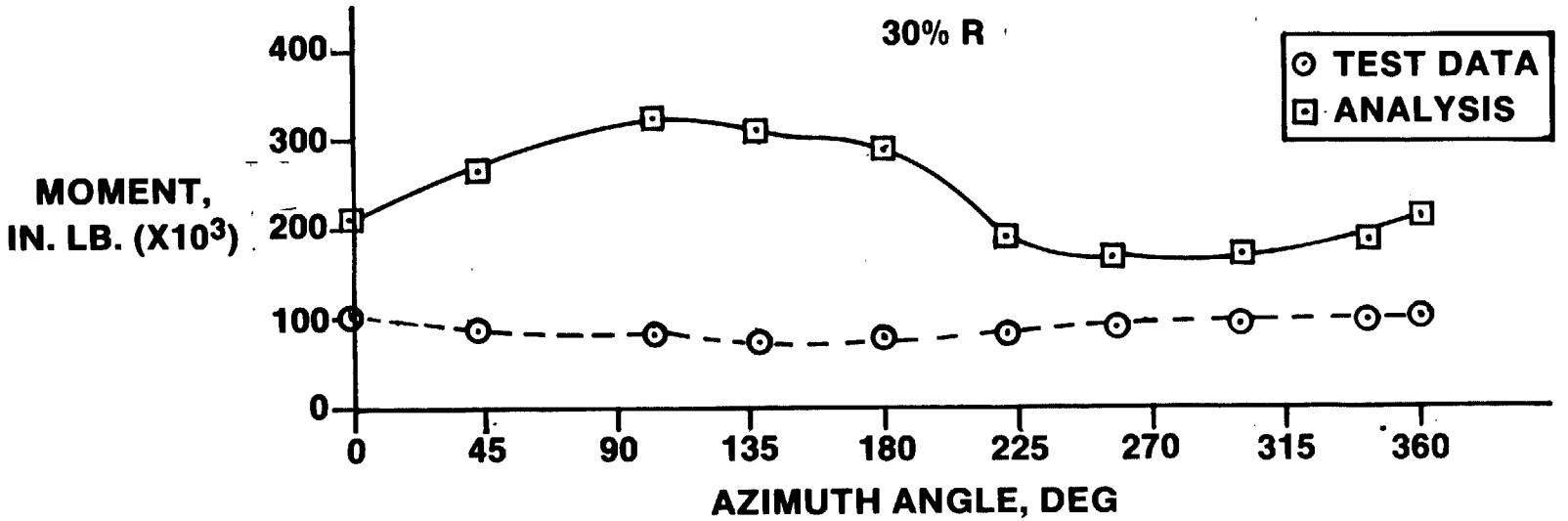

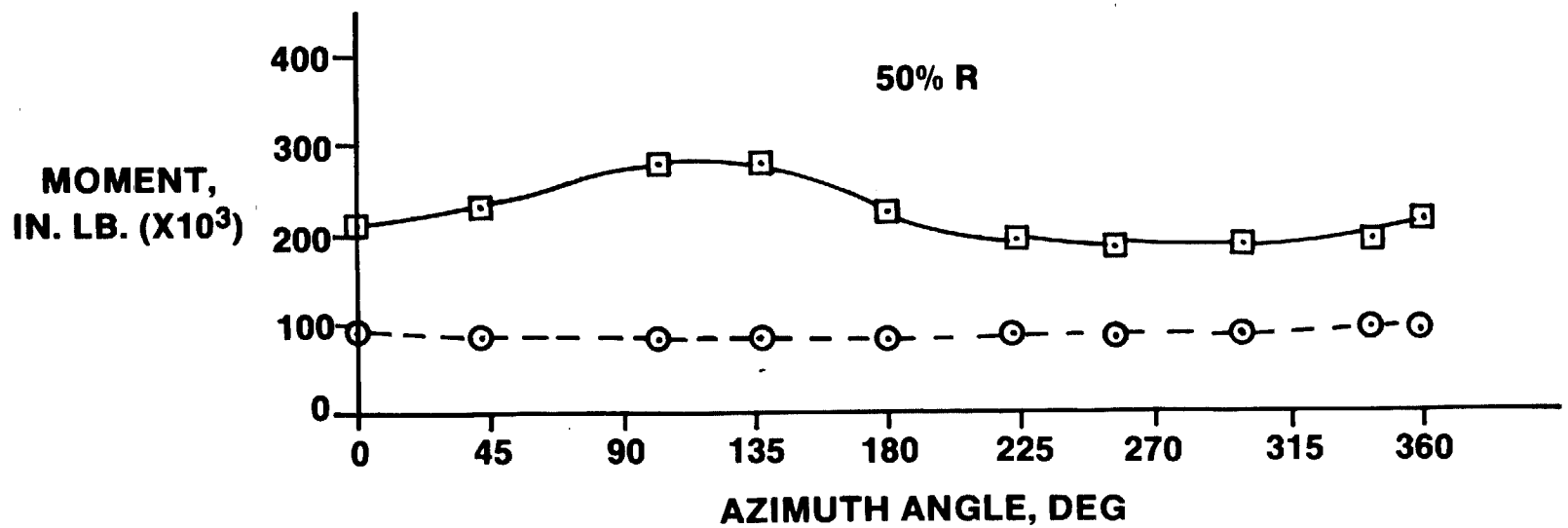

BLADE EDGEWISE BENDING MOMENT TIME HISTORIES
V = 67 KN

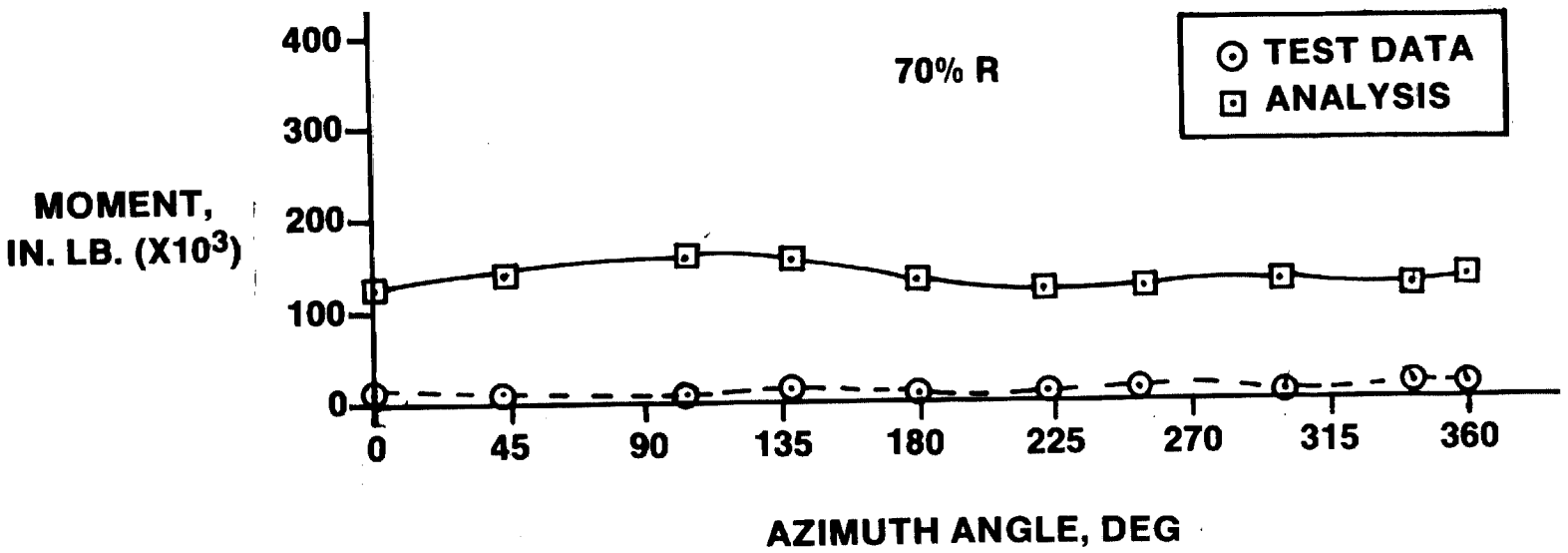

14. CORRELATION OF FUSELAGE VIBRATION

HUB VIBRATIONS AT 2/REV

Analytical and test hub vibrations at 2/rev in the longitudinal, lateral, and vertical directions are compared.

HUB VIBRATIONS AT 2/REV

LONGITUDINAL ACCELERATIONS, G'S

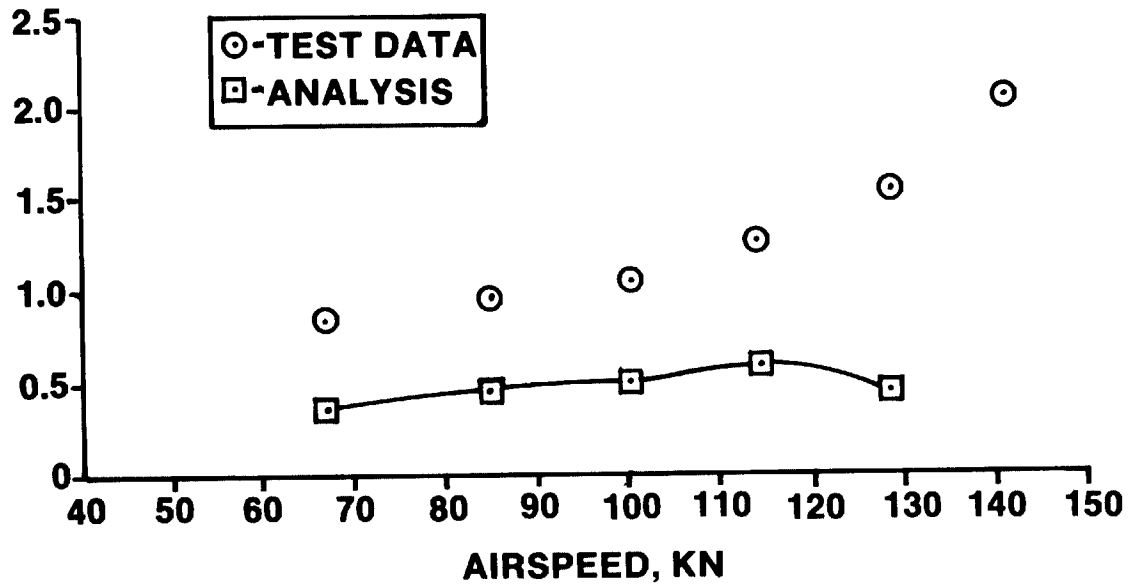

LATERAL ACCELERATIONS, G'S

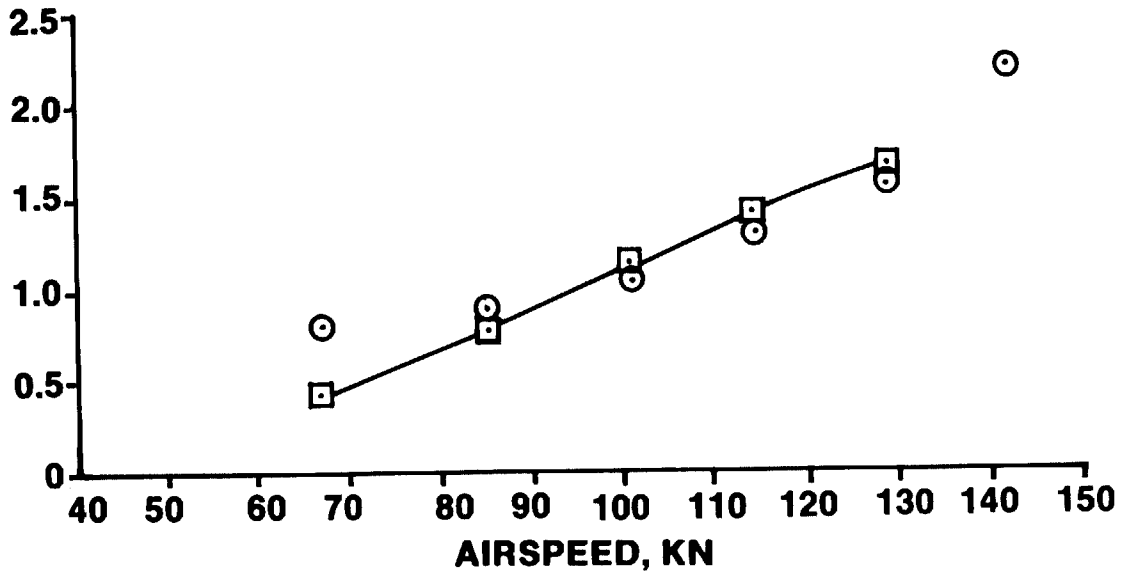

HUB VIBRATION AT 2/REV

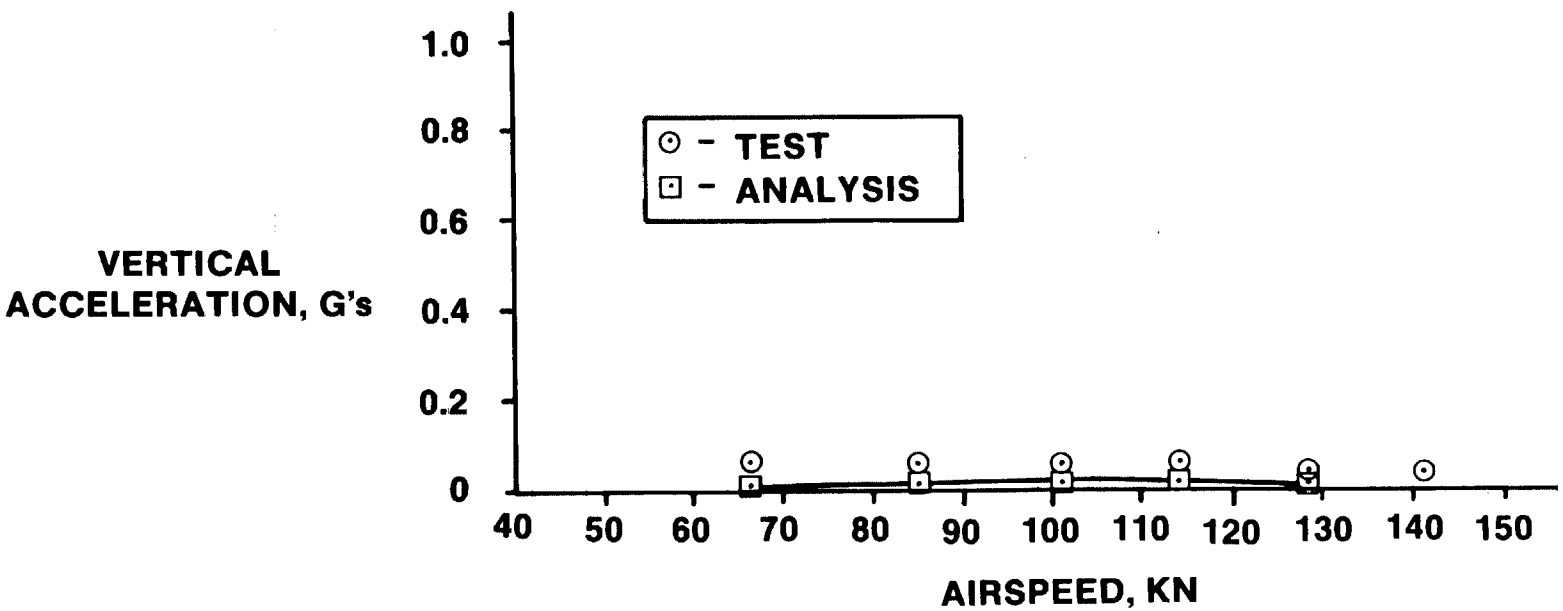

FUSELAGE VIBRATION AT 2/REV

Five points along the fuselage were selected to represent the fuselage vibration response in addition to the hub location. The five locations are listed below:

1) Nose Location

2) Pilot Location

3) Tailboom Junction

4) Elevator Location

5) Fin Location

The following five figures illustrate lateral and vertical vibration levels at 2/rev for the above locations. No correlation was done for the longitudinal direction since no test data were supplied in that direction.

The coupled rotor/fuselage analysis consistently overpredicts flight test data in both lateral and vertical vibration levels. As the airspeed increases, larger deviations from flight test are observed. Deviations of 2 to 1 are observed for the high speed conditions. An exception is in the vertical direction, at the vertical fin where vibration levels are underpredicted. In general, correlation with test data is more favorable at low airspeeds.

NOSE VIBRATION AT 2/REV

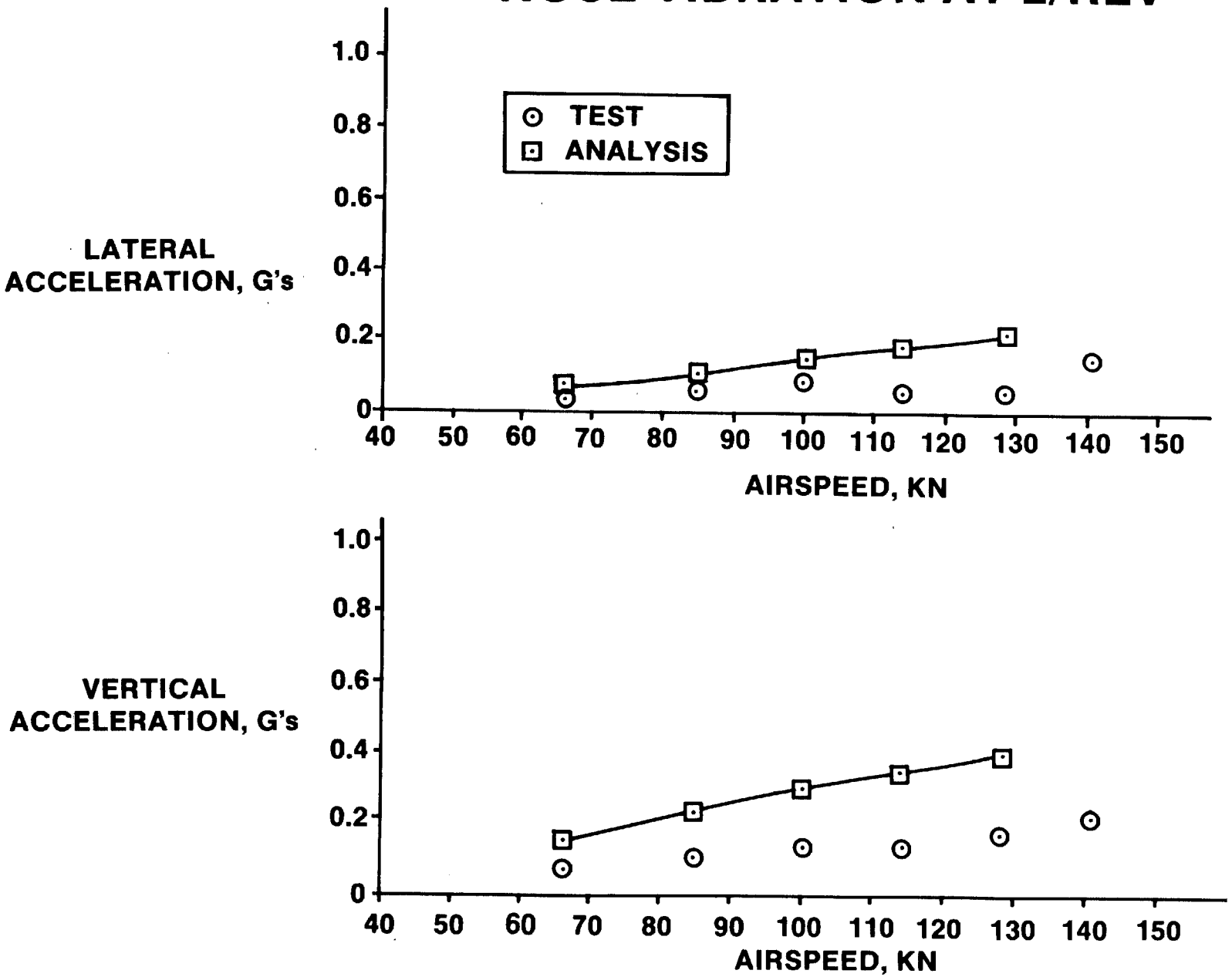

PILOT VIBRATION AT 2/REV

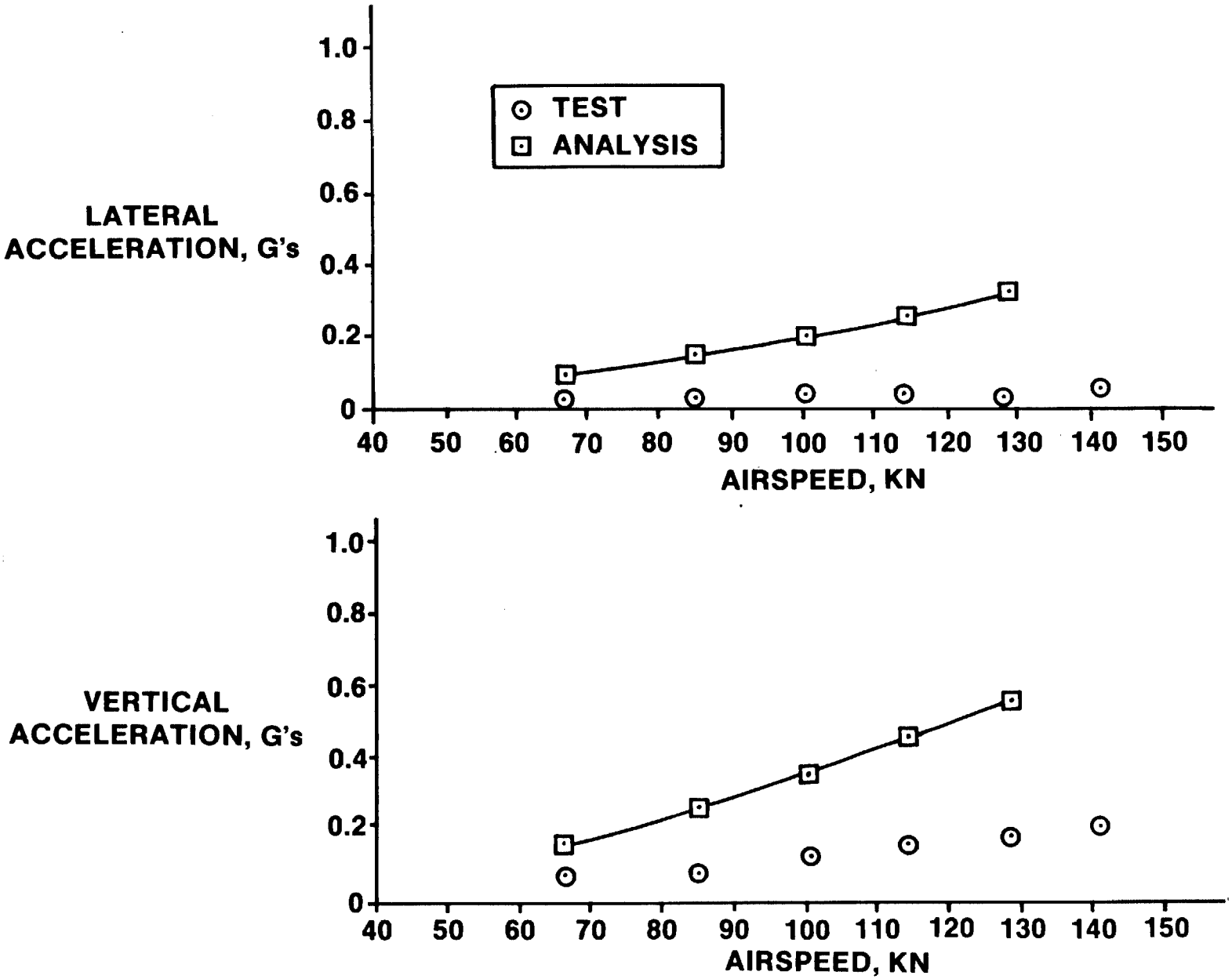

T/B JUNCTION VIBRATION AT 2/REV

LATERAL ACCELERATION, G's

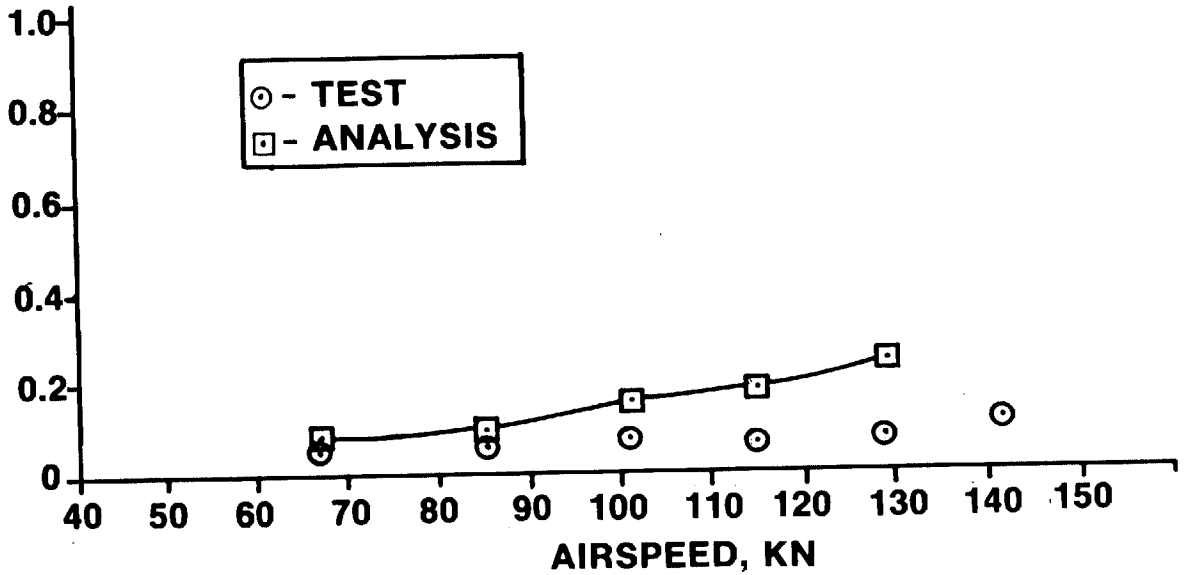

VERTICAL ACCELERATION, G's

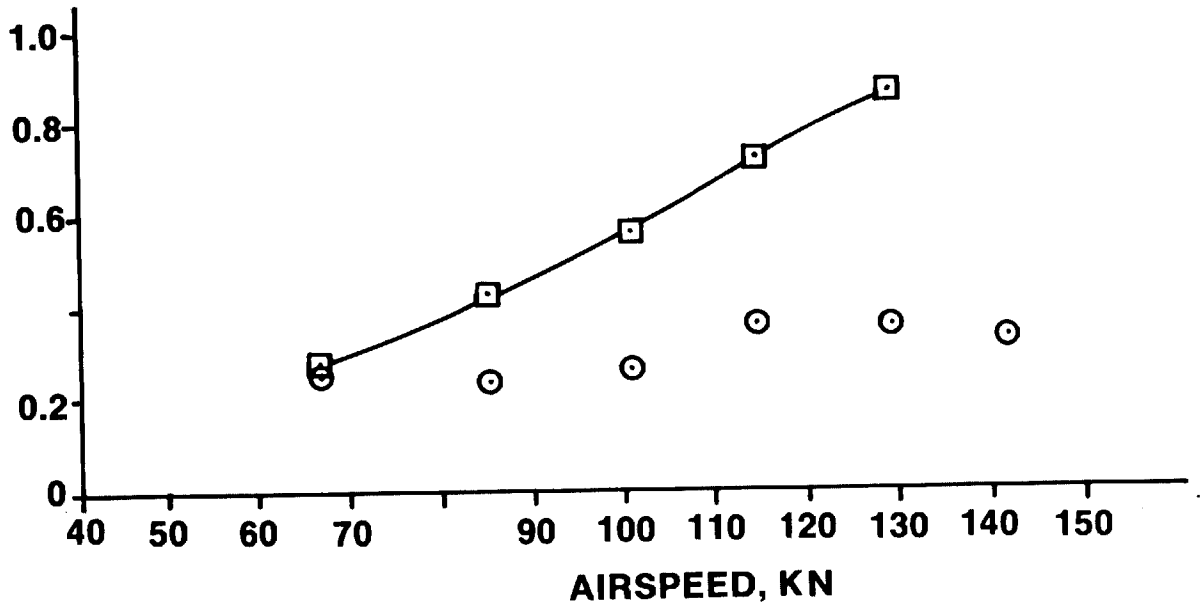

ELEVATOR VIBRATION AT 2/REV

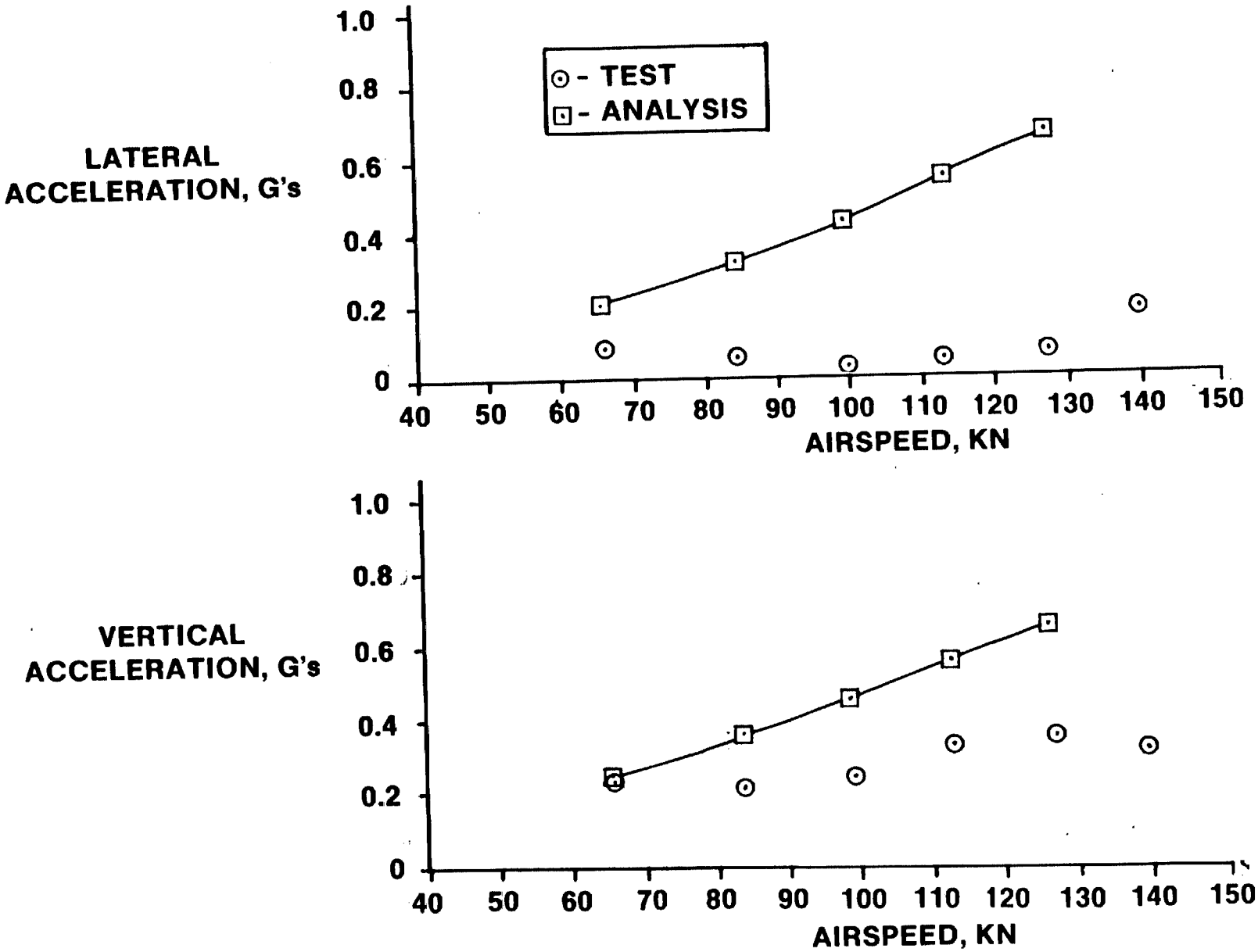

FIN VIBRATION AT 2/REV

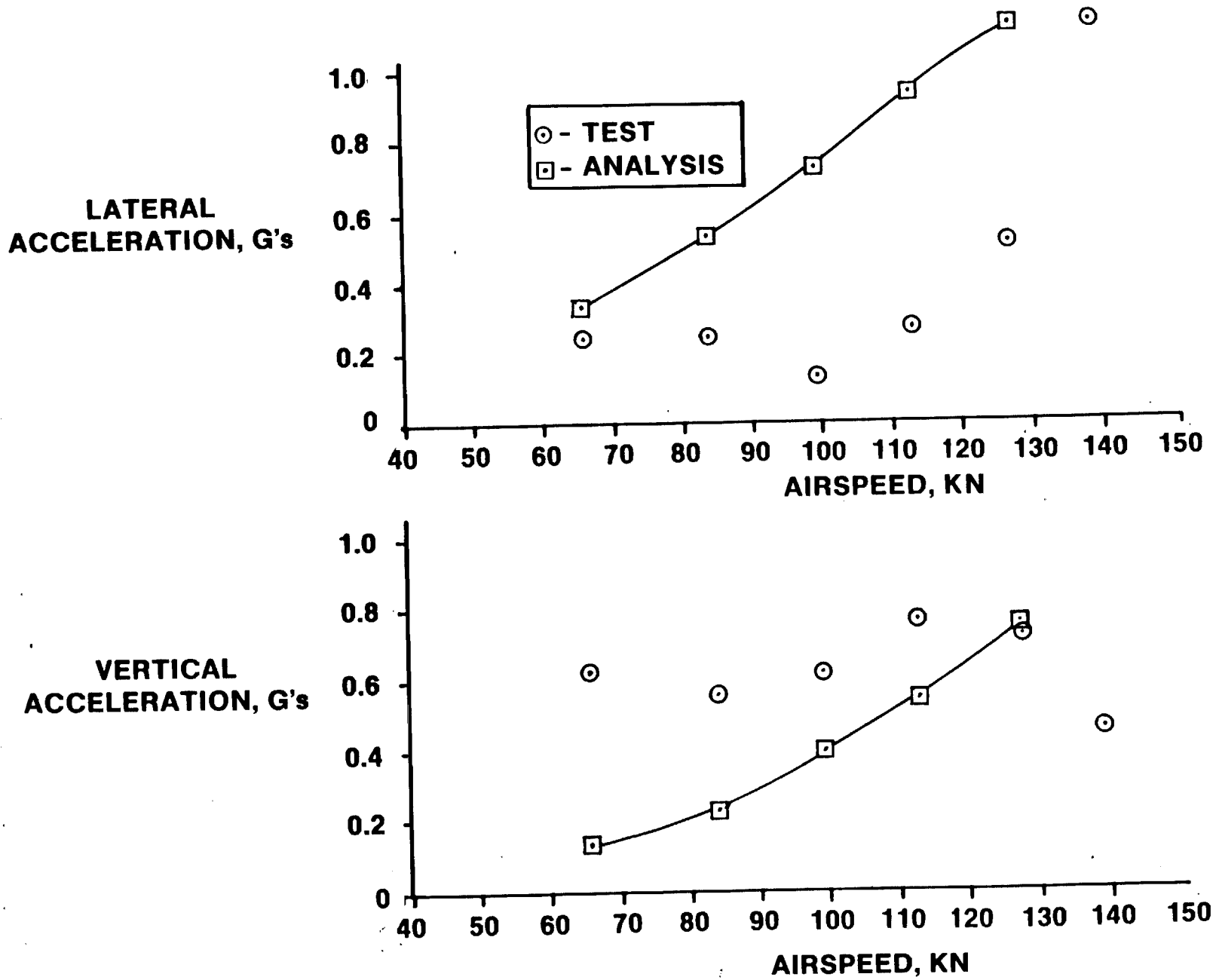

15. SENSITIVITY INVESTIGATION

SENSITIVITY OF HARMONICS OF BLADE BENDING MOMENT AT 50% RADIUS, V = 67 KNOTS

The assumptions that were made in the baseline model in order to achieve convergence were described on page 132. The effect of making these assumptions was investigated at V = 67 knots and the results presented in this figure. Included are the effects of:

a) Changing the amount of structural damping in the fuselage (2% instead of 10%).

b) Including the non-zero hub roll component of the 2nd fuselage mode.

Also investigated, for their possible effect on numerical integration accuracy were:

a) Reducing the size of the time step used in the time history integration (azimuth angle increment reduced from 5° to 1°).

b) Changing the number of blade flatwise modes from 9 to 8.

As can be seen in this figure, changing these parameters had almost no effect on blade response.

SENSITIVITY OF HARMONICS OF BLADE BENDING MOMENT AT 50 % RADIUS V = 67 KN

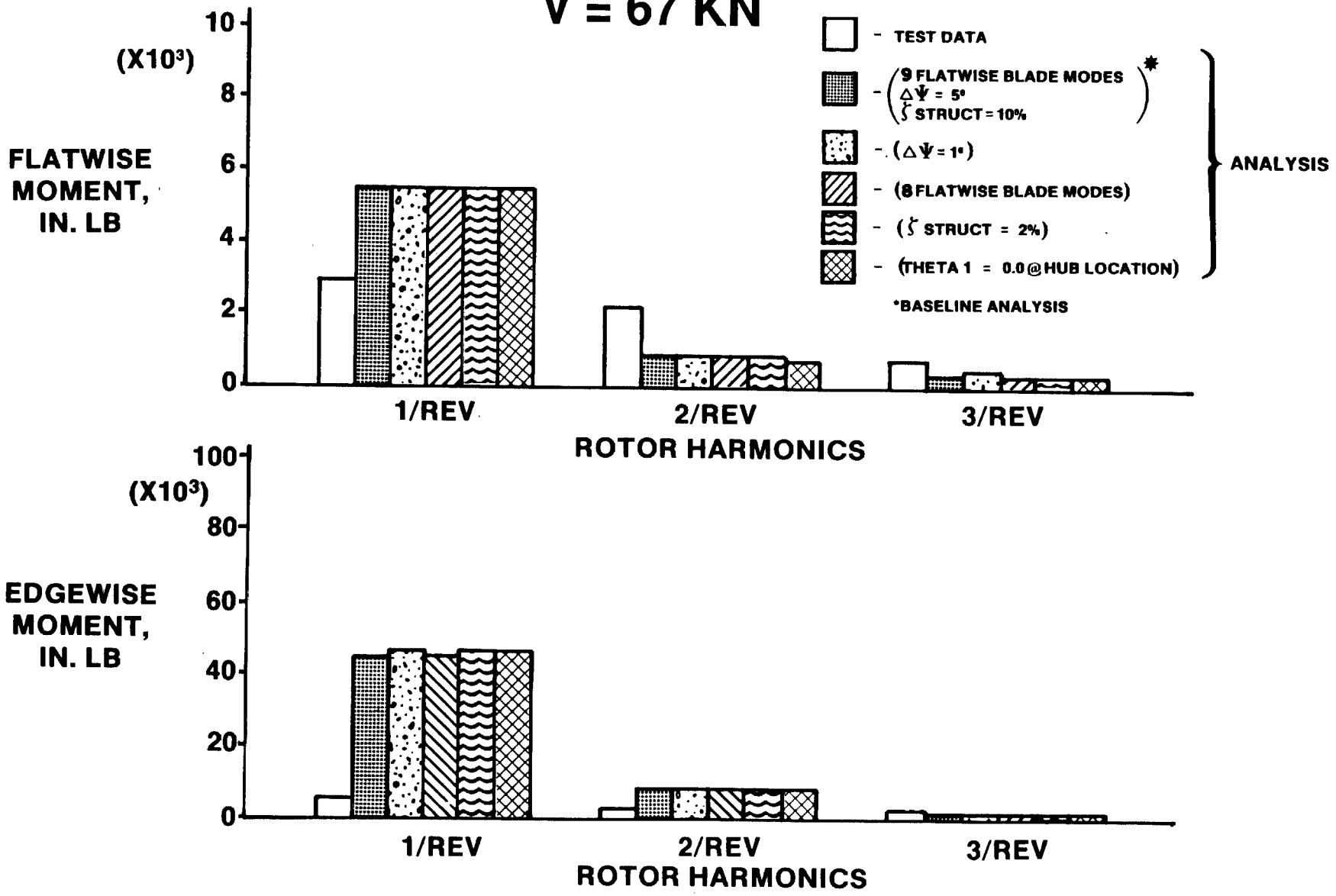

SENSITIVITY OF FUSELAGE VIBRATION AT 2/REV, V = 67 KNOTS

The following three figures show the effect that changing the same parameters had on fuselage vibration. As can be seen the effect was likewise small.

SENSITIVITY OF FUSELAGE VIBRATION AT 2/REV
V = 67 KN

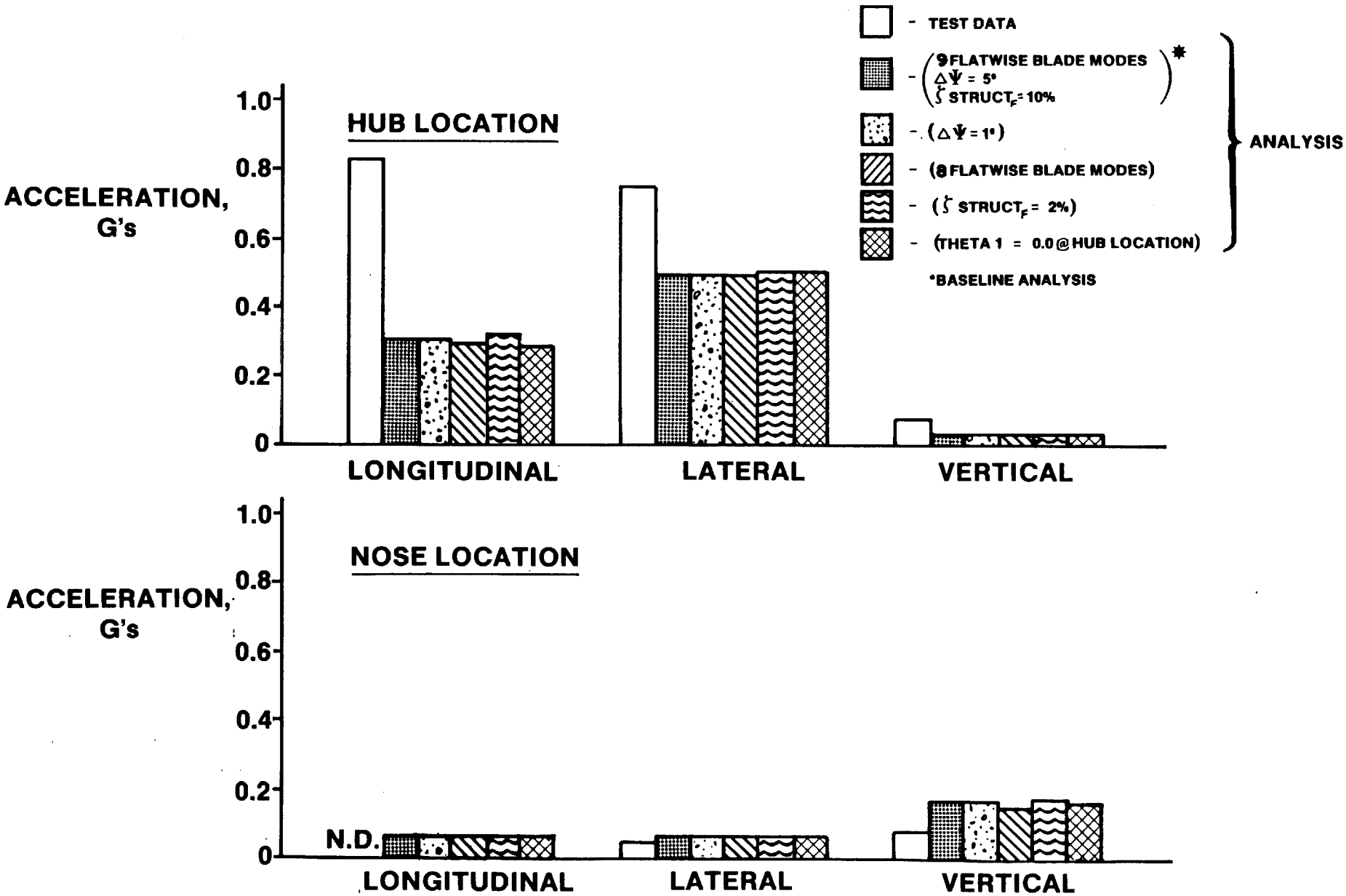

SENSITIVITY OF FUSELAGE VIBRATION AT 2/REV
V= 67 KN

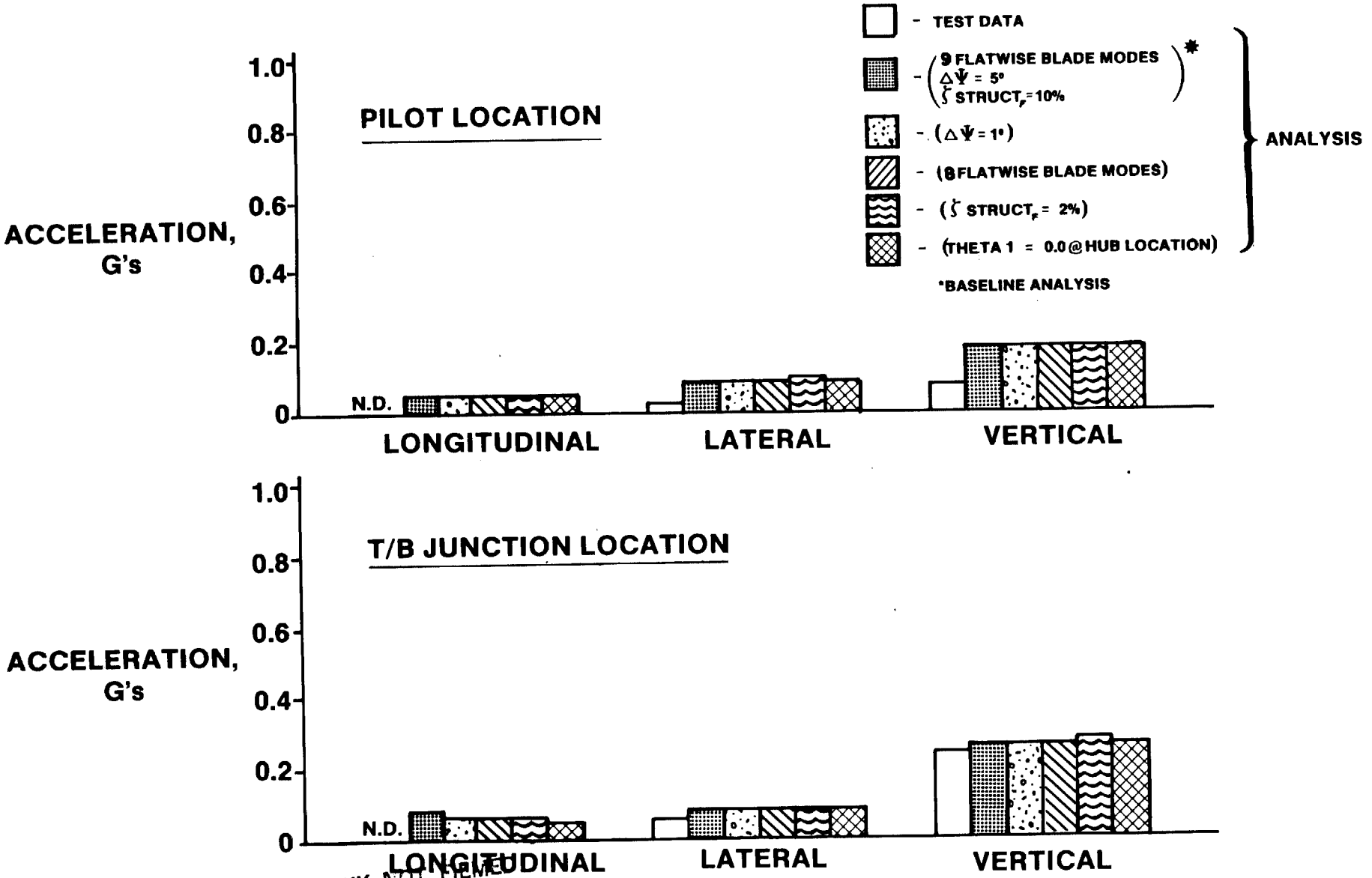

PRECEDING PAGE BLANK NOT FILMED

SENSITIVITY OF FUSELAGE VIBRATION AT 2/REV
V=67 KN

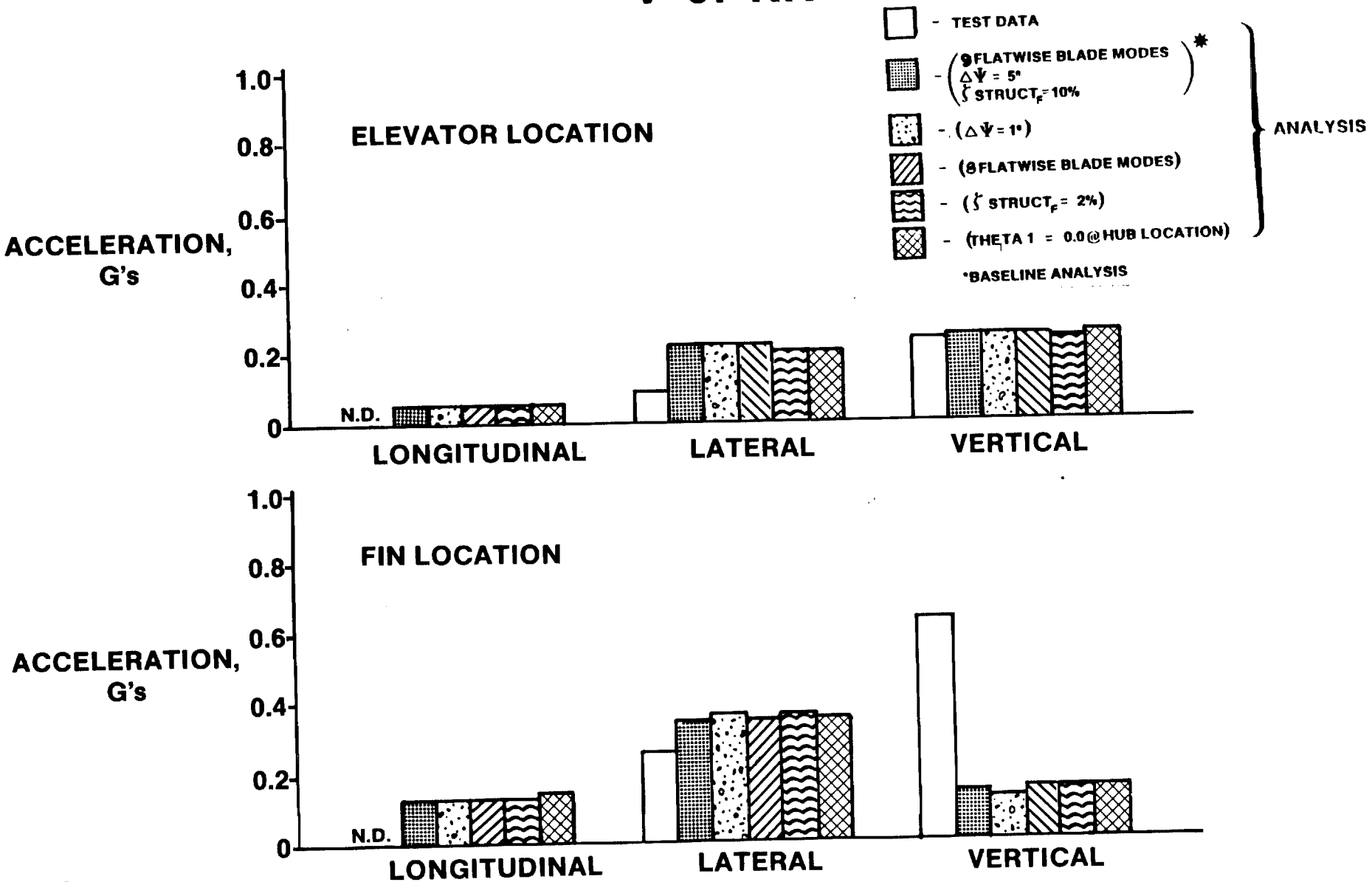

EFFECT OF VARIABLE INFLOW ON BLADE BENDING MOMENTS AT 50 PERCENT RADIUS (HUB FIXED V = 67 KNOTS)

A hub fixed comparison was done to determine the effects of variable inflow on blade bending moments. Both flatwise and edgewise blade bending moments are shown versus azimuth angle in the following figure. Analysis was conducted at 67 knots at 50 percent blade radius. The flatwise bending moment signature for uniform inflow is found to have the general shape as test data. However, a phase shift occurs and details of the curve are sacrificed. A much better signature is obtained with the use of variable inflow, particularly at azimuth angles 50 through 100 degrees.

The edgewise bending moments obtained from analysis are seen to have larger values than test by a factor of 2 or 3. Both uniform and variable inflow show these large variations.

EFFECT OF VARIABLE INFLOW ON BLADE BENDING MOMENTS AT 50% RADIUS (HUB FIXED V = 67 KN)

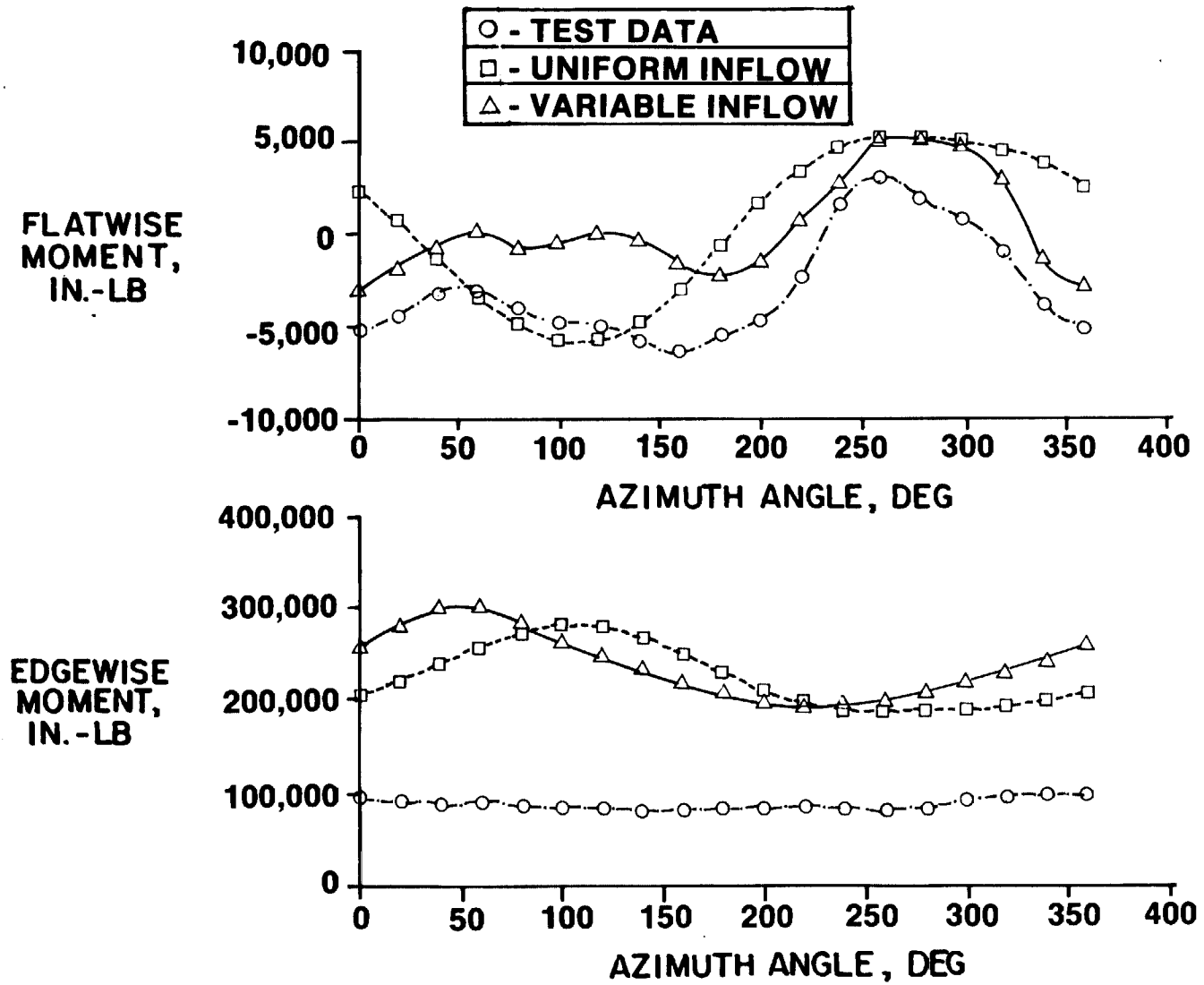

EFFECTS OF TORSIONAL BLADE MODE ON BLADE BENDING MOMENTS AT 50 PERCENT RADIUS (HUB FIXED V = 142 KNOTS)

The effects of torsional blade modes on blade bending moment at 142 knots and 50 percent radius are seen in the following figure. Flatwise and edgewise blade bending moments are shown versus azimuth angle. The flatwise bending moment signature for the no torsion condition shows fairly good correlation with test data. The trend and magnitude of flatwise moment are close and in phase. As torsion is added, fluctuations are encountered for the flatwise moment. The fluctuation oscillates about the test data. Therefore, better flatwise bending moment correlation is obtained from the no torsion condition.

Edgewise blade bending moments are seen to differ considerably from test data at the first 200 degrees of azimuth angle. Large edgewise moments are encountered with closer correlation after the 200 degree azimuth angle. Again, the effects of the blade torsional mode introduce additional harmonics but do not improve the correlation with test data.

EFFECT OF TORSIONAL BLADE MODE ON BLADE BENDING MOMENTS AT 50% RADIUS (HUB FIXED V = 142 KN)

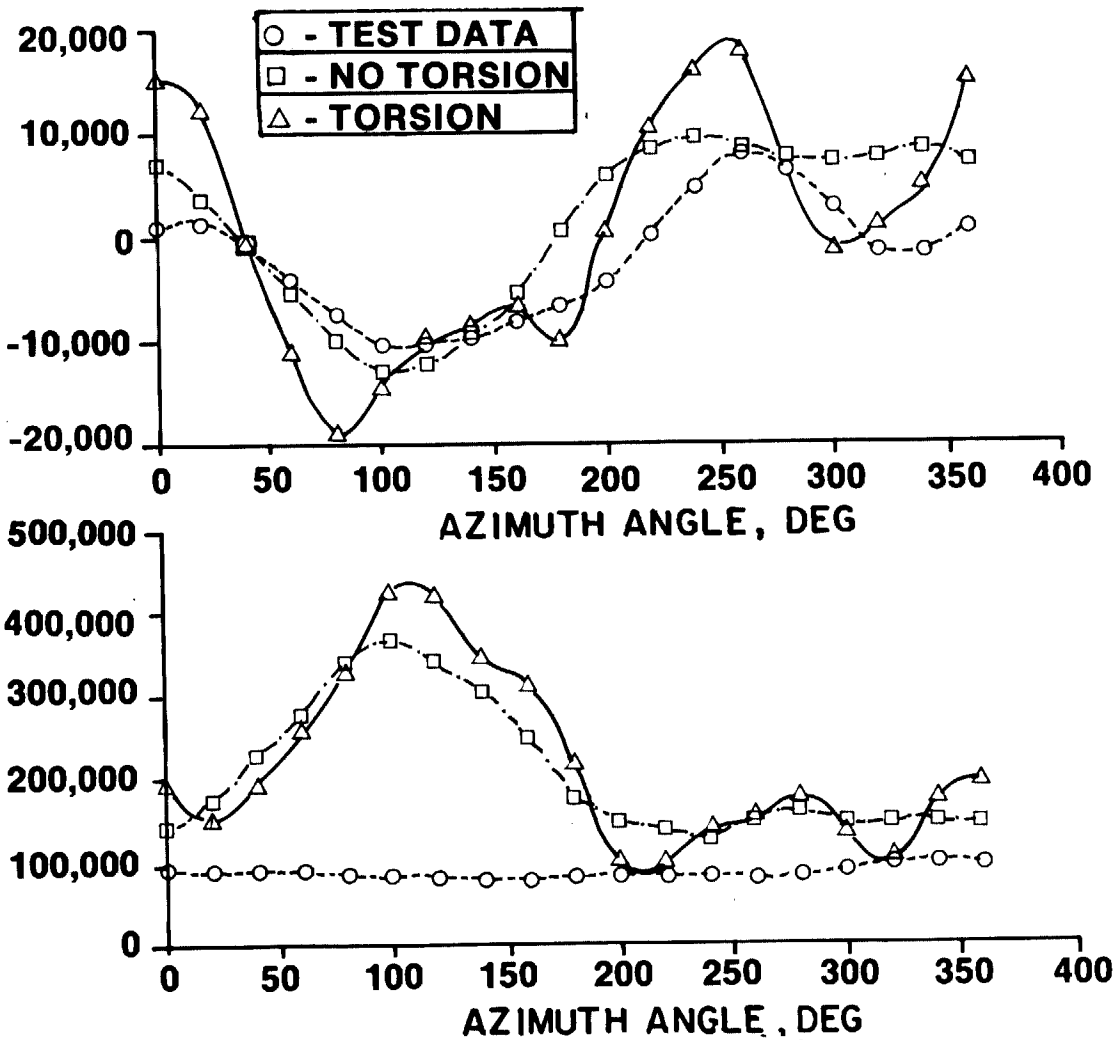

EFFECTS OF TORSION BLADE MODE ON BLADE BENDING MOMENTS AT 50 PERCENT RADIUS (HUB FIXED V = 142 KNOTS)

The following figure illustrates the effect of blade torsion mode on blade bending moments. The first three harmonics are shown comparing the effects of torsion with test data at 50 percent radius and 142 knots. Analyses were conducted with hub fixed.

EFFECT OF TORSION BLADE MODE ON BLADE BENDING MOMENTS AT 50% RADIUS (HUB FIXED V = 142 KN)

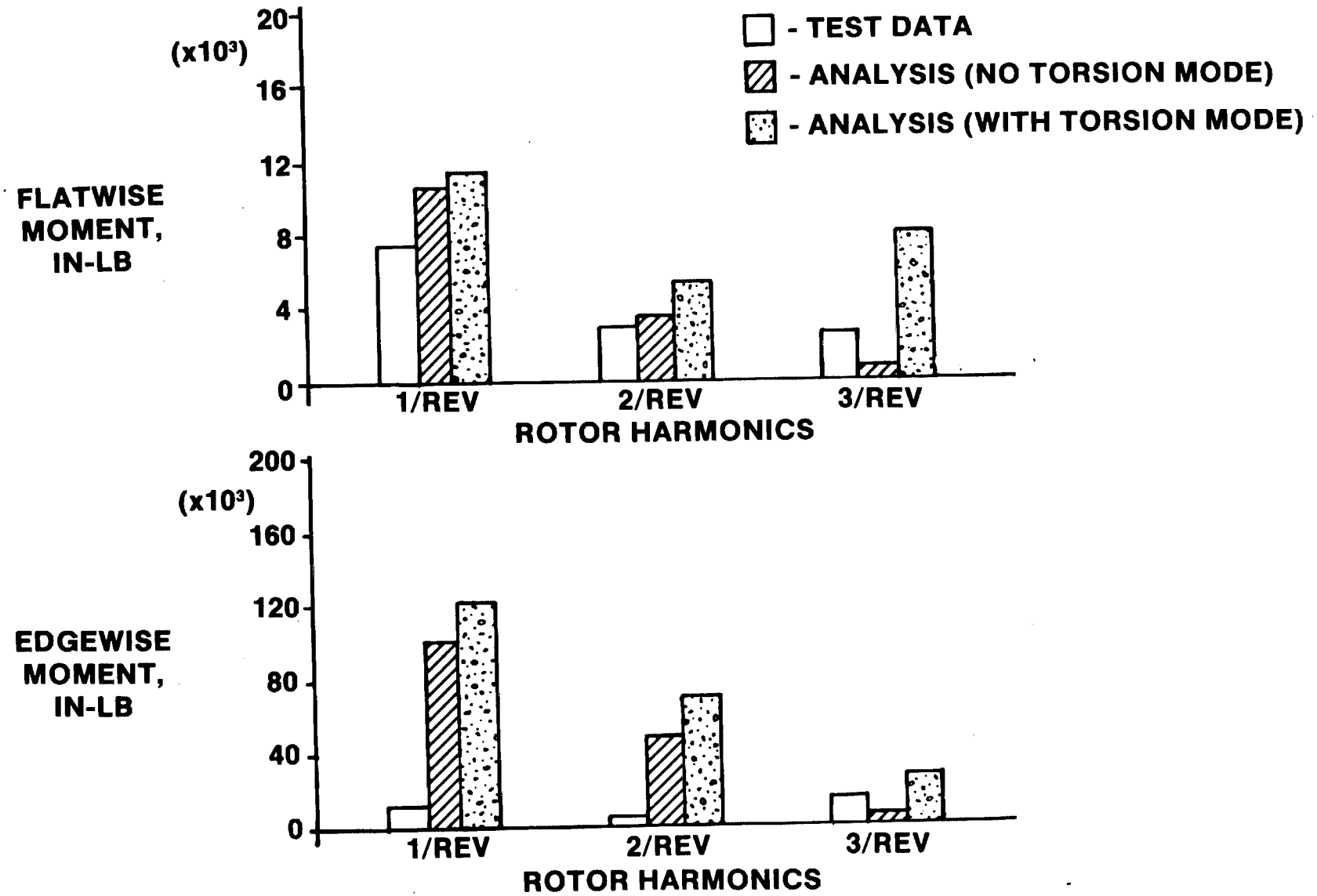

EFFECT OF AIRFRAME ON HUB LOADS AT 2P, PER BLADE

The traditional method of predicting airframe flight vibration was a two-step procedure involving uncoupled models of the rotor and fuselage.

1) Vibratory hub loads were first calculated from a hub-fixed rotor time history response.

2) These hub-fixed hub loads were then applied to a finite element model of the fuselage and the vibratory response of the latter was calculated.

This figure shows a comparison of 2/rev hub loads, per blade, calculated with the hub fixed and with the coupled rotor/fuselage model. The inclusion of the fuselage coupling effects is seen to cause significant changes in hub loads from those calculated with the hub fixed. This is an indication that the traditional uncoupled approach is not adequate, and that a fully coupled rotor/airframe system must be simulated.

EFFECT OF AIRFRAME ON HUB LOADS AT 2P, PER BLADE

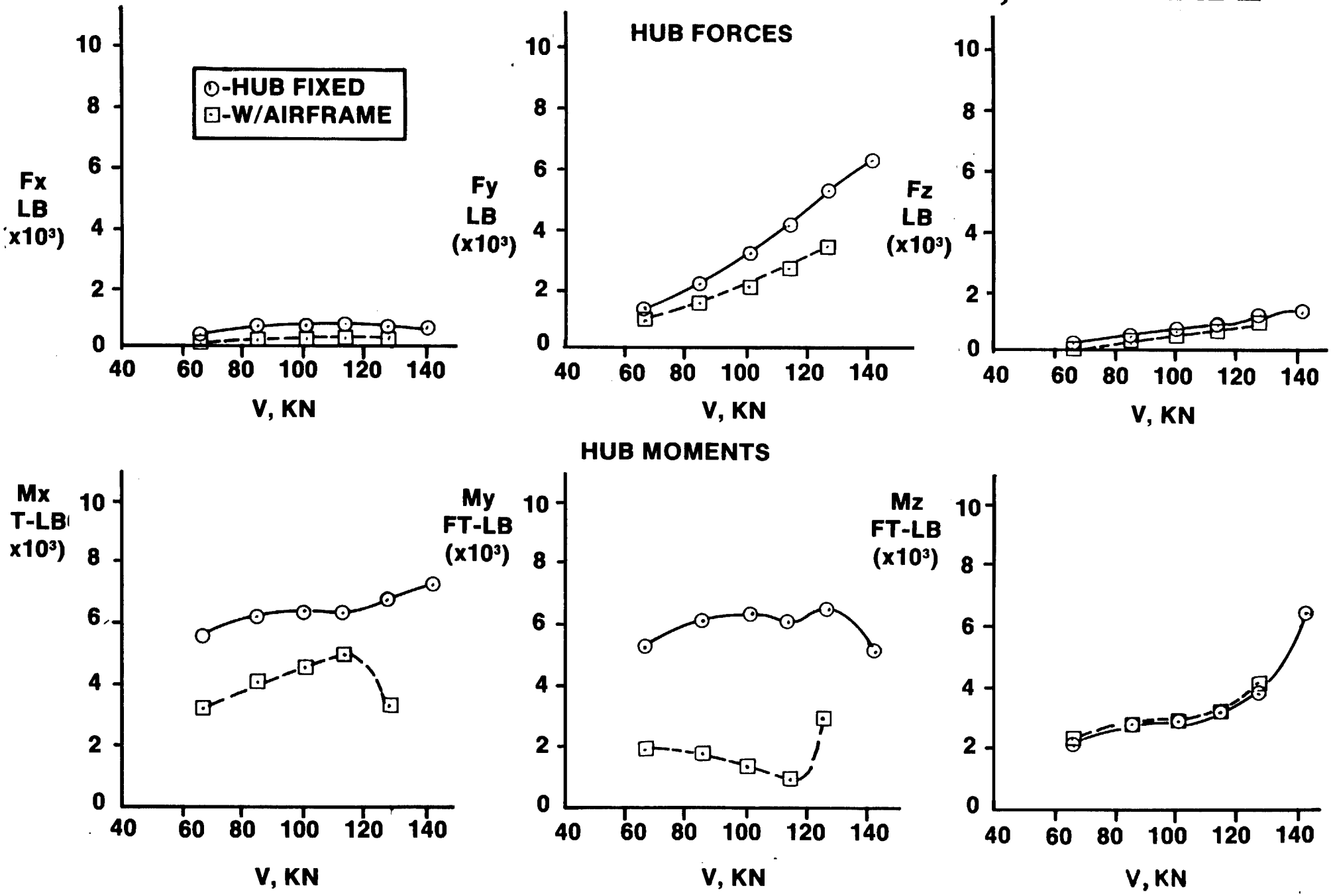

16. CONCLUDING REMARKS

CONCLUDING REMARKS

A comparison of predicted vibrations from the RDYNE analysis with flight test data for the AH-1G shows that RDYNE has a fair ability to predict vibrations for a helicopter with a teetering rotor. Specific conclusions are as follows:

1) Comparisons with the experimental data show that theory was able to predict trends of variations of 2P vibrations with airspeed, generally showing increases with airspeed. In some instances predicted magnitudes differed from measured results by factors of two or three to one. For some points, such as at the fin location, theory was not able to predict the proper shape of vibration variation with airspeed, owing perhaps to omission from the application of wake loads affecting the fin.

2) In attempting to trace the sources of the differences between theoretical predictions and the results of test data, the following results were obtained for blade bending moments. It was found that theory was able to represent trends of variations of blade flatwise bending moments with airspeed and radial position. The predicted flatwise bending moments rarely differed from the measurements by more than a factor of two to one. In the case of the edgewise moment there were gross overpredictions, particularly in the one and two per rev harmonics, and it is assumed that the differences are responsible for the differences between vibration predictions and test data. The assumption of pinned collective edgewise rotor modes, which was made owing to a lack of information on drive train properties, is a possible modeling deficiency.

3) Rotor-induced variable inflow improved the ability of the analysis to duplicate the azimuthal variation of measured flatwise bending moment yielding improvements in the harmonic content of the response. The edgewise bending moment was not significantly affected by variable inflow.

4) Omission of the torsional degree-of-freedom did not cause major changes in flatwise or edgewise bending moments, and appears to be a satisfactory approximation for vibration predictions, although torsion cannot be discounted as a factor affecting vibrations.

5) There were no significant sensitivities to number of blade modes, integration step size, fuselage structural damping and hub modal component.

17. REFERENCES

REFERENCES

1. Shockey, G. A., Williamson, J. W., Cox, C. R., "AH-1G Helicopter Aerodynamic and Structural Loads Survey," USAAMRDL-TR-76-39, April 1976.

2. Van Gaasbeek, J. R., "Validation of the Rotorcraft Flight Simulation Program (C81) Using Operational Loads Survey Flight Test Data," USAAVRADCOM-TR-80-D-4, November 1979.

3. Cronkhite, J. D., Berry, V.L., and Brunken, J. E., "A NASTRAN Vibration Model of the AH-1G Helicopter Airframe," U. S. Army Armament Command Report No. R-TR-74-045, June 1974.

4. Dompka, R.V., and Cronkhite, J. D., "Summary of AH-1G Flight Vibration Data for Validation of Coupled Rotor-fuselage Analyses", NASA CR 178160, Nov. 1986.

5. Sopher, R. and Hallock, D. H., "Time History Analysis for Rotorcraft Dynamics Based on a Component Approach," Journal of the American Helicopter Society, Vol. 31, No. 1, 1986.

6. Hsu, T. K. and Peters, D. A., "Coupled Rotor/Airframe Vibration Analysis by a Combined Harmonic-Balance Impedance Matching Method," Journal of the American Helicopter Society, Vol. 27, No. 1, 1982.

7. Kunz, D. L., "Response Characteristics of a Linear Rotorcraft Model," Journal of Aircraft, Vol. 19, No. 4, 1982.

8. Hohenemser, K. H. and Yin, S. K., "The Role of Rotor Impedance in the Vibration Analysis of Rotorcraft," Vertica, 3, (3/4), 1979.

9. Arcidiacono, P. J. and Sopher, R., "Review of Rotor Loads Prediction Methods," AGARD Conference Proceedings No. 334, London, England, May 1982.

10. Sopher, R., Studwell, R. E., Cassarino, S., and Kottapalli, S. B. R., "Coupled Rotor/Airframe Vibration Analysis," NASA CR 3582, November 1982.

Report Documentation Page

NASA National Aeronautics and Space Administration

1. Report No.	2. Government Accession No.	3. Recipient's Catalog No.
NASA CR-182031		

4. Title and Subtitle
CALCULATION OF FLIGHT VIBRATION LEVELS OF THE AH-1G HELICOPTER AND CORREALTION WITH EXISTING FLIGHT VIBRATION MEASUREMENTS

5. Report Date
APRIL 1990

6. Performing Organization Code

7. Author(s)
R. SOPHER AND W.J. TWOMEY

8. Performing Organization Report No.

10. Work Unit No.
505-63-51-01

9. Performing Organization Name and Address
UNITED TECHNOLOGIES CORPORATION
SIKORSKY AIRCRAFT DIVISION
6900 MAIN STREET
STRATFORD, CT 06601-1381

11. Contract or Grant No.
NAS1-17499

13. Type of Report and Period Covered
CONTRACTOR REPORT

12. Sponsoring Agency Name and Address
NATIONAL AERONAUTICS AND SPACE ADMINISTRATION
LANGLEY RESEARCH CENTER
HAMPTON, VA 23665-5225

14. Sponsoring Agency Code

15. Supplementary Notes
LANGLEY TECHNICAL MONITOR: RAYMOND G. KVATERNIK
FINAL REPORT (FOR TASK NO. 1 OF CONTRACT)

16. Abstract

~~The~~ NASA Langley Research Center is sponsoring a rotorcraft structural dynamics program with the ~~overall~~ objective to establish in the ~~United~~ States a superior capability to utilize finite element analysis models for calculations to support industrial design of helicopter airframe structures. In the initial phase of the program, teams from the major U. S. manufacturers of helicopter airframes will apply extant finite element analysis methods to calculate loads and vibrations of helicopter airframes, and perform correlations between analysis and measurements. The aforementioned rotorcraft structural dynamics program ~~has~~ was been given the acronym DAMVIBS (Design Analysis Method for Vibrations). ~~This~~ report describes Sikorsky's RDYNE Rotorcraft Dynamics Analysis used for the correlation study, the specifics of the application of RDYNE to the AH-1G, and comparisons of the predictions of the method with flight data for loads and vibrations on the AH-1G. RDYNE was able to predict trends of variations of loads and vibrations with airspeed, but in some instances magnitudes differed from measured results by factors of two or three to one. Sensitivities were studied of predictions to rotor inflow modeling, effects of torsional modes, number of blade bending modes, fuselage structural damping, and hub modal content.

ARE

17. Key Words (Suggested by Author(s))	18. Distribution Statement
AIRFRAME VIBRATIONS AH-1G HELICOPTER ROTORCRAFT DYNAMICS ANALYSIS DYNAMICS	UNCLASSIFIED - UNLIMITED Subject Category 39

19. Security Classif. (of this report)	20. Security Classif. (of this page)	21. No. of pages	22. Price
UNCLASSIFIED	UNCLASSIFIED	206	A10

NASA FORM 1626 OCT 86

11. Arcidiacono, P. J., "Prediction of Rotor Instability at High Forward Speeds - Volume 1 - Steady Differential Equations of Motion for A Helicopter Blade with Chordwise Mass Unbalance," USAAVLABS TR 68-16A, February 1969.

12. Chan, S.P., Cox, H. J., and Benfield, W. A., "Transient Analysis of Forced Vibrations of Complex Structural-Mechanical Systems," Journal of the Royal Aeronautical Society, Vol. 66, July 1962.